Calculation of aperture and far-field distributions from measurements in the Fresnel zone of large reflector antennas

th e

Calculation of aperture and far-field distributions from measurements in the Fresnel zone of large reflector antennas

by

C.A.M. Geus and J. Dijk

TECHNISCHE HOGESCHOOL EINDHOVEN
NEDERLAND
AFDELING DER ELEKTROTECHNIEK
VAKGROEP TELECOMMUNICATIE

EINDHOVEN UNIVERSITY OF TECHNOLOGY
THE NETHERLANDS
DEPARTMENT OF ELECTRICAL ENGINEERING
SECTION TELECOMMUNICATION

Calculation of aperture and far-field distributions from measurements in the Fresnel zone of large reflector antennas

by

C.A.M. Geus and J. Dijk

August 1978

TH-Report 78-E-87 ISBN 90 6144 087 4

Table of contents page

Summary

This report deals with the calculation of aperture field and radiation pattern, from Fresnelfield measurements of both amplitude and phase distributions radiated by large ($D >> \lambda$) reflector antennas.

A microwave measurement system based on the concept of microwave complex holograms is introduced.

The use of an existing antenna scanning system suggests measurements with a spherical scan. Equations for the Fresnel field of a large reflector antenna on a spherical surface will be derived. Also, the transformations necessary to calculate aperture and far fields will be given.

The cross-polarisation properties in the Fresnel zone will be investigated. For small boresight angles (large D/λ) the co-polarised and cross-polarised field distributions can be shown to result independently of co-polarised and cross-polarised aperture fields respectively.

It will be shown that an antenna test range of about 15 times the diameter of the reflector (D) is necessary to carry out Fresnel field measurements. Equations defining the angular test interval and the sampling distance will be derived.

In Ch. 4 results of measurements and calculations on the field of a small reflector antenna ($D \tilde{=} 10\lambda$) will be given.

Finally the authors wishes to thank Mrs. v.d. Ven - Pellegrino for typing the manuscript.

1.1 Introduction

The investigation of the far field characteristics of large reflector antennas often encounters a lot of problems because of the long distance and great altitudes at which a source (or receiver) has to be placed. Several methods of obtaining these characteristics from measurements at much shorter distances than $2D^2/\lambda$ were proposed. An excellent review of these methods is given by Ashton et al [1] and Hollis et al [2].
The three fundamental methods of obtaining the far field when measured in the near field are by:

a) arranging for the antenna to be illuminated by a plane wave generated within a short distance;
b) measuring the radiated fields in phase and amplitude of an antenna in the near field and calculating the far field;
c) changing the antenna to be tested in a prescribed way so that the field over a certain area in the near field closely resembles that of the far field of the true antenna.

Variations on these three methods have been developed, but all systems may be classified among one or occasionally two of these methods.
The plane wave illumination method (a), presently known as the compact range method, can be used for antenna pattern measurements, radar reflectivity measurements, etc. and yields accurate results [2].
The defocussing method (c) yields a rough approximation of the required far field pattern [1] and can only be used with systems that can be defocussed.
Method (b) uses phase and amplitude information of the near field to calculate the far field. The field measured at some plane, cylindrical or spherical surface is thereby transformed into the far field pattern. Use of this Field Transform Method requires also measurement of the phase pattern which was a prime difficulty at microwave frequencies. For this reason, only little attention has been paid to the measurement of the phase patterns in the past, hence calculations of aperture fields were not usually possible and information regarding aperture blocking and aperture field deformations was not obtained.
Using microwave holography and optical data handling, the Russian investigators Bakhrakh and Kurochkin [3], were the first to reconstruct the optical analogon of the radiation pattern of a large reflector antenna. Other authors proposed numerical data handling [4,5]. It is the purpose of this report to present

the necessary transformations for the calculation of the far field and aperture field measurements from Fresnel field·measurements on a spherical surface and to introduce a measurement bridge based on the principle of microwave complex holograms.

1.2 Literature

[1] R.W. Ashton et al "A study of the prediction of antenna performances from near field measurements", June 1975, Final Report Marconi Res. Labs. ESA contract 2239/75/HP.

[2] Johnson et al, "Determination of far field antenna patterns from near field measurements", Proc. IEEE Dec. 1973.

[3] L.D. Bakhrakh, A.P. Kurochkin, D.A. Dimitranko, W.M. Tseitlin and D.L. Arutyunyan, "Determination of the radiation pattern of a receiving antenna by means of a source in the Fresnel zone using holography and optical processing", Sov. Phys. Doklady, Vol. 16 no. 11 pp. 1004.

[4] R.H.T. Bates, "Holographic approach to radiation pattern measurements", pp. 1107-1208, Int. Jrnl Engng Sci., Vol. 9 - 1971.

[5] R.H.T. Bates and P.J. Napier,"A suggestion for determining antenna pattern phase from holographic type of measurement", Austr. Electr. Comm. p. 164, April 1971.

2. Field equations

2.1. Introduction

Radiation patterns of electrically large reflector antennas ($D >> \lambda$) can only be measured at distances greater than $2D^2/\lambda$, i.e. sometimes several kilometers. Measurements of the radiation patterns with the help of sources in the very far field like radio stars [1] and satellites are very well possible, but require accurate and often difficult tracking of these sources. Measurement at much shorter distances, i.e. in the Fresnel region, yield a Fresnel diffraction pattern instead of the Fraunhofer diffraction pattern (or radiation pattern), in which we are mainly interested. However, measurements of both phase and amplitude distributions in the Fresnel zone, for instance with microwave holographic techniques, give a complete picture of the radiating source under investigation. Therefore, with the use of appropriate transformations, the field in any plane from aperture to far field can be calculated accurately.

Measurements in the Fresnel region are very meaningful for large reflector antennas (large D) which are used at very high frequencies (small λ). The cross-polarisation characteristics of these antennas, which are important because of frequency re-use, will have to be investigated in the Fresnel region, too.

The Fresnel diffraction field of a large reflector antenna can be calculated by the scalar aperture method or by the current distribution method. The latter is a vectorial method and can be used to calculate cross-polarisation. The scalar aperture field method assumes a linearly polarised aperture field; consequently, only co-polarisation can be calculated by it. Silver [2] states that as a first approximation cross-polarisation can also be computed by applying the scalar aperture field method to the cross-polarised aperture field. Silver also shows that the radiation pattern calculated by the current distribution method is essentially the same as that calculated by the aperture plane method. Co-polarised and cross-polarised Fresnel fields can thus be calculated by using the current distribution method with the help of approximations which are similar to those used in the aperture field method. Using these methods, it will be shown that co-polarised and cross-polarised fields in the Fresnel and Fraunhofer region can be treated individually by applying the aperture field method to co-polarised and cross-

polarised aperture fields.
It is the purpose of this chapter to compare these two methods in order to derive field equations for the co-polar and cross-polar fields in the Fresnel zone and Fraunhofer region. The relations between these fields are given, and finally field reconstruction errors will be investigated.

2.2. The aperture field method

Assuming an aperture diameter D which is much greater than wavelength λ, and a linearly polarised aperture field E(x,y), Silver [2] shows that the scalar aperture field method can be used to calculate the diffraction field E_p in P (Fig. 2.2.1, page 40).

$$E_p = \frac{1}{4\pi} \iint_A E(x,y) . \frac{e^{-jkr_1}}{r_1} [(jk + \frac{1}{r_1}) \bar{e}_z . \bar{e}_r + jk \bar{e}_z . \bar{e}_s] dxdy \qquad (2.2.1.)$$

with: E(x,y): the aperture field, which is linearly polarised in the aperture A
r_1: distance from source point to field point
$\bar{e}_r$: direction unit vector from source to field point
$\bar{e}_z$: direction unit vector normal to the aperture
$\bar{e}_s$: direction unit vector defining the direction of the magnetic field $\bar{H} = \frac{1}{Z_o} \bar{e}_s \times \bar{E}(x,y)$
x,y: aperture coordinates
k: the wave number $k = 2\pi/\lambda$.

The aperture field can be represented by its amplitude and phase distribution:

$$E(x,y) = A(x,y) e^{j\psi(x,y)} \qquad (2.2.2.)$$

Silver [2, p. 161] shows that:

$$\bar{e}_s = \left(\frac{1}{k} \frac{\partial \psi}{\partial x}, \frac{1}{k} \frac{\partial \psi}{\partial y}, \sqrt{1 - \frac{1}{k^2} \left(\left(\frac{\partial \psi}{\partial x} \right)^2 + \left(\frac{\partial \psi}{\partial y} \right)^2 \right)} \right) \qquad (2.2.3.)$$

and uniform phase distribution ψ = constant then yields:

$$\bar{e}_s . \bar{e}_z = 1.$$

Depending on the mathematical approximations of the integral (2.2.1.), the space for z > 0 can be divided into 3 zones: the near-field zone, the

Fresnel field zone and the Fraunhofer zone.
Again, Silver states that for the near zone region of points in the immediate neighbourhood of the aperture no simplifying approximations can be made. This region extends several wavelengths outward of the aperture.
In the Fresnel region, several simplifying approximations are possible:
- the term $1/r_1$ in square brackets is negligible with respect to k.
- $1/r_1 \simeq 1/R$.
- the term $\bar{e}_z.\bar{e}_r$ can be approximated because R >> r where $x^2 + y^2 = r^2$:

$$\bar{e}_r = \frac{R\bar{e}_R - r.\bar{e}_r}{|R\bar{e}_R - r.\bar{e}_r|} \simeq \bar{e}_R \qquad (2.2.4.)$$

so $\bar{e}_z.\bar{e}_R = \cos\theta$
- the phase term e^{-jkr_1} can be approximated using:

$$\bar{r}_1 = r_1\bar{e}_r = R\bar{e}_R - r\bar{e}_r$$

$$r_1^2 = (\bar{r}_1.\bar{r}_1) = R^2 + r^2 - 2rR(\bar{e}_r.\bar{e}_R).$$

Hence

$$r_1^2 = R^2\left[1 + \frac{r^2 - 2rR(\bar{e}_r.\bar{e}_R)}{R^2}\right]$$

A binomial expansion yields

$$r_1 = R\left[1 + \frac{1}{2}\left(\frac{r^2-2rR(\bar{e}_r.\bar{e}_R)}{R^2}\right) - \frac{1}{8}\left(\frac{r^2-2rR(\bar{e}_r.\bar{e}_R)}{R^2}\right)^2 \ .....\right] \qquad (2.2.5.)$$

Neglecting all terms of the second and higher orders, this equation simplifies to the Fresnel approximation:

$$r_1 = R + \frac{r^2}{2R} - r(\bar{e}_r.\bar{e}_R) \qquad (2.2.6.)$$

with a maximum error of

$$|\Delta r_1| = \frac{r^2}{8R^3}\left(r^2 + 4R^2(\bar{e}_r.\bar{e}_R)^2 - 4rR(\bar{e}_r.\bar{e}_R)\right) \qquad (2.2.7.)$$

Applying spherical coordinates:

$x_p = R\sin\theta\cos\phi = R\alpha$
$y_p = R\sin\theta\sin\phi = R\beta$
$z_p = R\cos\theta$

the Fresnel approximation now yields

$$r_1 = R + \frac{r^2}{2R} - (x\alpha + y\beta)$$

hence the Fresnel diffraction field yields

$$E_{pFre} = \frac{jk}{2\pi R_{Fre}} \left(\frac{1 + \cos\theta}{2}\right) e^{-jkR_{Fre}} \iint E(x,y)\, e^{-jk\left(\frac{x^2 + y^2}{2R_{Fre}} - (x\alpha + y\beta)\right)} dxdy \qquad (2.2.8.)$$

For large values of R_{Fre} the term $r^2/2R$ becomes negligible and the Fresnel pattern transforms into the Fraunhofer or far field pattern.

$$E_{pFra} = \frac{jk}{2\pi R_{Fra}} \left(\frac{1 + \cos\theta}{2}\right) e^{-jkR_{Fra}} \iint E(x,y)\, e^{+ jk(x\alpha + y\beta)} dxdy \qquad (2.2.9.)$$

2.3. The current distribution method

Using the current distribution method or physical optics approximation, it is possible to calculate cross-polarised field components because here the field has a vectorial character [Silver, p. 88](Fig. 2.3.1, page 40)

$$\bar{E}_p = \frac{-jk^2}{4\pi\omega\varepsilon} \iint \{\bar{J} - (\bar{J}.\bar{e}_{r2}).\bar{e}_{r2}\} \frac{e^{-jkr_2}}{r_2} dS \qquad (2.3.1.)$$

The current density $\bar{J}$ is given by

$$\bar{J} = 2(\bar{n} \times \bar{H}_i) \qquad (2.3.2.)$$

$\bar{n}$ being the normal to the reflector surface and $\bar{H}_i$ the magnetic field incident on the reflector

$$\bar{H}_i = \left(\frac{\varepsilon}{\mu}\right)^{\frac{1}{2}} .(\bar{e}_\rho \times \bar{E}_i) \qquad (2.3.3.)$$

with

$$\bar{E}_i = \left[\left(\frac{\mu}{\varepsilon}\right)^{\frac{1}{2}} . \frac{P_T}{2\pi}\right]^{\frac{1}{2}} \frac{\sqrt{G_f(\psi,\xi)}}{\rho} \bar{e}_i(\psi,\xi)\, e^{-jk\rho} \qquad (2.3.4.)$$

where

P_T : total radiated power
G_f : gain of the feed
$\bar{e}_i$: polarisation vector.

If the feed is linearly polarised in the $\bar{e}_x$ direction:

$$\bar{e}_i(\psi,\xi) = \cos\xi\ \bar{e}_\psi - \sin\xi\ \bar{e}_\xi \tag{2.3.5.}$$

Equation (2.3.1.) can be simplified using the Fresnel and Fraunhofer approximations of section (2.2.).
Using (2.2.4.) with the vector $\bar{e}_\rho$ pointing to the reflector according to Fig. 2.3.1., one can write

$$(\bar{J}.\bar{e}_{r2}).\bar{e}_{r2} = \frac{(\bar{J}.(R\bar{e}_r - \rho\bar{e}_\rho)).(R\bar{e}_R - \rho.\bar{e}_\rho)}{|R.\bar{e}_R - \rho.\bar{e}_\rho|^2}$$

$$= \frac{(\bar{J}.R\bar{e}_R)R\bar{e}_R - (\bar{J}.\rho\bar{e}_\rho)R\bar{e}_R - (\bar{J}.R\bar{e}_R)\rho\bar{e}_\rho + (\bar{J}_\rho\bar{e}_\rho).\ \bar{e}_\rho}{|R\bar{e}_R - \rho.\bar{e}_\rho|^2} \tag{2.3.6.}$$

With $|R\bar{e}_R - \rho\bar{e}_\rho|^{-1} \simeq R^{-1}$ this equation becomes

$$(\bar{J}.\bar{e}_{r2}).\bar{e}_{r2} = \{(\bar{J}.R\bar{e}_R) - (\bar{J}.\rho\bar{e}_\rho)\}\ .\{\frac{\bar{e}_R}{R} - \frac{\rho}{R^2}\ \bar{e}_\rho\}.$$

Because $\rho^2 << R^2$, one term can be neglected and

$$\bar{J}' = \bar{J} - (\bar{J}.\bar{e}_r)\bar{e}_r = \bar{J} - (\bar{J}.\bar{e}_R)\bar{e}_R + \frac{\rho}{R}\ (\bar{J}.\bar{e}_\rho)\bar{e}_R + \frac{\rho}{R}\ (\bar{J}.\bar{e}_R)\bar{e}_\rho \tag{2.3.7.}$$

The third term of $\bar{J}'$ only contributes to the longitudinal field. If, in addition,

$$\rho << R, \tag{2.3.8.}$$

the last two terms of (2.3.7.) can be neglected, and only the transversal field components of $\bar{J}$ (i.e. the θ and ϕ components) will contribute to $\bar{J}'$:

$$\bar{J}' = (0,\ J_\theta,\ J_\phi) \tag{2.3.9.}$$

The exponent in (2.3.1.) can be approximated using (2.2.5.) by replacing r by ρ:

$$r_2 = R_{Fre} + \frac{\rho^2}{2R_{Fre}} - \rho(\bar{e}_\rho . \bar{e}_R) - \frac{\rho^2}{2R_{Fre}} (\bar{e}_\rho . \bar{e}_R)^2$$

The Fresnel field can thus be calculated from

$$\bar{E}_{pFre} = \frac{-jk^2}{4\pi\omega\varepsilon} \iint_S \bar{J}' \frac{e^{-jk[R_{Fre} + \frac{\rho^2}{2R_{Fre}} - \rho(\bar{e}_\rho . \bar{e}_R) - \frac{\rho^2}{2R_{Fre}} (\bar{e}_\rho \bar{e}_R)^2]}}{R_{Fre}} dS \quad (2.3.10)$$

where

$$dS = \rho^2 \sin\psi \sec\frac{\psi}{2} \, d\psi d\xi$$

The current density $\bar{J}$ is given by Collin and Zucker [4]:

$$\bar{J} = 2[(\frac{\varepsilon}{\mu})^{\frac{1}{2}} \frac{P_T}{2\pi}]^{\frac{1}{2}} \frac{G_f^{\frac{1}{2}}(\psi,\xi)}{\rho} e^{-jk\rho} . (\bar{n} \times (\bar{e}_\rho \times \bar{e}_i))$$

with $\bar{e}_i$ defining the polarisation of the field incident on the paraboloidal reflector, and $\bar{n}$ being the normal vector to this surface.
The vector product is given by [4]:

$$\bar{n} \times (\bar{e}_\rho \times \bar{e}_i) = \bar{n} \times (-\bar{e}_z \times \bar{e}_i) = -\cos\frac{\psi}{2} \bar{e}_i - (\bar{n}.\bar{e}_i)\bar{e}_z \quad (2.3.11)$$

Here $\bar{e}_i$ defines the polarisation of the ray reflected at the paraboloid, hence $\bar{e}_i$ describes the polarisation of the field in the aperture plane.
The aperture distribution is [4]:

$$\bar{E}_{ap} = \{[\frac{\mu}{\varepsilon}]^{\frac{1}{2}} . \frac{P_T}{2\pi}\}^{\frac{1}{2}} . \frac{G_f^{\frac{1}{2}}(\psi,\xi)}{\rho} e^{-jk\rho} . e^{-jk\rho\cos\psi} . \bar{e}_i \quad (2.3.12)$$

The current density $\bar{J}$ can now be expressed in terms of the aperture field as

$$\bar{J} = -2(\frac{\varepsilon}{\mu})^{\frac{1}{2}} e^{jk\rho\cos\psi} [\cos\frac{\psi}{2} . \bar{E}_{ap} + (\bar{n}.\bar{E}_{ap})\bar{e}_z] \quad (2.3.13)$$

The Fresnel field can be expressed in the aperture field using (2.3.9) to (2.3.13).
The $\bar{e}_z$ term in (2.3.13) will not contribute to E_ϕ and its contribution to E_θ is proportional to $\sin\theta$ which is nearly zero for the narrow beams we are concerned with. Keeping in mind that $\bar{J}'$ can be replaced by $\bar{J}$ in (2.3.10) if one does not account for the $\bar{e}_R$ component of the electric field (2.3.10) this

substitution in (2.3.10) yields

$$\bar{E}'_{pFre} = \frac{jk}{2\pi R_{Fre}} e^{-jkR_{Fre}} \iint_{S_1} \bar{E}_{ap} \, e^{+jk(2f-\rho)} \, e^{jk[\frac{r^2}{2R_{Fre}} - \rho(\bar{e}_\rho . \bar{e}_R) - \frac{\rho^2}{2R_{Fre}} (\bar{e}_\rho \bar{e}_R)}$$

Dropping the $\bar{e}_R$ component, we obtain

$$\bar{E}_{pFre} = (0, E'_{pFre_\theta}, E'_{pFre_\phi}) \qquad (2.3.14)$$

Here S_1 is the aperture plane and $dS_1 = r \, dr \, d\xi$ and $r = \rho \sin\psi = 2 f \tan \frac{1}{2}\psi$ while $2f - \rho = \rho\cos\psi$ is the definition of the paraboloid.
The inner product $(\bar{e}_\rho . \bar{e}_R)$ is given by

$$(\bar{e}_\rho . \bar{e}_R) = \cos\psi \cos\theta - \sin\psi \sin\theta \cos(\xi - \phi) \qquad (2.3.15)$$

In Appendix I it is shown that for small angles θ, the Fresnel integral yields

$$\bar{E}'_{pFre} = \frac{jk}{2\pi R_{Fre}} e^{-jkR_{Fre}} \iint \bar{E}_{ap} \, e^{jk\frac{r^2}{2R_{Fre}}} . e^{jkr\sin\theta a s(\xi-\phi)} \, r \, dr \, d\xi$$

$$\bar{E}_{pFre} = (0, E'_{pFre_\theta}, E'_{pFre_\phi}) \qquad (2.3.16)$$

For large values of R_{Fre} the quadratic phase term becomes negligible and the Fraunhofer or far field pattern is obtained

$$\bar{E}'_{pFra} = \frac{jk}{2\pi R_{Fra}} e^{-jkR_{Fra}} \iint \bar{E}_{ap} \, e^{jkr\sin\theta\cos(\xi-\phi)} r dr d\xi \qquad (2.3.17)$$

The true far field is then given by

$$\bar{E}_{pFra} = (0, E'_{pFra_\theta}, E'_{pFra_\phi})$$

2.4. Comparison of the aperture field method with the P.O. method

The Fresnel field obtained with the aperture field method (2.2.8) can be written as

$$E_{pFre} = \frac{jk}{2\pi R_{Fre}} e^{-jkR_{Fre}} \left(\frac{1 + \cos\theta}{2}\right) \iint E_{ap} \, e^{jk\frac{r^2}{2R_{Fre}} + jkr\sin\theta\cos(\xi-\phi)} \, r dr d\xi \qquad (2.4.1)$$

Comparison of (2.4.1) with (2.3.16) shows that for small angles θ the same radiation patterns are obtained by the aperture field method (2.2.8) applied to both aperture polarisations and with the aperture field approximation obtained from the P.O. method (2.3.16).

In general, a somewhat more accurate pattern is obtained from the surface currents directly rather than by the use of the aperture field, which involves a second application of Snell's law with its optical approximations [4].

Again, for small θ, both methods lead to the same equation of the far field. The aperture integrals (2.2.8) and (2.3.16) always yield far field components which are parallel to the aperture plane; hence, the $\bar{e}_R$ directed (longitudinal) component does not vanish. This is inherent in the aperture field method (2.2.8) because the basic equation (2.2.1) assumes a scalar field in the aperture.

The aperture field method (2.3.16) derived from the physical optics method yields an $\bar{e}_R$ component; however, this component may not be taken into consideration when calculating the actual field. In fact (2.3.16) yields (x,y,z) components of the calculated field since all (x,y,z) components of $\bar{J}$ are unequal to zero. In spherical coordinates:

$$\begin{bmatrix} E_R \\ E_\theta \\ E_\phi \end{bmatrix} = \begin{bmatrix} \sin\theta\cos\phi & \sin\theta\sin\phi & \cos\theta \\ \cos\theta\cos\phi & \cos\theta\sin\phi & -\sin\theta \\ -\sin\phi & \cos\phi & \end{bmatrix} \begin{bmatrix} E_x \\ E_y \\ E_z \end{bmatrix}$$

with

$$\begin{cases} E_i = \dfrac{-jk^2}{4\pi\omega\epsilon R_{Fre}} \iint_S J_i \, e^{-jk\left[R_{Fre} + \frac{\rho^2}{2R_{Fre}} - \rho(\bar{e}_\rho . \bar{e}_R)\right]} \, dS \\ i = (x,y,z) \end{cases} \tag{2.4.2}$$

Since the aperture field method (2.3.16) only takes into account E_x and E_y (E_z was neglected in (2.3.13)), the values of E'_R and E'_θ calculated by this method will be different from the actual field E_R, E_θ. However, because $J'_R = 0$ (Eq. 2.3.9), also $E_R = 0$. From (2.4.2.)

$$E_R = \sin\theta \cos\phi \, . \, E_x + \sin\theta \sin\phi \, . \, E_y + \cos\theta \, . \, E_z = 0 \tag{2.4.3}$$

and $E'_R = \sin\theta \cos\phi \, . \, E_x + \sin\theta \sin\phi \, . \, E_y$
hence $E_R = E'_R + \cos\theta \, . \, E_z = 0$
Hence,

$$E_Z = \frac{-E'_R}{\cos\theta} = - \frac{\sin\theta}{\cos\theta} (\cos\theta \, E_x + \sin\phi \, E_y) \tag{2.4.4}$$

and

$$E_\theta = \cos\theta \cos\phi \, E_x + \cos\theta \sin\phi \, E_y - \sin\theta \, E_z \tag{2.4.5}$$

$$E'_\theta = \cos\theta \cos\phi \, E_x + \cos\theta \sin\phi \, E_y \tag{2.4.6}$$

$$E_\theta = E'_\theta - \sin\theta \, E_z$$

Substitution of (2.4.4) and (2.4.6) in Eq. (2.4.5) leads to a correction of E'_θ :

$$E_\theta = E'_\theta + \frac{\sin^2\theta}{\cos\theta} (\cos\phi \, E_x + \sin\phi \, E_y) \tag{2.4.7}$$

The actual $E_{\theta,\phi}$ field can thus be calculated by the aperture field method (2.3.19) if the resultant E'_R, E'_θ fields are modified according to (2.4.7) and (2.4.3). This correction then leads to:

$$\begin{pmatrix} E_\theta \\ E_\phi \end{pmatrix} = \begin{pmatrix} (\cos\theta + \frac{\sin^2\theta}{\cos\theta}) \cos\phi & (\cos\theta + \frac{\sin^2\theta}{\cos\theta}) \sin\phi \\ - \sin\phi & \cos\phi \end{pmatrix} \begin{pmatrix} E_x \\ E_y \end{pmatrix} \tag{2.4.9}$$

with $E_R = 0$.
Using

$$\cos\theta + \frac{\sin^2\theta}{\cos\theta} = \frac{1}{\cos\theta}$$

we may write

$$\begin{pmatrix} E_\theta \\ E_\phi \end{pmatrix} = \begin{pmatrix} \frac{\cos\phi}{\cos\theta} & \frac{\sin\phi}{\cos\theta} \\ -\sin\phi & \cos\phi \end{pmatrix} \cdot \begin{pmatrix} E_x \\ E_y \end{pmatrix} \qquad (2.4.10)$$

Here E_x and E_y are the components calculated by the aperture field method (2.4.2).

2.5. Co-polarised and cross-polarised field distributions

The distant radiation field from a linearly polarised antenna can be completely specified in terms of two spatially orthogonal vector components. The definition of these vectors in terms of co-polarised and cross-polarised components is to some extend an arbitrary one, and at least three different definitions are commonly used in the literature. The definition employed here has the particular advantage that the calculated field components at any point in space, correspond directly to the components measured using standard antenna-range techniques.
This definition given by Ludwig [5] depends on the antenna axis, giving the principal electric vector, which is taken as reference polarisation.
Taking the x-axis as a reference, the co-polar (R-reference) and the cross-polar (C-cross-polar) field components can be related to the field components E_θ and E_ϕ [5]:

$$\begin{pmatrix} R \\ C \end{pmatrix} = \begin{pmatrix} \cos\phi & -\sin\phi \\ \sin\phi & \cos\phi \end{pmatrix} \begin{pmatrix} E_\theta \\ E_\phi \end{pmatrix} \qquad (2.5.1)$$

With (2.4.10) the co-polar and cross-polar fields can be expressed in E_x and E_y:

$$\begin{pmatrix} R \\ C \end{pmatrix} = \begin{pmatrix} 1 + (\frac{1}{\cos\theta} - 1)\cos^2\phi & (\frac{1}{\cos\theta} - 1)\sin\phi\cos\phi \\ (\frac{1}{\cos\theta} - 1)\sin\phi\cos\phi & 1 + (\frac{1}{\cos\theta} - 1)\sin^2\phi \end{pmatrix} \cdot \begin{pmatrix} E_x \\ E_y \end{pmatrix} \tag{2.5.2}$$

For small values of θ:

$$\frac{1}{\cos\theta} - 1 \simeq 0$$

and (2.5.2) yields around the boresight axis:

$$\begin{pmatrix} R \\ C \end{pmatrix} = \begin{pmatrix} 1 & 0 \\ 0 & 1 \end{pmatrix} \cdot \begin{pmatrix} E_x \\ E_y \end{pmatrix} \tag{2.5.3}$$

For $\theta = 0$, Eq. (2.5.3) is exact and the choise of the x-axis as a reference now becomes obvious. Hence, if the y-axis was chosen as a reference, R and C should be interchanged in (2.5.1) to (2.5.3).
The inversion of (2.5.2) yields

$$\begin{pmatrix} E_x \\ E_y \end{pmatrix} = \cos\theta \begin{pmatrix} 1 + (\frac{1}{\cos\theta} - 1)\sin^2\phi & -(\frac{1}{\cos\theta} - 1)\sin\phi\cos\phi \\ -(\frac{1}{\cos\theta} - 1)\sin\phi\cos\phi & 1 + (\frac{1}{\cos\theta} - 1)\cos^2\phi \end{pmatrix} \cdot \begin{pmatrix} R \\ C \end{pmatrix} \tag{2.5.4}$$

2.6. Field equations expressed in Fourier transforms

Using the Fourier transform pair

$$f(x,y) = \int_{-\infty}^{\infty}\int_{-\infty}^{\infty} e(\alpha,\beta)\, e^{-j\frac{2\pi}{\lambda}(\alpha x + \beta y)}\, d\tfrac{\alpha}{\lambda} d\tfrac{\beta}{\lambda} = F\{e(\alpha,\beta)\} \tag{2.6.1}$$

$$e(\alpha,\beta) = \int_{-\infty}^{\infty}\int_{-\infty}^{\infty} f(x,y)\, e^{j\frac{2\pi}{\lambda}(\alpha x + \beta y)}\, dxdy = F^{-1}\{f(x,y)\} \tag{2.6.2}$$

the far field distribution (2.3.17) for one vector component can be written as the inverse Fourier transform of the aperture distribution:

$$E_{p_{Fra}}(\alpha,\beta) = \frac{jk}{2\pi R_{Fra}}\, e^{-jkR_{Fra}} . F^{-1}\{E_{ap}(x,y)\} \tag{2.6.3}$$

with $E_{ap}(x,y) = 0$ outside the aperture.
From (2.6.3) it is apparent that Fourier transformation of the far field yields the aperture distribution:

$$E_{ap}(x,y) = -jkR_{Fra}\, e^{+jkR_{Fra}}\, F\{E_{P_{Fra}}(\alpha,\beta)\} \qquad (2.6.4)$$

However, in the above Fourier integrals the integration limits of α and β are infinite, but in practice the observed far field pattern can only be known for α and β with

$$\alpha^2 + \beta^2 = \sin^2\theta < 1.$$

For this reason it is theoretically impossible to calculate the aperture distribution from a measured far field pattern. In practice, however, Fourier integration over limited α and β with $\alpha^2 + \beta^2 << 1$, yields good results if it can be shown that the contribution of the integrand is negligible for values of α and β above the integration limits.
Similarly to (2.6.3) the Fresnel field can be calculated from

$$E_{P_{Fre}}(\alpha,\beta) = \frac{jk}{2\pi R_{Fre}}\, e^{-jkR_{Fre}}\, F^{-1}\{E_{ap}(x,y)\, e^{-jk\frac{x^2+y^2}{2R_{Fre}}}\} \qquad (2.6.5)$$

Thus the aperture field can be calculated from the Fresnel field:

$$E_{ap}(x,y) = -j\lambda R_{Fre}\, e^{jkR_{Fre}}.e^{jk\frac{x^2+y^2}{2R_{Fre}}}\, F\{E_{P_{Fre}}(\alpha,\beta)\} \qquad (2.6.6)$$

Substitution of (2.7.6) in (2.7.3) yields

$$E_{P_{Fra}}(\alpha,\beta) = \underbrace{\frac{R_{Fre}}{R_{Fra}}\, e^{jk(R_{Fre} - R_{Fra})}}_{C_1}.F^{-1}\{F\{E_{P_{Fre}}(\alpha,\beta)\, e^{jk\frac{x^2+y^2}{2R_{Fre}}}\} \qquad (2.6.7)$$

In Appendix II a two-dimensional convolution is derived from (2.6.7):

$$E_{P_{Fra}}(\alpha,\beta) = \frac{jR_{Fre}C_1}{\lambda} e^{\frac{-jkR_{Fre}}{2}(\alpha^2+\beta^2)} \int_{-\infty}^{\infty}\int_{-\infty}^{\infty} E_{P_{Fre}}(\alpha',\beta') e^{\frac{-jkR_{Fre}}{2}(\alpha'^2+\beta'^2)} .$$

$$. e^{jkR_{Fre}(\alpha\alpha'+\beta\beta')} d\alpha' d\beta' \qquad (2.6.8)$$

The last term of (2.6.8) shows that this equation is an inverse Fourier transform of the (α',β') domain to the $(\alpha R_{Fre}, \beta R_{Fre})$ domain.
Defining $s = \alpha . R_{Fre}$

$t = \beta R_{Fre}$ and $C_2 = jR_{Fre} C_1/\lambda$

(2.6.8) can be formulated as a Fourier transform:

$$E_{P_{Fra}}(\alpha,\beta) = \frac{C_2}{R_{Fre}^2} e^{\frac{-jkR_{Fre}}{2}} F^{-1}\{E_{P_{Fre}}(\frac{s}{R_{Fre}}, \frac{t}{R_{Fre}}) e^{-jkR_{Fre}(s^2+t^2)}\} \qquad (2.6.9)$$

Instead of using a two-dimensional convolution, the far field can be calculated from the measured Fresnel field with the help of an inverse two-dimensional Fourier transform. Again, it must be stated that Fourier integration may be limited to certain maximum angles α and β if the contribution of the field beyond these angles is negligible.

2.7. An upper limit to the angle from boresight θ

In the previous sections it was stated that θ must be small in order that the aperture field method should yield good results.
Approximation of the phase factor exp(jkr) leads to a truncation of a binomial (alternating) series with a maximum error of (2.2.7)

$$|\Delta r_1| = \frac{r^2}{8R^3} (r - 2R(\bar{e}_r . \bar{e}_R))^2$$

Here we state

$$|\Delta r_1| < \lambda/128 \qquad (2.7.1)$$

as a reasonable criterion, because errors involved in phase measurements

are of the same order.

$$\left|\frac{r^2}{2R}\left(\frac{r}{2R} - (\bar{e}_r.\bar{e}_R)\right)^2\right| < \frac{\lambda}{128}$$

$$\left|\frac{r}{2R} - (\bar{e}_r.\bar{e}_R)\right| < \sqrt{\frac{\lambda R}{64r^2}}$$

$$|\bar{e}_r.\bar{e}_R| < \sqrt{\frac{\lambda R}{64r^2}} - \frac{r}{2R} \qquad (2.7.2)$$

Since $\bar{e}_r.\bar{e}_R = \sin\theta\cos(\xi-\phi)$ an upper limit for $|\sin\theta|$ is found from (2.7.2)

$$|\sin\theta| < \sqrt{\frac{\lambda R}{64r^2}} - \frac{r}{2R} \qquad (2.7.3)$$

The minimum of the right-hand term of (2.6.3) is found for $r = \frac{D}{2}$. So

$$|\sin\theta| < \sqrt{\frac{\lambda R}{16D^2}} - \frac{D}{4R} \qquad (2.7.4)$$

If we define m as a ratio between R_{Fre} and the usual far field criterion $2D^2/\lambda$, equation (2.7.4) leads to

$$|\sin\theta| < \sqrt{\frac{1}{8m}} - \frac{m}{8}\left(\frac{\lambda}{D}\right) \qquad (2.7.5)$$

$$m = \frac{2D^2}{\lambda R_{Fre}} \qquad (2.7.6)$$

In the far field the term $r^2/2R_{Fra}$ is neglected; thus the far field criterion states a mimimum distance R_{far} giving a maximum phase contribution for the neglected term of:

$$k.\frac{r^2}{2R_{far}}\Big|_{max} = \frac{kD^2}{8R_{far}} = \frac{kD^2}{8}.\left(\frac{\lambda}{2D^2}\right) = \frac{\pi}{8} \qquad (2.7.7)$$

with

$$R_{Fra} > R_{far} = \frac{2D^2}{\lambda} \qquad (2.7.8)$$

2.8. A lower limit to angle θ and an estimation of the errors introduced by truncating the angle of measurement

In order to apply the field equations of section 6, the Fresnel field can only be recorded for angles θ satisfying Eq. (2.7.5). If the measurement of the Fresnel field is truncated at some angle $\hat{\theta}$, errors will occur in the aperture field which has been reconstructed from the recorded data.
From the point of view of measurement and data processing the angle $\hat{\theta}$ should be kept as small as possible, while the field transforms (2.6.6) and (2.6.9) still yield accurate results. In order to find a lower limit for $\hat{\theta}$, the errors involved in the use of field transforms with truncated integration limits, have to be calculated.
It is convenient here to investigate only the one-dimensional case since in the two-dimensional case the calculations become rather laborious without yielding any fundamental new insight [6].
Truncation of the Fresnel field measurements to

$$-\frac{\hat{\alpha}}{2} \leqslant \alpha \leqslant \frac{\hat{\alpha}}{2} \tag{2.8.1}$$

yields a measured Fresnel field:

$$\tilde{E}_{Fre}(\alpha) = E_{Fre}(\alpha)\ P_{\hat{\alpha}}(\alpha) \tag{2.8.2}$$

with

$$\begin{aligned} P_{\hat{\alpha}}(\alpha) &= 1 \text{ for } |\alpha| < \frac{\hat{\alpha}}{2} \\ P_{\hat{\alpha}}(\alpha) &= \tfrac{1}{2} \text{ for } |\alpha| = \frac{\hat{\alpha}}{2} \\ P_{\hat{\alpha}}(\alpha) &= 0 \text{ for } |\alpha| > \frac{\hat{\alpha}}{2} \end{aligned} \tag{2.8.3}$$

Application of (2.6.6) in the one-dimensional case yields

$$\tilde{E}_{ap}(x) = C.e^{\frac{jkx^2}{2R_{Fre}}} \int_{-\infty}^{\infty} E_{Fre}(\alpha)\, P_{\hat{\alpha}}(\alpha)\, e^{+jk\alpha x}\, \frac{d\alpha}{\lambda} \tag{2.8.4}$$

With

$$F^{-1}\{P_{\hat{\alpha}}(\alpha)\} = \frac{\hat{\alpha}}{\lambda} \cdot \frac{\sin(\frac{\pi\hat{\alpha}}{\lambda} x)}{(\frac{\pi\hat{\alpha}}{\lambda})} \tag{2.8.5}$$

and (2.6.5), a one-dimensional convolution yields:

$$\tilde{E}_{ap}(x) = e^{\frac{jkx^2}{2R_{Fre}}} [E_{ap}(x)\ e^{\frac{-jkx^2}{2R_{Fre}}} * \frac{\hat{\alpha}}{\lambda} \operatorname{sinc}\ (\frac{\pi\hat{\alpha}x}{\lambda})] \tag{2.8.6}$$

For very large values of $\hat{\alpha}$, (2.8.5) approaches a δ-function and (2.8.6) yields the exact aperture distribution.

For small values of $\hat{\alpha}$, equation (2.8.6) cannot be evaluated analytically (because of the quadratic phase factor); hence computer calculations should be performed for various values of $\hat{\alpha}$, R_{Fre} and $E_{ap}(x)$ in order to find a lower limit for $\hat{\alpha}$ yielding enough information to reconstruct $E_{ap}(x)$ accurately (see the next chapter for a computer reconstruction).

Here we are mainly interested in an analytic expression for the lower limit of $\hat{\alpha}$, which can be obtained from the transform of the Fresnel field into the far field. Calculation of the aperture field from the truncated far field then yields an expression for the minimum number of side lobes which are necessary to calculate an accurate aperture field.

Assuming that the truncated far field was obtained exactly, a lower bound of $\hat{\alpha}$, yielding an accurate aperture field, can be given.

With (2.6.8), the far field can be calculated from the truncated Fresnel field [7].

$$\tilde{E}_{P_{Fra}}(\alpha) = C \int_{-\infty}^{\infty} E_{P_{Fre}}(\alpha')\ P_{\hat{\alpha}}(\alpha')\ e^{\frac{-j\pi R_{Fre}}{\lambda}(\alpha'-\alpha)^2}\ d\alpha' \tag{2.8.7}$$

Substitution of (2.6.5) yields

$$\tilde{E}_{P_{Fra}}(\alpha) = C' \int_{-\infty}^{\infty}\int_{-\infty}^{\infty} E_{ap}(x)\ .e^{\frac{-jkx^2}{2R_{Fre}} + j2\pi\frac{\alpha'}{\lambda}x}\ dx.P_{\hat{\alpha}}(\alpha')e^{\frac{-j\pi R_{Fre}}{\lambda}(\alpha'-\alpha)^2}\ d\alpha' \tag{2.8.8}$$

where C and C' are important factors.

Because

$$\exp[-jk\frac{x^2}{2R_{Fre}} - jk\frac{R_{Fre}}{2}(\alpha-\alpha')^2]\ \exp[jk\alpha' x] =$$

$$\exp[-j\frac{k}{2}R_{Fre}(\alpha'-\alpha-\frac{x}{R_{Fre}})^2]\ \exp[jk\alpha x]$$

equation (2.8.8) can be formulated as

$$\tilde{E}_{P_{Fra}}(\alpha) = C'\int_{-\infty}^{\infty} E_{ap}(x)\ e^{jk\alpha x}\,dx \int_{-\infty}^{\infty} P_{\hat{\alpha}}(\alpha')\exp[-j\frac{k}{2}R_{Fre}(\alpha'-\alpha-\frac{x}{R_{Fra}})^2]d\alpha' \qquad (2.8.9)$$

and with definition of

$$B_{\hat{\alpha}}(\alpha) = \int_{-\infty}^{\infty} P_{\hat{\alpha}}(\alpha')\ \exp[-j\frac{k}{2}R_{Fre}(\alpha-\alpha')^2]d\alpha' \qquad (2.8.10)$$

the Fraunhofer field yields

$$\tilde{E}_{P_{Fra}}(\alpha) = C'\int_{-\infty}^{\infty} E_{ap}(x)\ B_{\hat{\alpha}}(\alpha+\frac{x}{R_{Fra}})\ e^{jk\alpha x}\,dx \qquad (2.8.11)$$

With the well-known Fresnel integrals [8]

$$C(x) = -C(-x) = \sqrt{\frac{2}{\pi}}\int_0^x \cos t^2\,dt$$

$$S(x) = -S(-x) = \sqrt{\frac{2}{\pi}}\int_0^x \sin t^2\,dt \qquad (2.8.12)$$

formula (2.8.10) can be calculated:

$$B_{\hat{\alpha}}(\alpha) = \sqrt{\frac{\lambda}{2R_{Fre}}}\,[\{C(\sqrt{\frac{\pi R_{Fre}}{\lambda}}(\frac{\hat{\alpha}}{2}+\alpha)) + C(\sqrt{\frac{\pi R_{Fre}}{\lambda}}(\frac{\hat{\alpha}}{2}-\alpha))\} +$$

$$-j\{S(\sqrt{\frac{\pi R}{\lambda}}(\frac{\hat{\alpha}}{2}+\alpha)) + S(\sqrt{\frac{\pi R}{\lambda}}(\frac{\hat{\alpha}}{2}-\alpha))\}] \qquad (2.8.13)$$

Assuming that

$$\alpha^2 . R_{Fre} >> \lambda \qquad (2.8.14)$$

then $B_{\hat{\alpha}}(\alpha)$ is nearly constant if $|\alpha| \leq \frac{\hat{\alpha}}{2}$.
Hence $B_{\hat{\alpha}}(\alpha+\frac{x}{R}) \tilde{=}$ constant if

$$|\alpha| \leq (\frac{1}{2}\hat{\alpha} - \frac{D}{R_{Fre}}) \qquad (2.8.15)$$

and with asymptotic expansion of the Fresnel integrals:

$$B_{\hat{\alpha}}(\alpha + \frac{x}{R}) \simeq (1-j)\sqrt{\frac{\lambda}{\pi R_{Fre}}} - \frac{j\lambda}{2\pi R_{Fre}}\left\{\frac{\exp(-j\pi\frac{R_{Fre}}{\lambda}A^2)}{A} + \frac{\exp(-j\pi\frac{R_{Fre}}{\lambda}B^2)}{B}\right\} \tag{2.8.16}$$

with

$$A = \alpha' + \frac{\hat{\alpha}}{2} + \frac{x}{R_{Fre}}$$

$$B = \alpha' - \frac{\hat{\alpha}}{2} - \frac{x}{R_{Fre}}$$

Using the fact that

$$\frac{1}{A} \simeq \frac{1}{B} \simeq \frac{1}{\hat{\alpha}}$$

substitution of (2.8.16) in (2.8.11) yields

$$\tilde{E}_{Fra}(\alpha) = E_{Fra}(\alpha) + \frac{1+j}{\sqrt{\pi}}\sqrt{\frac{\lambda}{R_{Fre}\hat{\alpha}^2}}\left[E_{P_{Fre}}(-\frac{\hat{\alpha}}{2})\exp\{\frac{-j\pi R}{\lambda}(\alpha + \frac{\hat{\alpha}}{2})^2\}\right.$$

$$\left. + E_{P_{Fre}}(\frac{\hat{\alpha}}{2})\exp\{\frac{j\pi R}{\lambda}(\frac{\hat{\alpha}}{2} - \alpha)^2\}\right] \tag{2.8.17}$$

From (2.8.17) it may be seen that the error in pattern reconstruction may be small because of condition (2.8.14). Therefore in order to reconstruct the pattern in the interval $[-\frac{\hat{\alpha}f}{2}, \frac{\hat{\alpha}f}{2}]$ it is necessary to know the Fresnel field in the interval $[-\frac{\hat{\alpha}}{2}, \frac{\hat{\alpha}}{2}]$ with

$$\frac{\hat{\alpha}}{2} \geq \frac{\hat{\alpha}f}{2} + \frac{D}{2R} \tag{2.8.18}$$

or with $\hat{\alpha}_f = M(\frac{\lambda}{D})$, $\frac{M}{2}$ being the approximate number of sidelobes and (2.7.6):

$$\hat{\alpha} > \frac{\lambda}{D}(M + \frac{m}{2}) \tag{2.8.19}$$

The upper limit of $\hat{\alpha}$ or $\sin\theta$ from equation (2.7.5) then gives

$$\sqrt{\frac{1}{m}} - m\left(\frac{\lambda}{D}\right) \geq \frac{\lambda}{D}\left(M + \frac{m}{2}\right) \tag{2.8.20}$$

The solution of this equation yields [6]:

$$m \leq \frac{1}{2}.\left(\frac{8D}{5\lambda}\right)^{2/3} - \frac{4}{15}M \tag{2.8.21}$$

and the minimum value of R_{Fre} is then:

$$R_{Fre} \geq \left(\frac{2D^2}{\lambda}\right) . \frac{1}{\frac{1}{2}\left(\frac{8D}{5\lambda}\right)^{2/3} - \frac{4}{15}M} = \frac{2D^2}{\lambda} . \frac{1}{m_{max}} \tag{2.8.22}$$

In order to find a lower limit for $\hat{\alpha}$, the minimum number of side lobes M /2 yielding an accurate aperture field, has to be calculated using (2.8.6), keeping in mind that the quadratic phase term is negligible in reconstructions from the far field

$$\tilde{E}_{ap}(x) = E_{ap}(x) * \frac{\hat{\alpha}}{\lambda} \operatorname{sinc}\left(\frac{\hat{\alpha}.x.\pi}{\lambda}\right) \tag{2.8.23}$$

For a uniform aperture distribution

$$E_{ap}(x) = \begin{cases} 1 & |x| < \frac{D}{2} \\ \frac{1}{2} & |x| = D/2 \\ 0 & |x| > D/2 \end{cases} \tag{2.8.24}$$

The reconstructed field is given by

$$\tilde{E}_{ap}(x) = \frac{1}{\pi}\left[Si\left\{\frac{\pi\hat{\alpha}}{\lambda}\left(\frac{D}{2} + x\right)\right\} + Si\left\{\frac{\pi\hat{\alpha}}{\lambda}\left(\frac{D}{2} - x\right)\right\}\right] \tag{2.8.25}$$

with

$$Si(y) = \int_0^y \frac{\sin x}{x}\, dx \tag{2.8.26}$$

Starting from a tapered aperture field

$$E'_{ap}(x) = (1 - ax^2).E_{ap}(x) \tag{2.8.27}$$

where $E_{ap}(x)$ is given by (2.8.24), the reconstructed field is:

$$\tilde{E}'_{ap}(x) = (1 - ax^2).\tilde{E}_{ap}(x) + R(x,\hat{\alpha},a) \qquad (2.8.28)$$

where

$$R(x,\hat{\alpha},a) = \frac{2a\lambda^2}{\pi^3\hat{\alpha}^2}\{(\sin\beta\,\frac{D}{2} - \beta\frac{D}{2}\cos\beta\frac{D}{2})\cos\beta x - \beta x\sin\beta\frac{D}{2}\sin\beta x\} \qquad (2.8.29)$$

with $\beta = \frac{\pi\hat{\alpha}}{\lambda}$

and where $\tilde{E}_{ap}(x)$ is given by Eq. (2.8.25).

Putting $\hat{\alpha} = M(\frac{\lambda}{D})$, then M/2 is the approximate number of sidelobes and (2.8.28) becomes:

$$\tilde{E}'_{ap}(x) = (1 - ax^2).\frac{1}{\pi}\,[Si\{\frac{M\pi}{D}(\frac{D}{2} + x)\} + Si\{\frac{M\pi}{D}(\frac{D}{2} - x)\}]$$

$$+ \frac{2aD^2}{M^2\pi^3}\{(\sin\frac{M\pi}{2} - \frac{M\pi}{2}\cos\frac{M\pi}{2})\cos\frac{M\pi x}{D} - \frac{M\pi x}{D}\sin\frac{M\pi}{2}\sin\frac{M\pi x}{D}\} \qquad (2.8.30)$$

Substitution of $x = yD$ and

$$a = (1 - c).\frac{4}{D^2}$$

yields:

$$\tilde{E}'_{ap}(yD) = (1 - 4(1-c)y^2\,\frac{1}{\pi}\,[Si\{M\pi(y + \frac{1}{2})\} + Si\{M\pi(\frac{1}{2}-y)\}]$$

$$+ \frac{8(1 - c)}{M^2.\pi^3}\{\sin\frac{M\pi}{2} - \frac{M\pi}{2}\cos\frac{M\pi}{2})\cos M\pi y - M\pi y\,\sin\frac{M\pi}{2}\sin M\,\pi y\} \qquad (2.8.31)$$

Hence $\tilde{E}'_{ap}(yD)$ is only dependent on the edge illumination c and the number of sidelobes M/2. Numerical evaluation of (2.8.31) shows a small oscillatory error in the reconstructed field and a large overshoot of about 9% at the edge known as the Gibbs effect (Fig. 2.8.1 - 2.8.4).

This overschoot always appears when reconstructing a discontinuous distribution like (2.8.24) or (2.8.26) from their truncated spectra.

Apart from this unevitable overshoot at the edge, the aperture distribution can be reconstructed accurately (Table 2.8.1 and 2.8.2).

A maximum relative error of 3% within 90% of the aperture yields $M_\varepsilon = 60$ for uniform illumination as can be seen from Table (2.8.1).
The overshoot at the edge yields large relative errors, but it is of minor importance when calculating the far field from this distribution if the edge is weakly illuminated. This is due to the fact that in that case the contribution of the field at the edge to the far field is small. Since the far field is calculated by performing (Fourier) integration over the aperture and the fact that errors in reconstructing the aperture field are oscillatory, the first lobes of the far field can be calculated accurately for small values of M. (In fact, here the true far field truncated to M/2 lobes yields the calculated aperture field!).

Figures (2.8.1) to (2.8.2) give some insight into the behaviour of the reconstructed aperture field distribution for various values of M assuming F(x) is uniform. Note that the amplitude of the error $\tilde{F}(x)-F(x)$ becomes smaller for larger values of M, and that the point of maximum overshoot shifts to y = 0.5 for larger values of M.
In figures (2.8.3) to (2.8.4) the reconstructed field in the case of a 15 dB tapered aperture field (2.8.27) is given for M = 20 and M = 60 respectively.

Numerical calculations show a maximum overshoot of 9.5% for the uniformly illuminated aperture and a somewhat larger overshoot of 11.5% in the tapered case (M = 20) due to the error term (2.8.29).

Finally it can be concluded that the Fresnel field for M = 6 yields enough information to calculate a few sidelobes of the far field, but that for calculating an accurate aperture field the value of M should be approximately 60.

Table 2.8.1 Absolute relative error ε, for uniform aperture illumination

$$\varepsilon = \left|\frac{\tilde{F}(x) - F(x)}{F(x)}\right| = 100$$

$F(x) = F(y\frac{D}{2}) = 1$

y \ M	20	40	60	80	100	120
$0 < y < 0.3$	2.4%	1.6	0.9	0.7	0.5	0.4
0.3 - 0.35	4.2	2.0	1.1	0.8	0.8	0.5
0.35 - 0.40	5.4	2.8	1.3	1.0	1.1	0.7
0.40 - 0.45	7.8	2.9	2.2	2.7	1.6	1.2
0.45 - 0.46	9.5	5.2	3.5	2.6	2.1	1.8
0.46 - 0.47	7.1*	6.4	3.4	2.8	2.7	1.6
0.47 - 0.48	13.5	7.4*	4.0	1.8	3.4	0.7
0.48 - 0.49	31	13.5	7.4*	7.0	5.0	1.8
0.49 - 0.50	--	--	--	--*	--*	--*

* Denotes the interval with maximum overshoot.

Table 2.8.2. Absolute relative error ε, for -15 dB tapered illumination

$F(x) = 1 - ax^2$

$F(x) = F(y\frac{D}{2}) = 1 - ax^2$; $a = 0.822$

y \ M	20	40	60	80	100	120
0 - 0.3	4.7 %	2.4	1.6	1.2	1.1	0.5
0.3 - 0.35	6.7	2.8	2.2	1.7	1.3	0.9
0.35 - 0.40	7.1	3.4	3.1	2.3	1.9	1
0.40 - 0.45	14	5.5	4.4	2.6	2.7	1.6
0.45 - 0.46	11.5*	7.3	5.1	3.9	3.1	2.6
0.46 - 0.47	7	5*	5.4	3.9	3.7	2.4
0.47 - 0.48	15.7	9.9	7.2*	1.8	4.6	1.5
0.48 - 0.49	38	9.7	5.6	5.7*	6.4	8.3
0.49 - 0.50	20	15	--	--	--*	--

Note: Since calculations were performed with y-steps of 0.01, some of the given percentages are averages for the given interval.

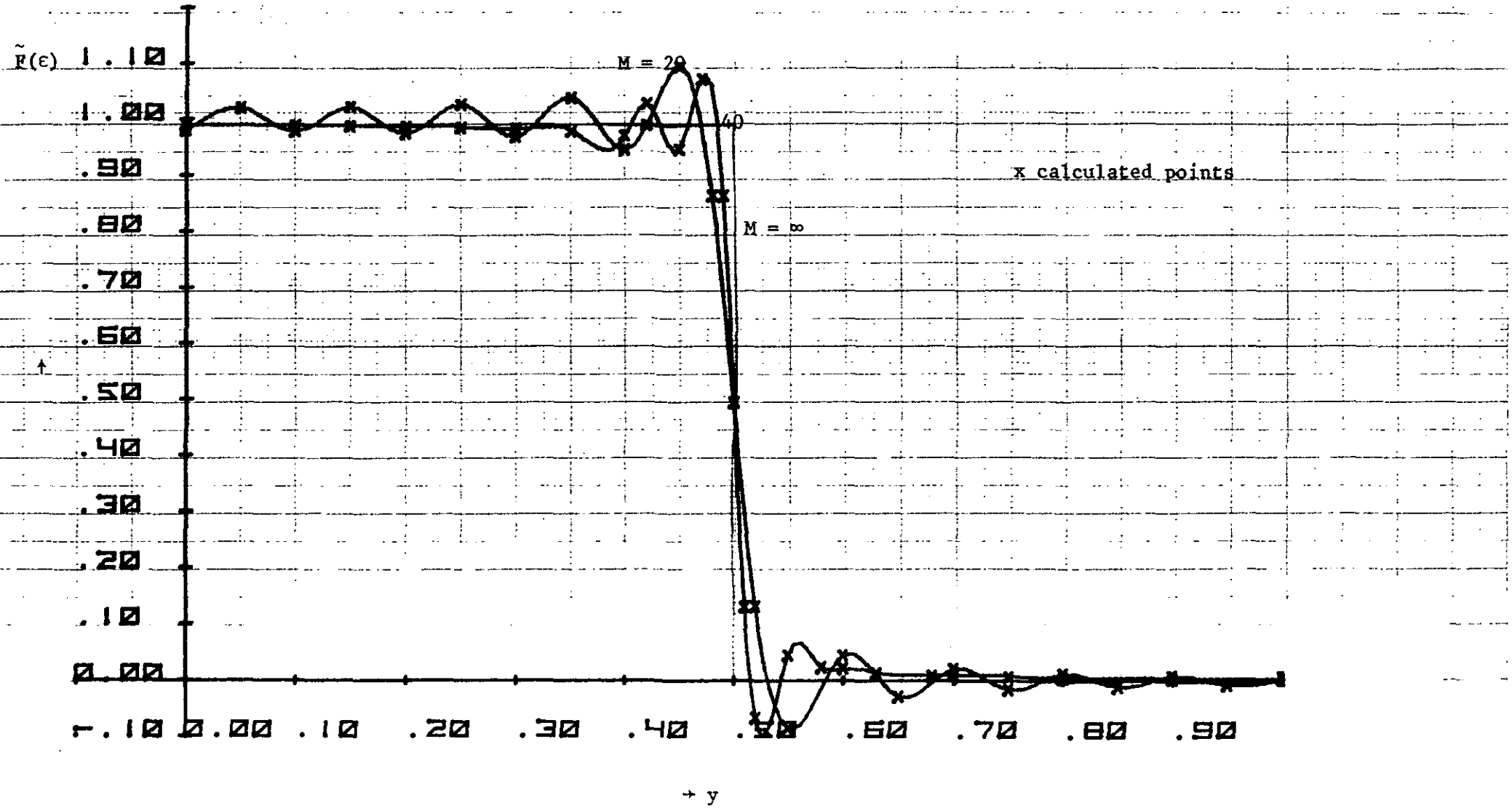
$\tilde{F}(\epsilon)$
1.10
1.00
.90
.80
.70
.60
.50
.40
.30
.20
.10
0.00
M = 20
40
M = ∞
x calculated points
-.10
0.00
.10
.20
.30
.40
.50
.60
.70
.80
.90
y

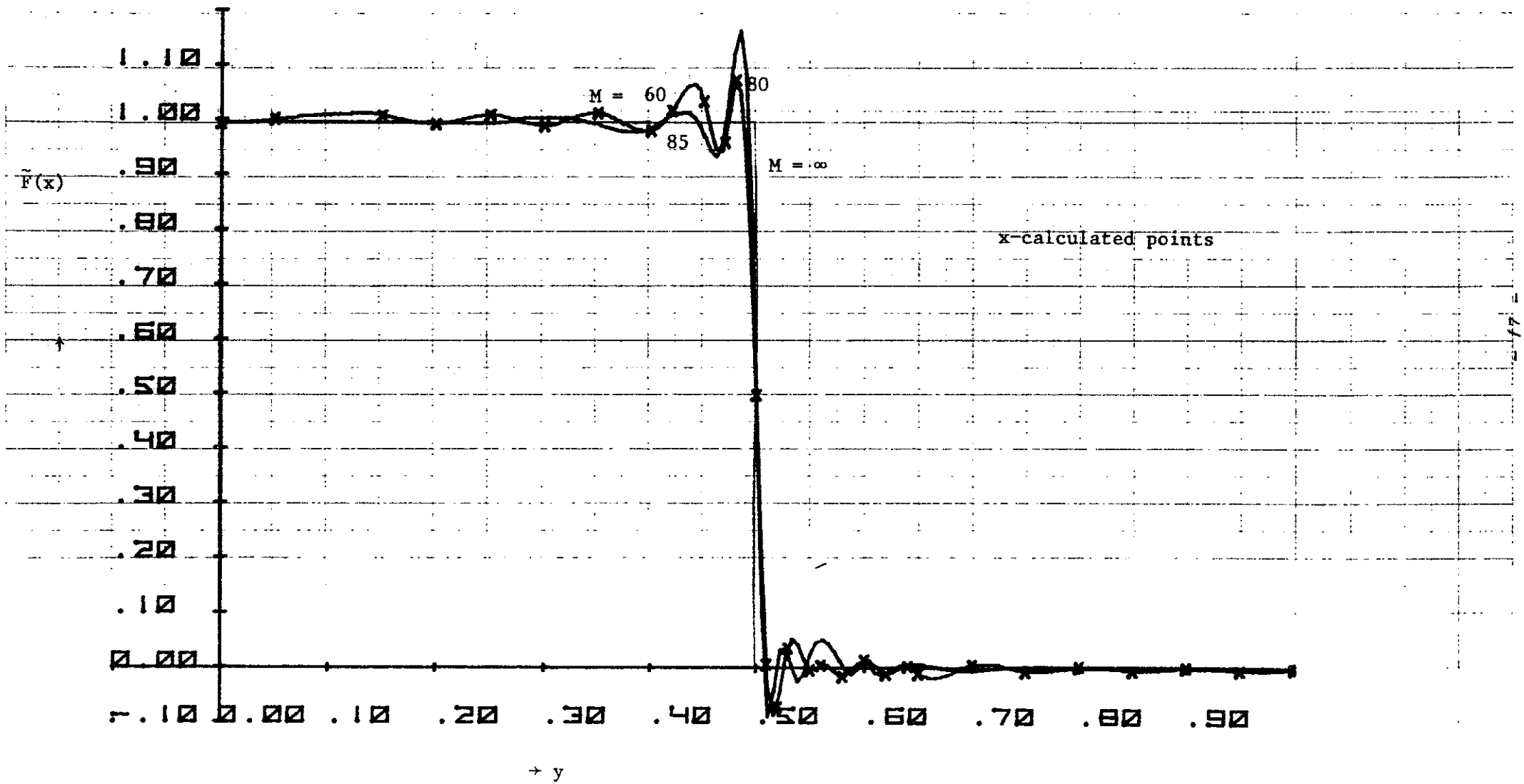

Fig. 2.8.2. Reconstructed aperture field in case of a uniformly illiminated aperture (eq. (2.8.23))

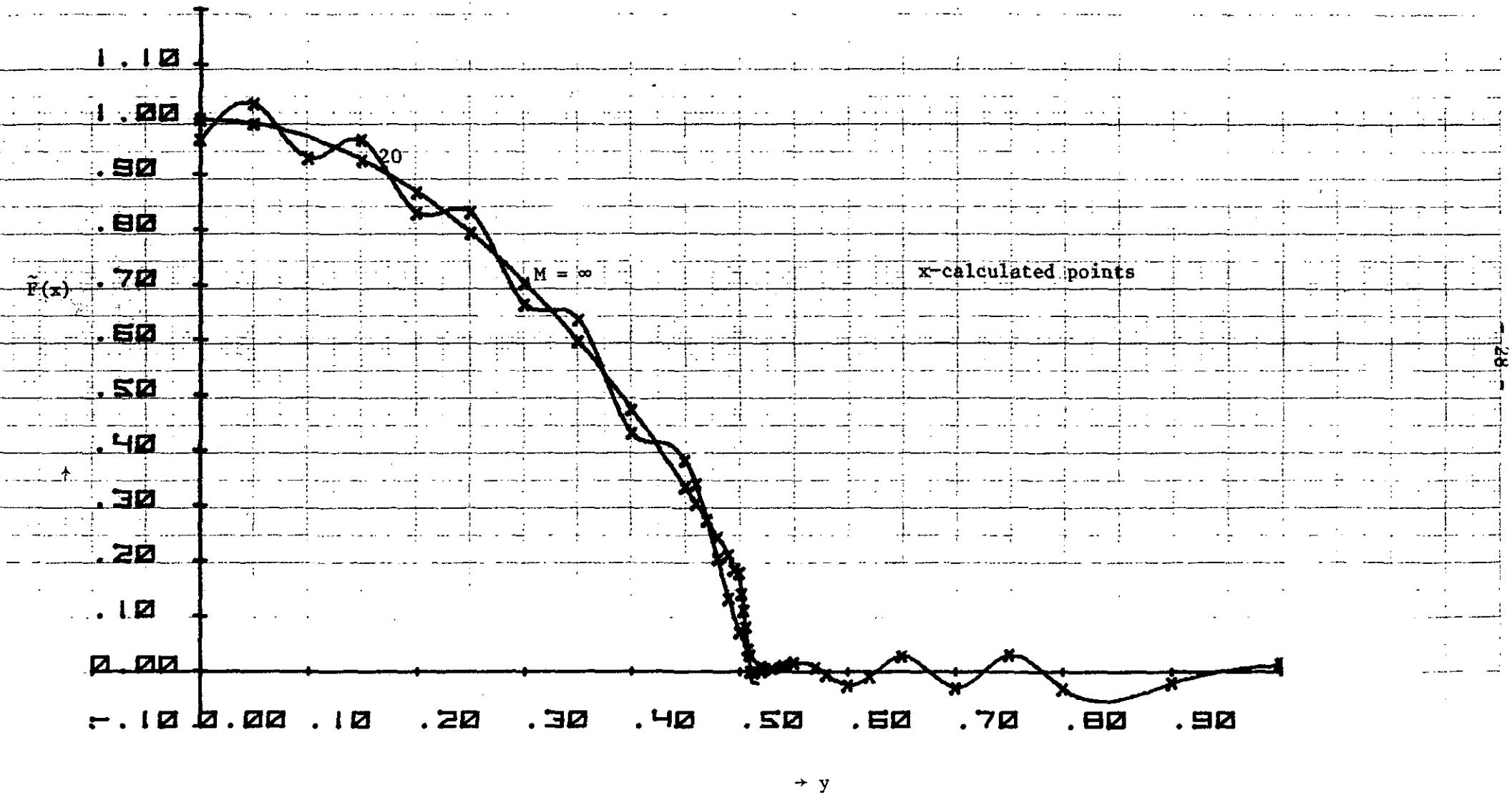

...n field in case of a "5 d3 tapered illumination (eq. (2.8.28))

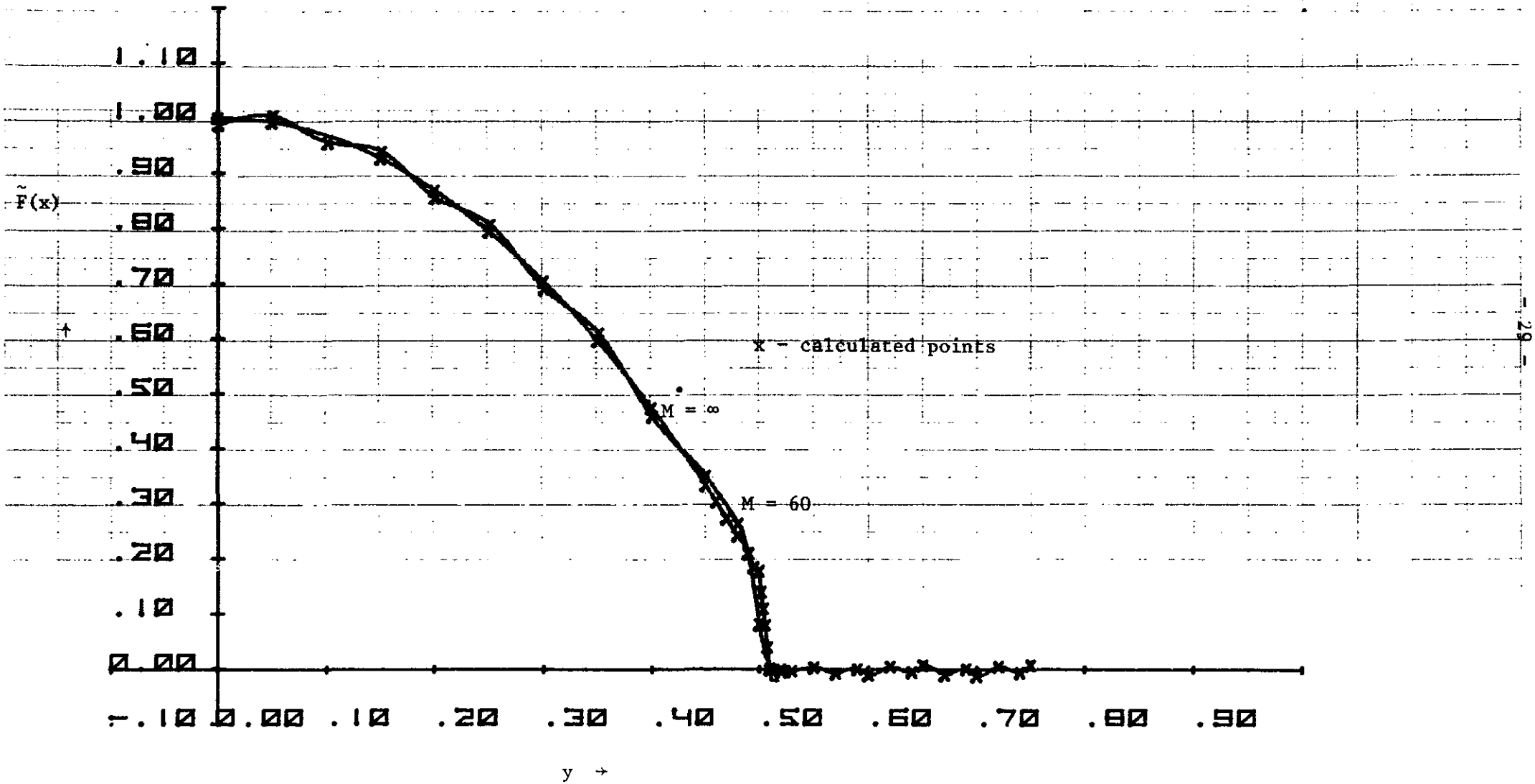

Fig. 2.8.4. Reconstructed aperture field in case of a 15 dB tapered illumination (eq. (2.8.28))

2.9. A lower limit to R_{Fre}

Since a given maximum truncation error in exp(jkr) yields a maximum value of θ for a particular value of R_{Fre}, a truncation error of

$$|\Delta r_1| < \frac{\lambda}{16\gamma} \tag{2.9.1}$$

where $\gamma > 1.0$ yields a more general result than (2.7.1)(where $\gamma = 8$). Then (2.7.5) changes into

$$|\sin\theta| < \sqrt{\frac{1}{m.\gamma}} - \frac{m}{8}\left(\frac{\lambda}{D}\right) \tag{2.9.2}$$

Figure (2.9.1) gives some idea of θ_{max} for various m and γ. Then (2.8.22) yields

$$R_{Fre} > \left(\frac{2D^2}{\lambda}\right) \cdot \frac{1}{\left(\frac{8}{5}\frac{D}{\lambda}\right)^{2/3} \cdot \frac{1}{\sqrt[3]{\gamma}} - \frac{4}{15}M} \tag{2.9.3}$$

For values of $\lambda/D > 100$ this equation can be approximated by

$$R_{Fre} > \lambda \left[\frac{2}{\left(\frac{8}{5\sqrt[3]{\gamma}}\right)^{2/3}} \cdot \left(\frac{D}{\lambda}\right)^{4/3} + \gamma\frac{M^2}{18}\right]$$

or

$$R_{Fre} > 1{,}7\ \sqrt[3]{\gamma} \cdot D \cdot \sqrt[3]{\frac{D}{\lambda}} + \gamma\frac{M^2}{18}.\lambda \tag{2.9.4}$$

(Figures 2.9.2 to 2.9.4).
Since $(D/\lambda)^{1/3}$ varies slowly if (D/λ) varies from 150 to 500, which is an interesting range here, a rule of thumb for R_{Fre} can be derived from (2.9.4)

$$\begin{aligned} R_{Fre} &> 20\ D + \frac{8M^2}{18}\lambda \quad ; \gamma = 8 \\ R_{Fre} &> 10\ D + \frac{M^2}{18}\lambda \quad ; \gamma = 1 \end{aligned} \tag{2.9.5}$$

Equations (2.9.5) would hold if they were derived for the aperture field method; however, the aperture field method derived from the more accurate physical optics method requires some terms containing ρ/R neglected.

$\gamma = 1$

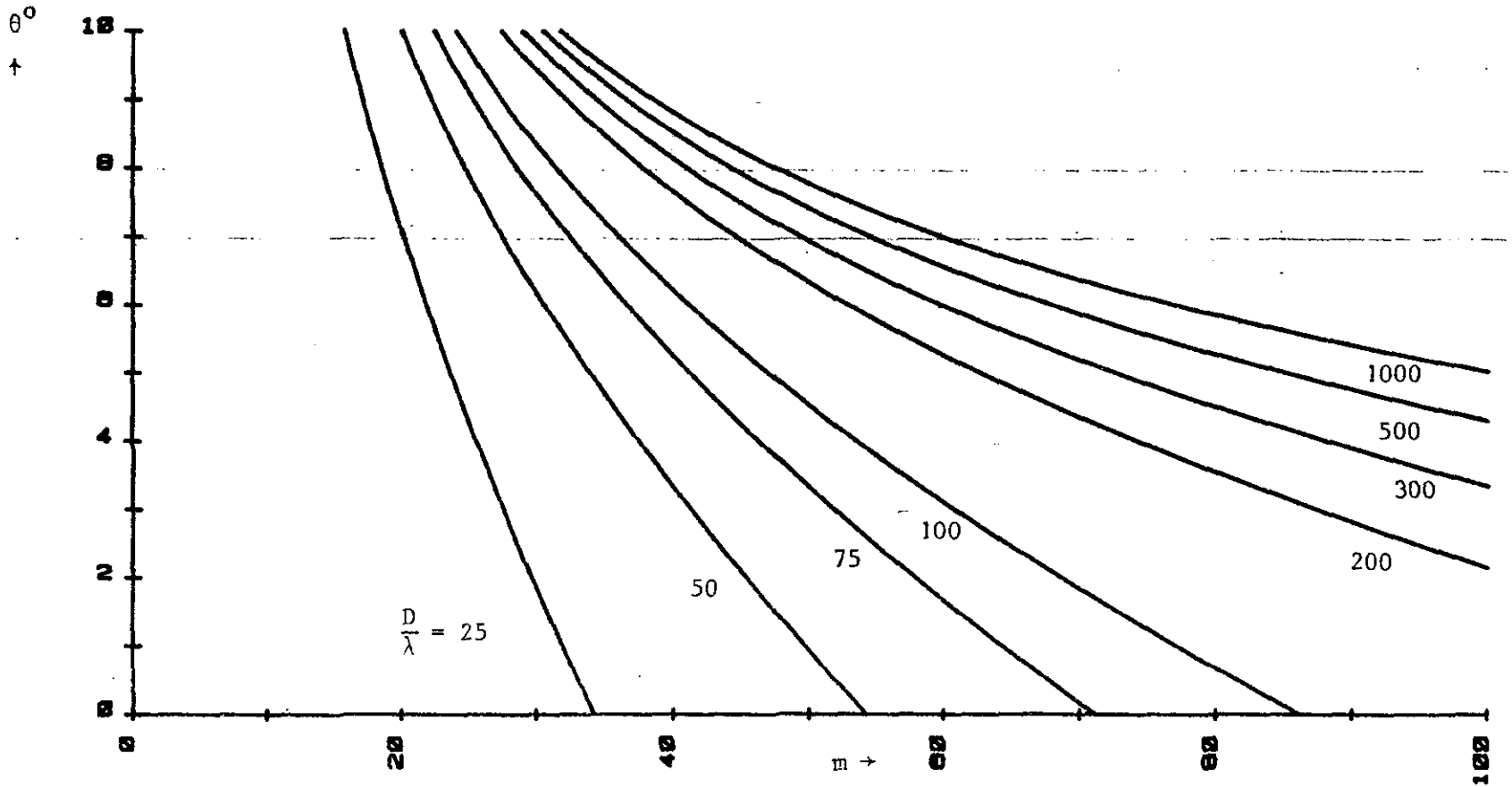

Fig. 2.9.1. An upper limit to θ as function of the number of reductions m

$\gamma = 8$

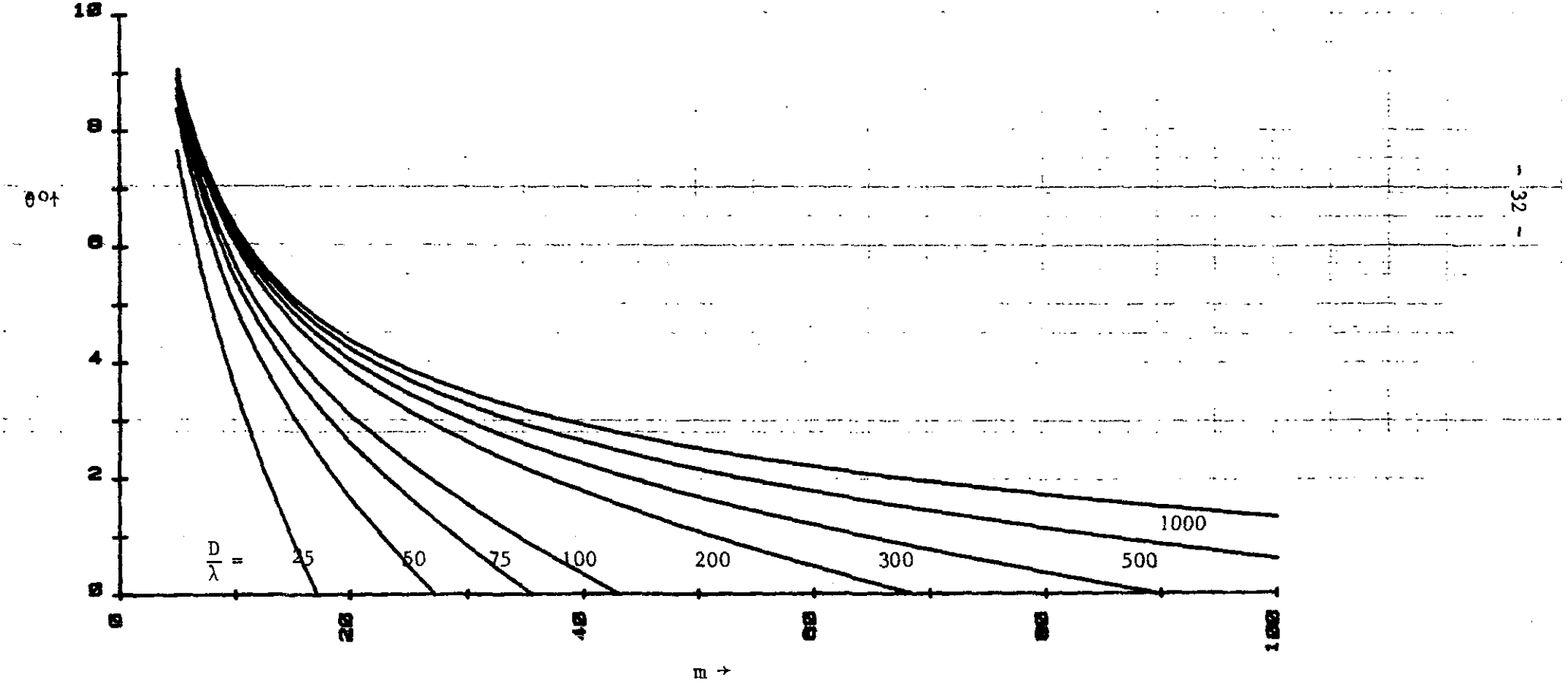

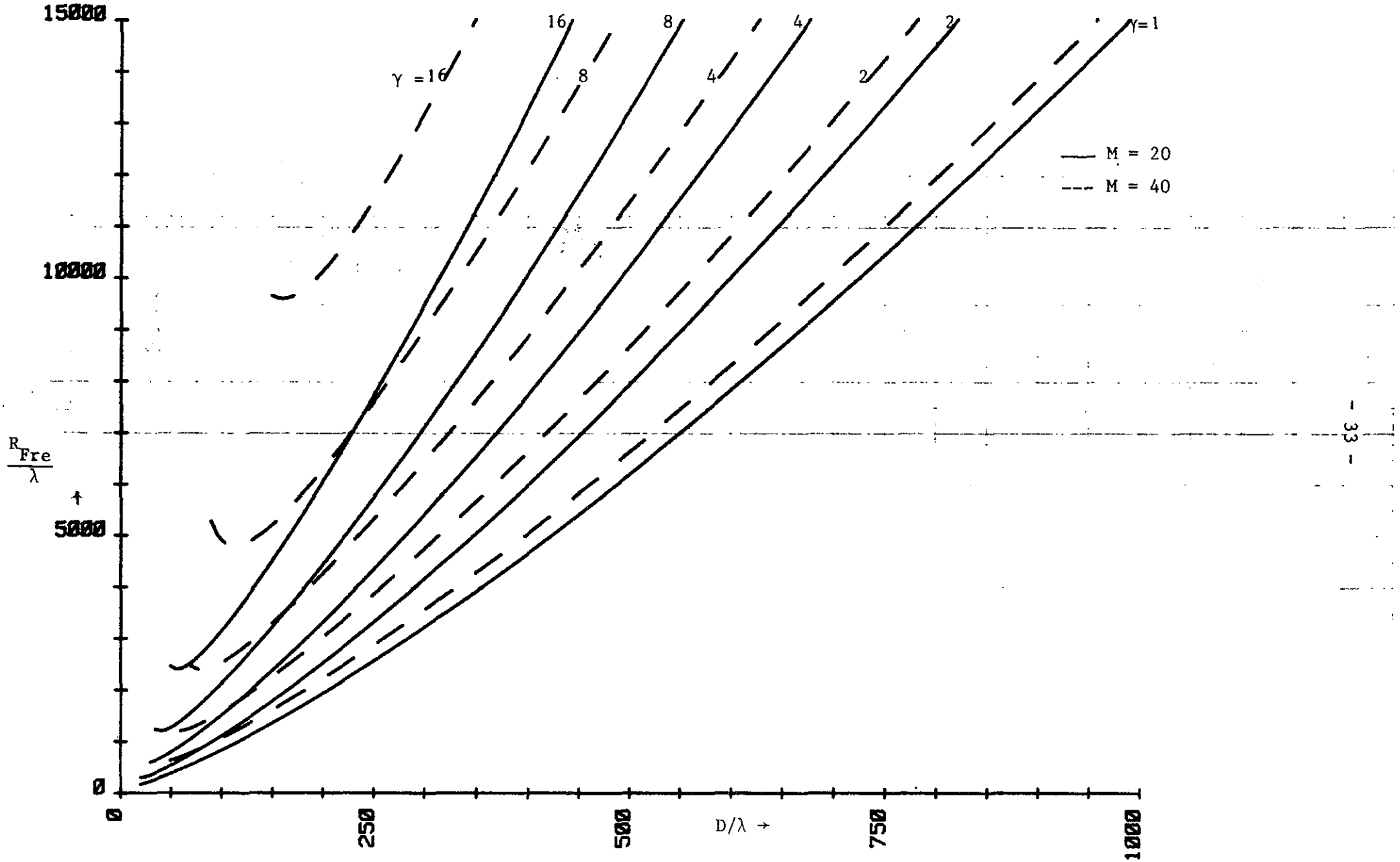

Fig. 2.9.3. Minimum of $R_{Fre/\lambda}$ as a function of D/λ, with M and γ as parameters

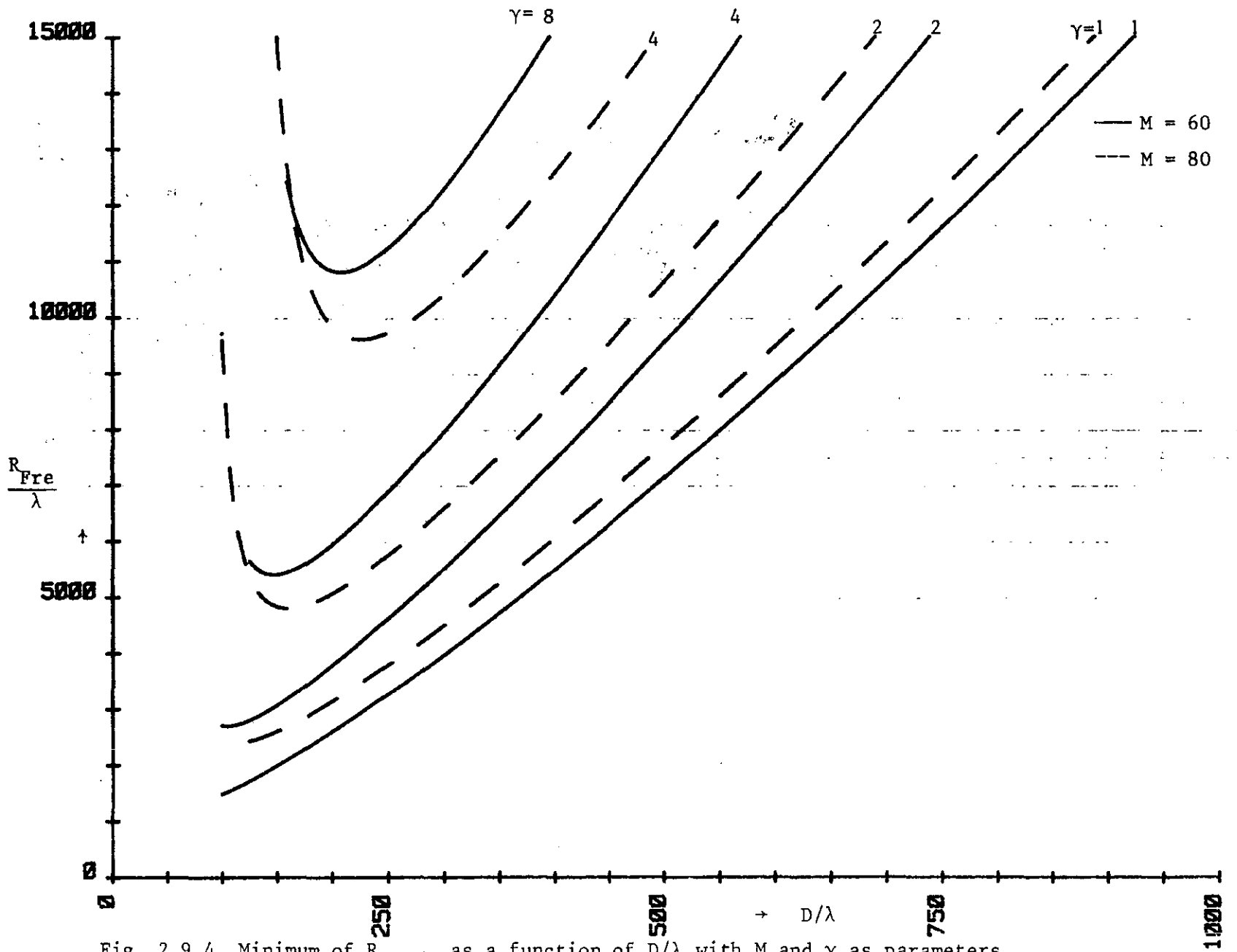

Fig. 2.9.4. Minimum of $R_{Fre/\lambda}$ as a function of D/λ with M and γ as parameters

From (2.3.7)

$$\left|\frac{\rho}{R_{Fre}}(\bar{J}.\bar{e}_R).\bar{e}_\rho\right| << \left|\bar{J} - (\bar{J}.\bar{e}_R)\bar{e}_R\right| \qquad (2.9.6)$$

and from appendix I, for small θ and small ρ/R:

$$A(\theta) \sim 0 \qquad (2.9.7)$$

which leads to the Fresnel integral (2.3.16).

Hence, if R_{Fre} = 10 D, maximum errors of about 5% are introduced in the integrand of the Fresnel field equation (2.3.10), as can readily be seen from (2.9.6). Also, because θ_{min} is generally smaller for smaller values of m (Eq. 2.8.19), (2.9.7) will be satisfied better for larger values of R_{Fre}, hence

$$R_{Fre} > 20\ D$$

will give better results.

2.10. Calculation of the antenna gain from the reconstructed aperture field

If only one aperture polarisation is considered (x-polarised), the gain function is given by Silver [2]:

$$g_x(\alpha,\beta) = \frac{4\pi}{\lambda^2}\frac{\left|\int_A E_x(x,y)\ e^{jk(\alpha x + \beta y)}\ dxdy\right|^2}{\int_A |E_x(x,y)|^2\ dxdy} \qquad (2.10.1)$$

Taking cross-polarisation into account, the power per unit solid angle in the far field is given by

$$P_{tot} = P_x + P_y = \frac{1}{2}\left(\frac{\varepsilon}{\mu}\right)^{1/2} R_{Fra}^2 \left\{\left|\int_A E_x(x,y)\ e^{jk(\alpha x + \beta y)}dxdy\right|^2 + \right.$$

$$\left. + \left|\int_A E_y(x,y)\ e^{jk(\alpha x + \beta y)}\ dxdy\right|^2\right\} \qquad (2.10.2)$$

and the power transmitted through the aperture

$$P_{ap} = \frac{1}{2}\left(\frac{\varepsilon}{\mu}\right)^{1/2} \int_A \{|E_x(x,y)|^2 + |E_y(x,y)|^2\}\, dxdy \qquad (2.10.3)$$

Hence the gain becomes

$$g_{xy}(\alpha,\beta) = \frac{4\pi}{\lambda^2} \cdot \frac{\left|\int_A E_x(x,y)e^{jk(x\alpha + \beta y)}dxdy\right|^2 + \left|\int E_y(x,y)e^{jk(x\alpha + \beta y)}dxdy\right|^2}{\int_A \{|E_x(x,y)|^2 + |E_y(x,y)|^2\}dxdy} \qquad (2.10.4)$$

The maximum gain generally occurs at the main axis $\alpha = \beta = 0$, where the far field cross-polar component is also zero:

$$g_{max}(0,0) = \frac{4\pi}{\lambda^2} \frac{\left|\int_A E_x(x,y)\, dxdy\right|^2}{\int_A \{|E_x(x,y)|^2 + |E_y(x,y)|^2\}dxdy} \qquad (2.10.5)$$

The gain calculated from the reconstructed aperture field thus becomes

$$\tilde{g}(0,0) = \frac{4\pi}{\lambda^2} \frac{\left|\int_A \tilde{E}_x(x,y)\, dxdy\right|^2}{\int_A \{|\tilde{E}_x(x,y)|^2 + |\tilde{E}_y(x,y)|^2\, dxdy} \qquad (2.10.6)$$

Because the reconstructed field $\tilde{\tilde{E}}_{ap}$ is the aperture field as "seen" from a distance R_{Fre} before the aperture, this equation takes into account aperture blocking and phase errors, but also the introduced reconstruction errors. Fortunately the latter errors will largely cancel out because integration is performed over the whole aperture as was already stated in section 2.8. Using (2.6.3)

$$E_{P_{Fra}}(\alpha,\beta) = C(R_{Fra}) \iint E_{ap}(x,y)\, e^{jk(x\alpha + \beta y)}dxdy \qquad (2.10.7)$$

with

$$C(R_{Fra}) = \frac{jke^{-jkR_{Fra}}}{2\pi R_{Fra}}$$

The gain (2.10.1) or (2.10.5) can also be calculated from the Fraunhofer field distribution, using Parsevals theorem:

$$\iint_A |E_{ap}(x,y)|^2 \, dxdy = \left|\frac{1}{C(R_{Fra})}\right|^2 \int_{-\infty}^{\infty}\int_{-\infty}^{\infty} |E_{P_{Fra}}(\alpha,\beta)|^2 \, \frac{d\alpha}{\lambda} \frac{d\beta}{\lambda} \qquad (2.10.8)$$

Substitution of (2.10.7) and (2.10.8) in (2.10.1) then leads to

$$g_x(\alpha,\beta) = \frac{4\pi}{\lambda^2} \frac{|E_{P_{Fra,x}}(\alpha,\beta)|^2}{\int_{-\infty}^{\infty}\int_{-\infty}^{\infty} |E_{P_{Fra,x}}(\alpha,\beta)|^2 \, \frac{d\alpha}{\lambda} \frac{d\beta}{\lambda}} \qquad (2.10.9)$$

Similarly, (2.10.6) leads to

$$\tilde{g}(0,0) = \frac{4\pi}{\lambda^2} \frac{|\tilde{E}_{P_{Fra,x}}(0,0)|^2}{\int_{-\infty}^{\infty}\int_{-\infty}^{\infty} \{|\tilde{E}_{P_{Fra,x}}(\alpha,\beta)|^2 + |\tilde{E}_{P_{Fra,y}}(\alpha,\beta)|^2\} \, \frac{d\hat{\alpha}}{\lambda} \frac{d\hat{\beta}}{\lambda}} \qquad (2.10.10)$$

Since the side lobes of the far field contain little power, the integral in the denominator of (2.10.10) can be approximated by integration over the main lobe and a few side lobes, instead of integration to infinity.
The Fresnel field gain for one polarisation for $\alpha = \beta = 0$ can be derived from (2.10.2) and (2.10.3) using (2.6.5):

$$g_{Fre}(0,0) = \frac{4\pi}{\lambda^2} \frac{\left| \int_A E_{ap,x}(x,y) \, e^{\frac{-jk(x^2+y^2)}{2R_{Fre}}} \, dxdy \right|^2}{\int_A |(E_{ap,x}(x,y)|^2 \, dxdy} \qquad (2.10.11)$$

From (2.6.5) and (2.6.3) it can be seen that the gain reduction factor:

$$\gamma = \frac{g_{Fre}(0,0)}{g(0,0)} = \left|\frac{E_{P_{Fra}}(0,0)}{E_{P_{Fre}}(0,0)}\right|^2 \cdot \left|\frac{R_{Fre}}{R_{Fra}}\right|^2 \qquad (2.10.12)$$

With (2.7.6):

$$m = \frac{R_{Fra}}{R_{Fre}}$$

this equation reduces to

$$\gamma = \frac{1}{m^2} \left|\frac{E_{P_{Fra}}(0,0)}{E_{P_{Fre}}(0,0)}\right|^2 \qquad (2.10.19)$$

For a tapered circular aperture field:

$$E_{ap}(x,y) = 1 - a(x^2 + y^2)$$

the gain reduction is easily shown to be

$$\gamma = \frac{1}{m^2} \left| \frac{(2-a)\ \sin(\frac{\pi m}{16}) + j\{\frac{16a}{\pi m}\ \sin(\frac{\pi m}{16}) - a.\cos(\frac{\pi m}{16})\}}{\frac{\pi}{4}\ (\frac{1}{2} - \frac{a}{4})} \right|^2 \qquad (2.10.20)$$

For a uniform illumination a = 0, which leads to

$$\gamma = \left[\frac{\sin(\frac{\pi m}{16})}{\frac{\pi m}{16}} \right]^2 \qquad (2.10.21)$$

as was already stated by Silver [2].
For m = 16, 32, 48, etc., the value of $\gamma \approx 0$ because the Fresnel field on axis is then zero. From (2.10.21) it can also be seen that for m = 0, 24, 40, 56 the value of γ reaches relative maxima.
Fig. (2.10.1) shows the value of γ, for tapered illuminations, to have a similar behaviour.
Evaluation of the Fresnel field outside the z-axis (α or $\beta \neq 0$) requires numerical calculation of (2.6.5). Analytical evaluation of (2.3.16) in case of the circular, uniformly illuminated aperture leads to a Hankel transform, which in turn leads to Lommel functions, as was shown by Papoulis [9]. From these functions it can be seen that the Fresnel field on the z-axis is not always a maximum, as is the case in the far field.
Application of the gain reduction factor γ which is derived on the z-axis, thus not always yields maximum recieved power.
Since evaluation of Hankel transforms, is difficult for nonuniform aperture distributions and only restricted to circularly symmetrical aperture fields, the Fourier integrals from section 2.6 are preferred for further analysis.

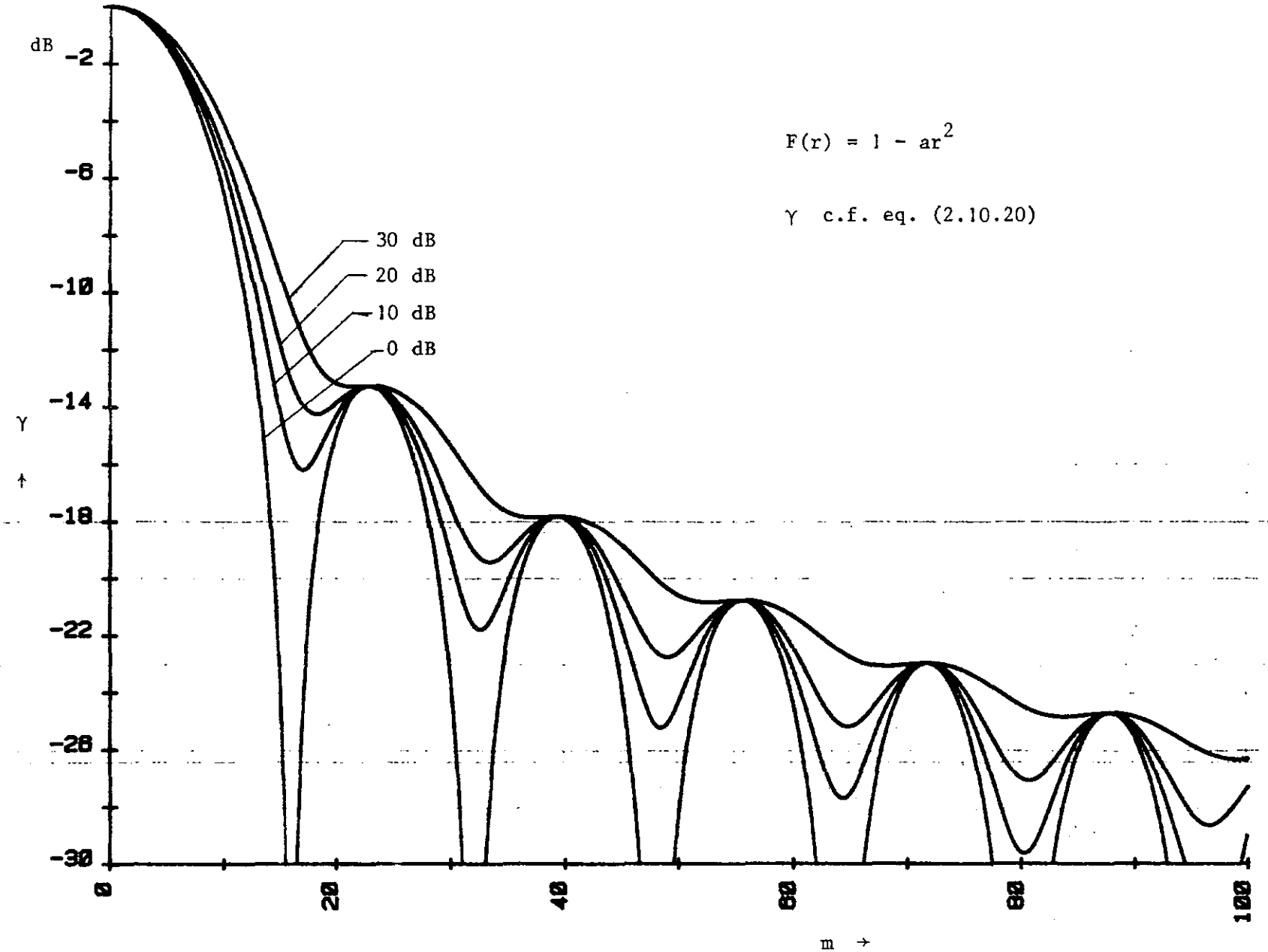

$F(r) = 1 - ar^2$

γ c.f. eq. (2.10.20)

Fig. 2.10.1

Gain reduction factor γ as a function of edge illumination and the reduction factor m

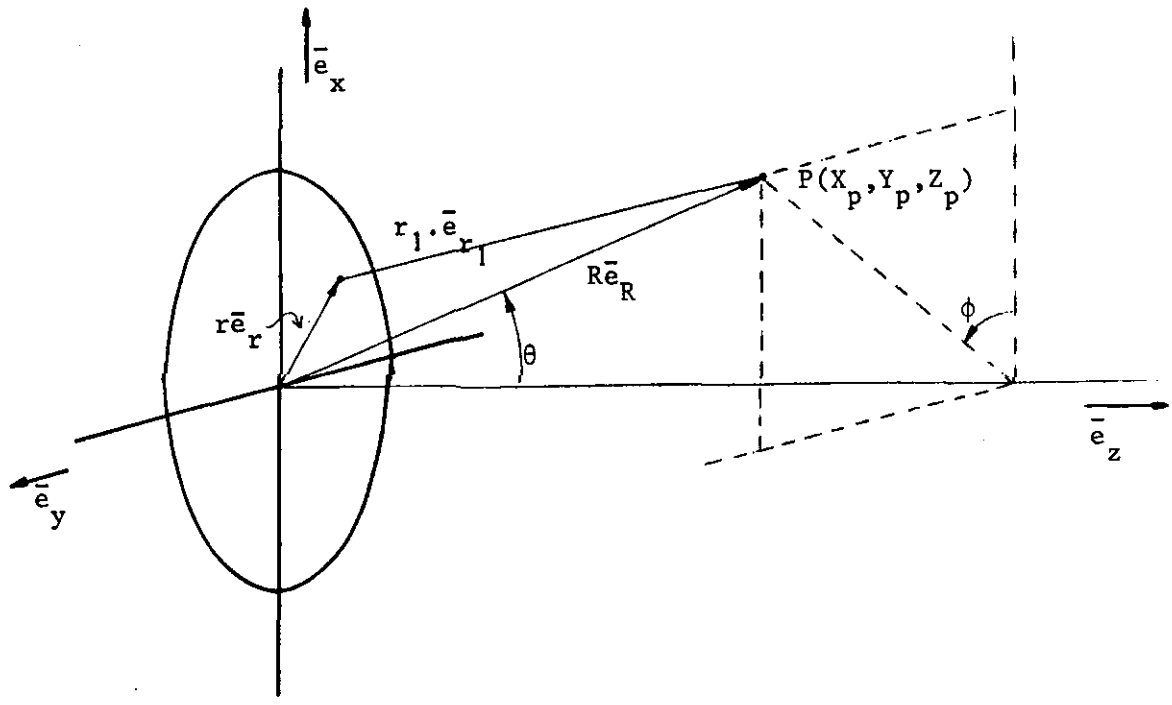

Fig. 2.2.1. Coordinate system for the aperture field method.

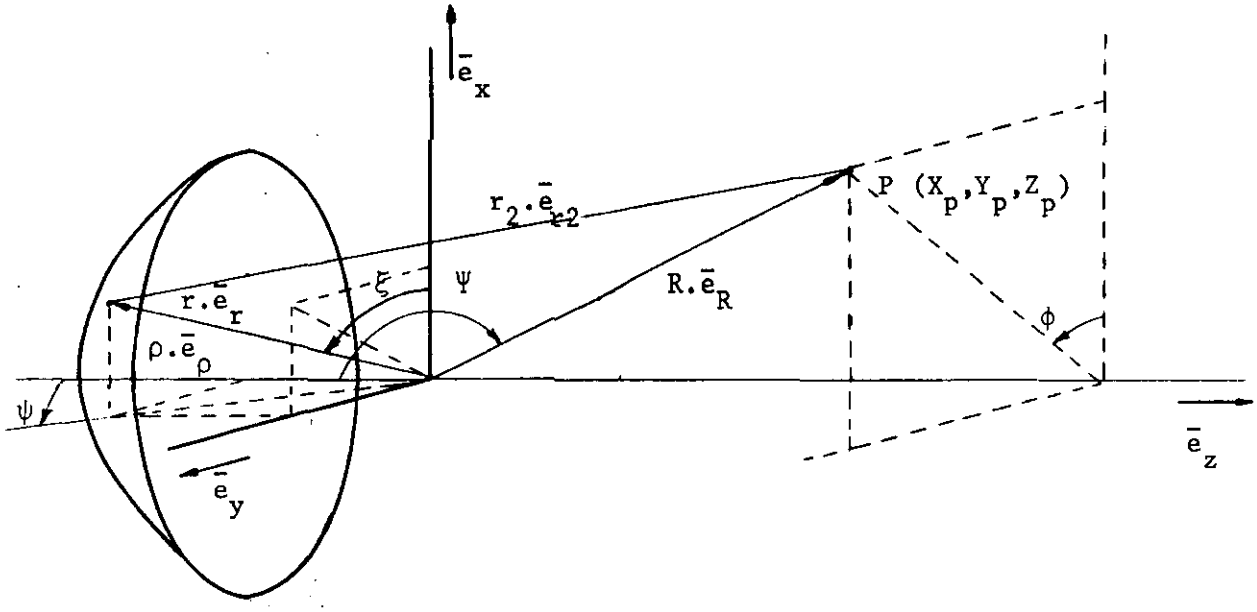

Fig. 2.3.1. Coordinate system for the current distribution method.

Appendix I

The exponent of (2.3.16) can be evaluated using (2.3.14) and (2.3.15):

$$\exp\{jk[2f - \rho - \rho(\cos\psi\cos\theta - \sin\psi\sin\theta\cos(\xi-\phi)) + \frac{\rho^2}{2R_{Fre}}$$

$$- \frac{\rho^2}{2R_{Fre}}(\cos^2\psi\cos^2\theta - \tfrac{1}{2}\sin2\psi\cos2\theta\cos(\xi-\phi) + \sin^2\psi\sin^2\theta\cos^2(\xi-\phi))]\}$$

$$= \exp\{jk[2f - \rho - \rho(\cos\psi + \cos\psi(\cos\theta-1) - \sin\psi\sin\theta\cos(\xi-\phi))$$

$$+ \frac{\rho^2}{2R_{Fre}}(1 - (\cos^2\psi + \cos^2\psi(\cos^2\theta-1) - \tfrac{1}{2}\sin2\psi\cos2\theta\cos(\xi-\phi)$$

$$+ \sin^2\psi\sin^2\theta\cos^2(\xi-\phi))]\}$$

Since $\rho + \rho\cos\psi = 2f$

$$\exp\{\} = \exp\{jk[-\rho(\cos\psi(\cos\theta-1) - \sin\psi\sin\theta\cos(\xi-\phi))$$

$$+ \frac{\rho^2}{2R_{Fre}}(1-\cos^2\psi) + \frac{\rho^2}{2R_{Fre}}(\cos^2\psi(\cos^2\theta-1) - \tfrac{1}{2}\sin2\psi\sin2\theta\cos(\xi-\phi)$$

$$+ \sin^2\psi\sin^2\theta\cos^2(\xi-\phi))]\}$$

With $r = \rho\sin\psi$

$$\exp\{\} = \exp\{jk[+\rho\cos\psi(1-\cos\theta) + r\sin\theta\cos(\xi-\phi)$$

$$+ \frac{r^2}{2R_{Fre}} + \frac{\rho^2}{2R_{Fre}}(\cos^2\psi(\cos^2\theta-1) - \frac{1}{2}\sin2\psi\sin2\theta\cos(\xi-\phi))$$

$$+ \frac{r^2}{2R_{Fre}}\sin^2\theta\cos^2(\xi-\phi)]\}$$

$$\exp\{\} = \exp\{jk[r\sin\theta\cos(\xi-\phi) + \frac{r^2}{2R_{Fre}}]\} \quad \exp\{jkA(\theta)\}$$

With $A(\theta) = \frac{\rho^2}{2R_{Fra}}(-\sin^2\theta\cos^2\psi - \frac{1}{2}\sin2\psi\sin2\theta\cos(\xi-\phi))$

$$+ \frac{r^2}{2R_{Fre}}(\sin^2\theta\cos^2(\xi-\phi))$$

For small angles θ and $\rho << R_{Fre}$ $\quad A(\theta)\big|_{\theta \to 0} = 0.$

Hence

$$\exp\{\} = \exp\{jk[\frac{r^2}{2R_{Fre}} + r\sin\theta\cos(\xi-\phi)]\}.$$

Appendix II

The Fraunhofer field can be expressed as

$$E_{P_{Fra}} = C_1\, F^{-1}\{F\{E_{P_{Fre}}(\alpha,\beta)\}.e^{jk(\frac{x^2+y^2}{2R_{Fre}})}\}$$

Since the inverse Fourier transform of a product of two Fourier transforms can be expressed as a convolution, we calculate

$$F^{-1}\{e^{jk(\frac{x^2+y^2}{2R_{Fre}})}\} = \int_{-\infty}^{\infty}\int_{-\infty}^{\infty} e^{j\frac{\pi}{\lambda R_{Fre}}(x^2+y^2)}\, e^{j\frac{2\pi}{\lambda}(\alpha x+\beta y)}\, dxdy$$

$$= \exp[-j\frac{\pi R_{Fre}}{\lambda}(\alpha^2+\beta^2)]\int_{-\infty}^{\infty}\int_{-\infty}^{\infty}\exp[j\{(\sqrt{\frac{\pi}{\lambda R_{Fre}}}\,x + \sqrt{\frac{\pi R_{Fre}}{\lambda}}\,\alpha)^2+(\sqrt{\frac{\pi}{\lambda R_{Fre}}}\,y + \sqrt{\frac{\pi R_{Fre}}{\lambda}}\,\beta)^2\}]dxdy$$

$$= \exp[-j\frac{\pi R_{Fre}}{\lambda}(\alpha^2+\beta^2)].\frac{\lambda R_{Fre}}{\pi}\{\int_{-\infty}^{\infty} e^{jS^2}\, dS\}^2$$

With the well known Fresnel integral:

$$\int_{-\infty}^{\infty} e^{jS^2}\, dS = \sqrt{\pi}\,\exp(j\frac{\pi}{4})$$

this equation yields:

$$F^{-1}\{e^{jk(\frac{x^2+y^2}{2R_{Fre}})}\} = j\lambda R_{Fre}\, e^{\frac{-j\pi R_{Fre}}{\lambda}(\alpha^2+\beta^2)}$$

Using the definitions (2.6.1) and (2.6.2), it is not hard to show that

$$E_{Pra} = C_1.F^{-1}\{F\{E_{P_{Fre}}(\alpha,\beta)\}.F\{j\lambda R_{Fre}\, e^{\frac{-jR_{Fre}}{\lambda}(\alpha^2+\beta^2)}\}\}$$

$$E_{P_{Fra}} = C_1.\frac{1}{\lambda^2}.E_{P_{Fre}}(\alpha,\beta)^{**}j\lambda R_{Fre}\, e^{\frac{-j\pi R_{Fre}}{\lambda}(\alpha^2+\beta^2)}$$

Hence

$$E_{P_{Fra}}(\alpha,\beta) = C_2 \int_{-\infty}^{\infty}\int_{-\infty}^{\infty} E_{P_{Fre}}(\alpha',\beta')\, e^{\frac{-j\pi R_{Fre}}{\lambda}[(\alpha-\alpha')^2 + (\beta-\beta')^2]} d\alpha' d\beta'$$

with $C_2 = jR_{Fre}C_1/\lambda$

Literature

[1] P.G. Smith, Transactions on Ant. & Prop. AP 14, nr. 2.

[2] Silver, S. "Antenna Theory and Design", Chap. 6 & 5, Mc GrawHill 1949.

[3] Maanders, E.J., Doctor's Thesis THE Report 75-E-60.

[4] Collin and Zucker, p. 41-48, Part II, Inter Univ. Elect. Series, 1969.

[5] Ludwig A.C., "The definition of cross-polarisation", IEEE Trans. AP, Jan. 1973, pp. 116-119.

[6] Geus, C.A.M., "Antennemetingen m.b.v. microgolfholografie", Master's Thesis, Eindhoven University of Technology, Nov. 1975.

[7] V.I. Turchin, N.M. Tseytlin and A.K. Chandaer,"Measurements on antenna patterns based on radiation from a source in the Fresnel zone with the help of computer processing", Radio Eng.& Elect.Phys. Vol.18,p.527-535 April '74.

[8] M. Abramowitz and I. Stegun, "Handbook of mathematical functions", Dover 1970.

[9] A. Papoulis, "Systems and transforms with applications in optics", Ch. 9 & 5, McGraw Hill 1968.

3. Computer simulations of Fresnel field measurements

3.1. Introduction

Fresnel field integrals can be evaluated with the well-known Fourier transfroms, which can be calculated at equidistant points with the use of discrete Fourier transform techniques. In this chapter a short review of this transform will be given in order to explain the calculated bandwidth and sampling distance. The Fresnel field distribution will be given for the special case of a circular symmetric illuminated aperture. In order to simulate measurements, the calculated distribution will be truncated to some "measurement" interval, in order to reconstruct aperture and far field distributions.
Information concerning the required dynamic range of the measurement equipment will be obtained from reconstructions of the aperture distributions from simulated low dynamic range Fresnel field measurements.

3.2. A short review of the discrete Fourier transform

Fourier integrals can be approximated accurately with the use of the discrete Fourier transform [1,2].
Consider a periodically continued time function f(t) with the two side bandwidth B and periode T. The Fourier spectrum of f(t) is then given by

$$F(f) = \int_0^T f(t)\, e^{-j2\pi ft} dt \qquad (3.2.1)$$

According to the sampling theorem the function f(t) is uniquely defined by N = B.T equidistant samples at a time distance

$$\tau_s = \frac{T}{N} = \frac{1}{B} \qquad (3.2.2)$$

The time function can be represented by a Fourier series

$$f(t) = \sum_0^{N-1} A(m) e^{j2\pi \frac{m}{T} t} \qquad (3.2.3)$$

with

$$A(m) = \frac{1}{T} \int_0^T f(t)\, e^{-j2\pi \frac{m}{T} t}\, dt \qquad (3.2.4)$$

Hence, samples in the time domain can be expressed in samples from the frequency domain

$$f(n\tau_s) = \sum_{o}^{N-1} \frac{1}{T} F\left(\frac{m}{T}\right) e^{j2\pi\frac{mn}{N}} \tag{3.2.5}$$

Similarly, using the periodically continued frequency function,

$$F\left(\frac{m}{T}\right) = \frac{1}{B}\sum_{o}^{N-1} f\left(n\frac{1}{B}\right) e^{-2j\pi\frac{mn}{N}} \tag{3.2.6}$$

If we define the discrete Fourier transform as

$$f_o(n) = \frac{1}{N}\sum_{o}^{N-1} F_o(m) e^{j2\pi\frac{mn}{N}} \tag{3.2.7}$$

and the inverse discrete Fourier transform as

$$F_o(m) = \sum_{o}^{N-1} f_o(n) e^{-j2\pi\frac{mn}{N}} \tag{3.2.8}$$

then (3.2.7) and (3.2.8) form a discrete Fourier transform pair as can be seen from the substitution of (3.2.8) in (3.2.7).
The inverse discrete Fourier transform $F_o(m)$ of $f_o(n) = f(n\tau_s)$ equals the sample value of the Fourier integral (3.2.1) apart from a factor B^{-1}.

$$\left.\begin{aligned} F\left(\frac{nB}{N}\right) &= B.F_o(m) \\ n &= m \end{aligned}\right\} \tag{3.2.9}$$

Apart from a factor T/N the discrete Fourier transform (D.F.T) $f_o(n)$ of $F_o(m) = F\left(\frac{m}{T}\right)$ is equal to $f(t)$:

$$f\left(\frac{n}{B}\right) = \frac{N}{T} f_o(n) \tag{3.2.10}$$

A time-limited function is not band-limited; hence, application of the discrete Fourier transform yields samples which are approximately equal to samples from the Fourier integral. This approximation is all the better as overlap owing to periodic continued spectra is less [1]. The error, called alaising distortion will be exactly zero for band-limited spectra. In order to apply D.F.T., the spectrum of the time limited function has to be so truncated that the contribution of the truncated part of the spectrum to the inverse transform yields

a negligible error [2].
Computer routines performing the discrete Fourier transform in a fast way are called "Fast Fourier Transform Procedures". The number of samples of these routines is generally a power of two, while the samples lie in the interval [0, N-1]. Application of F.F.T.-routines to N samples of a time function in the interval [0, N-1] always yields N samples in the frequency domain that also lie in the interval [0, N-1].
If the time function has non-zero values for the negative values of the argument, then with the use of the periodically continued function a new time function can be defined in the interval $0 \leq t < T$, yielding the same Fourier transform. Since the (F.F.T.) frequency spectrum is also one period of a periodically continued spectrum, the samples for negative frequencies are in the interval [N/2, N-1].
A two-dimensional F.F.T.

$$X[k,l] = \sum_{0}^{M-1}\sum_{0}^{N-1} X[m,n]\, e^{2j\pi\left[\frac{km}{M} + \frac{ln}{N}\right]} \tag{3.2.11}$$

can be performed with the one-dimensional F.F.T. applied to all rows of matrix X, followed by a one dimensional F.F.T. performed on all columns of the matrix (this is equal to a sequential summation over two different indices in a double sum).

3.3. The upper limit to the angular sample distance in the Fresnel field

The Fourier transform of the Fresnel field distribution equals the aperture field (apart from a phase factor). According to the sampling theorem of Shannon, the sample distance (of the Fresnel field) should be thus that no overlap of spectra (aperture field) occurs. Because the aperture field is zero outside the aperture, its "bandwidth" is limited to D, the aperture diameter.
The Fourier integral

$$E(\alpha,\beta) = \iint_{A} F(x,y)\, e^{\frac{j2\pi}{\lambda}(\alpha x + \beta y)}\, dxdy \tag{3.3.1}$$

can be approximated with D.F.T. as

$$E_o(k\Delta\alpha,\ l\Delta\beta) = \sum_{0}^{N-1}\sum_{0}^{M-1} F(n\Delta x,\ m\Delta y)\, e^{j\frac{2\pi}{\lambda}\left(\frac{ml}{M} + \frac{nk}{N}\right)} \tag{3.3.2}$$

In the sample point the exponent of (3.3.2) can be written as

$$\exp\left[j2\pi\left\{\frac{k\Delta x\ n\Delta x}{\lambda} + \frac{m\Delta y\ 1\Delta\beta}{\lambda}\right\}\right] = \exp\left[j2\pi\left\{\frac{ml}{M} + \frac{nk}{N}\right\}\right]$$

hence

$$N\Delta x = \frac{\lambda}{\Delta\alpha} \tag{3.3.3}$$

and

$$M\Delta y = \frac{\lambda}{\Delta\beta} \tag{3.3.4}$$

The sampling theorem now states that

$$N\Delta x \geqslant D$$
$$N\Delta y \geqslant D$$

which leads to

$$\Delta\alpha \leqslant \frac{\lambda}{D} \tag{3.3.5}$$
$$\Delta\beta \leqslant \frac{\lambda}{D} \tag{3.3.6}$$

From these equations it can be seen that the sample distance in the Fresnel field, may not exceed the far-field beamwidth.
Once the values of $\Delta\alpha$ and $\Delta\beta$ are chosen, the values of M and N determine the resolution Δx and Δy in the aperture. Calculation of the far field from this aperture field yields poor resolution since $\Delta\alpha$ and $\Delta\beta$ are the same as in the Fresnel field.
An increase in the values of M and N yields smaller values of $\Delta\alpha$ and $\Delta\beta$ in the far field as can be seen from (3.3.3) and (3.3.4). This increase, by merely adding zero samples outside the aperture, unfortunately also increases computer time which is proportional to the number of complex multiplications F(M,N). If M and N are each a power of two [3]:

$$F(M,N) \simeq MN\ ^{2}\log MN \tag{3.3.7}$$

Transformation of an 128 x 64 matrix by the author's Algol 60 FFT routine,

took nearly 100 seconds of computer time. An increase in M and N by a factor of 2 leads to more than 400 secs computer time for a twice better resolution.
Since data reduction depends on the sample distance $\Delta\alpha$, the quantity of data within the measurement interval yields the value of $N\Delta x$, giving only meaningful results for $N\Delta x \leq D$. Because there is no optimum value of Δx, computer time can only be a compromise between resolution in the Fresnel field and resolution in the calculated aperture field.

3.4. Results of computer simulations

In section 2.8 it was already stated that general insight into Field transforms can only be obtained by computer calculations of two-dimensional field distributions of various parameters like aperture diameter, frequency, measurement interval, sample distance, aperture field distribution and the number of reductions. This, however, would consume too much computer time. Computer simulations for a particular aperture field, aperture diameter and wavelength yield enough insight into and confidence in the equations described in chapter 2.
Recent Russian work [4] on far field reconstruction errors in the one-dimensional case yields a somewhat larger value of the minimal Fresnel field angular sector $\hat{\alpha}$ then is given by (2.8.19) if a 1-3% inaccuracy of the main lobe is required. A larger value of the minimum $\hat{\alpha}$ always yields more accurate results as was to be expected. Because the Fast Fourier transform of the Fresnel field requires the number of samples to be a power of two, extra samples of the Fresnel field taken outside the absolute minimum sector $\hat{\alpha}$ can replace the zero samples without increasing computer time.
Data reduction thus leads to measurement of the Fresnel field within the minimum sector $\hat{\alpha}$, yielding a minimum number of samples, while measurement outside this sector leads to more samples and a more accurate far field pattern in the same processor time (if N was chosen large enough).
For the computer simulations an 128 x 64 matrix was chosen. The computer program, written in Algol 60, is given by [5].
In the present example we consider a circular aperture with diameter D=3 m and with a tapered aperture distribution

$$E(r) = 1 - ar^2 \quad , \quad |r| < D/2$$
$$E(r) = 0 \quad , \quad |r| > D/2$$

A 15-dB taper yields $a = (1 - \frac{1}{4\sqrt{2}}).(\frac{2}{D})^2 = 0.365$

The far field criterion now gives

$$\frac{2D^2}{\lambda} = 1800 \text{ m.}$$

According to (2.8.21) the maximum number of reduction is

$$m = \frac{1}{2}(\frac{8D}{5\lambda})^{2/3} - \frac{4}{15}M = 30.65 - \frac{4}{15}M.$$

For our calculations: m = 10

then $R_{Fre} = 180$ meters.

The upper limit of the angle from boresight is (2.7.5)

$$\arcsin(\sqrt{\frac{1}{8m}} - \frac{m}{8}(\frac{\lambda}{D})) = 6.179^\circ$$

while the lower limit is given by

$$\arcsin(\frac{\lambda}{D}\left[\frac{M+m}{2}\right]) = 1.43^\circ \text{ if } M = 5$$

Because angles from boresight in the Fresnel field and far field are small, equation (2.5.3) is valid; hence the copolar field can be calculated directly from Fresnel or Fourier transforms of the aperture field without the use of the coordinate transform (2.5.2).

In order to verify computer calculations, the field on the main axis will now be given (2.3.17):

$$E_{far}(\theta,\phi) = \frac{jk}{2\pi R_{Fra}} e^{-jkR_{Fra}} \iint E(r)\, e^{jk\, r\sin\theta\cos(\xi-\phi)}\, r dr d\xi$$

Substitution of $u = k\frac{D}{2}\sin\theta$

and

$$r' = 2r/D$$

yields

$$E_{far}(\theta,\phi) = \frac{jk}{2\pi R_{Fra}} e^{-jkR_{Fra}} \left(\frac{D}{2}\right)^2 \int_0^{2\pi}\int_0^1 \left[1 - a\left(\frac{D}{2}\right)^2 r'^2\right] e^{jur'\cos(\xi-\phi)} r'dr'd\xi$$

With

$$J_o(ur') = \int_0^{2\pi} e^{jur'\cos(\xi-\phi)} d\xi$$

this equation leads to a Hankel transform of the aperture field:

$$E_{far}(\theta,\phi) = \frac{jke^{-jkR_{Fra}}}{2\pi R_{Fra}} \cdot \left(\frac{D}{2}\right)^2 \cdot \left[(1-a\frac{D^2}{4}) \frac{J_1(u)}{u} + 2.a.\frac{D^2}{4} \frac{J_2(u)}{u^2}\right] \qquad (3.4.1)$$

where $J_1(u)$ and $J_2(u)$ are the Bessel functions of the first and the second order. Note that the far field is a function of u only; therefore, the far field is circularly symmetric. The illumination efficiency η , defined by the relation [6]

$$\eta = \frac{1}{A} \frac{\left| \int_A E_{ap}(x,y)\, dxdy \right|^2}{\int_A |E_{ap}(x,y)|^2\, dxdy} = \frac{A_{eff}}{A} \qquad (3.4.2)$$

can be calculated with the help of (3.4.1), since the numerator of (4.3.2) equals the square of the far field modulus on the main axis, apart from a constant factor.

For the given illumination it is easily shown [5] that

$$\eta = 2 \frac{(\frac{1}{2} - aD^2)^2}{(\frac{1}{2} - \frac{aD^2}{4} + \frac{a^2D^4}{96})} \qquad (3.4.3)$$

Substitution of a = 0.365 yields

$$\eta = 0.85975$$

From (3.4.1) it follows that the field strength on the main axis in the far field is:

$$|E_{far}(0,0)| = 0.23$$

and in the Fresnel field, using (2.10.2)

$$|E_{Fre}(0,0)|_{m=10} = 1.2943$$

The Fresnel field of Fig. 3.4.1 was calculated from an aperture distriburion with sample spacing

$\Delta x = 3$ cm
$\Delta y = 6$ cm

With M = 64 and N = 128, the Fresnel field sample spacing is then:

$$\Delta\alpha = \frac{\lambda}{N\Delta x} = 0.0026 \text{ or } 8.95'$$

$$\Delta\beta = \frac{\lambda}{M\Delta y} = 0.0026 \text{ or } 8.95'$$

In Fig. 3.4.2 the same distribution, truncated at -50 dB,is given with a dB scale.
The rotation symmetry of the aperture field also yields rotation symmetry in the Fresnel field. From Fig. 3.4.2 a good symmetry is observed for amplitudes larger than about -45 dB. Sample values below -45 dB show that symmetry is disturbed owing to aliasing distortion.

Fig. 3.4.3. shows the phase distribution in the Fresnel region which oscillates strongly because of constructive and destructive interference in this region.

The calculated Fresnel field is now truncated from $-2^{\circ}23'$ to $+2^{\circ}23'$ in azimuth and elevation in order to simulate measurements over an interval for M = 40, yielding 32 x 32 samples. From this distribution, the aperture distribution is reconstructed in Fig. 3.4.4. Fig. 3.4.5. shows the reconstructed phase in the aperture.

Numerical output of the program yields the relative construction error ε.

Table 3.4.1. Relative construction error in relation to taper and radius

	|ε| interval	0<|r|<135	135<|r|<144	144<|r|<150	|r|=150	Taper
M = 40		<0.9%	<5.6%	<16.9%	11.4%	15 dB
M = 40		<0.15%	<3.3%	<12.3%	82%	30 dB
M = 15		<6.3%	<25.5%	<73 %	83.7%	0 dB

Table 3.4.2. Absolute reconstruction error

The phase error was:

taper		abs. error \ interval	0<|r|<96	96<|r|<138	138<|r|<147	|r|=150
M=40	15 dB		<0.0039 rad	<0.0193 rad	<0.02	0.079
M=40	30 dB		<0.0014 rad	<0.0097 rad	<0.0116	0.053
M=15	0 dB		<0.0224	<0.0490	<0.0678	0.19

In Fig. 3.4.6 is given the amplitude of the far field reconstructed from the truncated Fresnel field. Owing to aliasing distortion the circular symmetry of the sidelobes is disturbed.
In order to calculate the far field for a twice larger bandwidth, the Fresnel field resolution has to be twice better in the case of an equally large (128 x 64) matix.
Truncation of this Fresnel field to $|\alpha| < 2^{o}23'$ and $|\beta| < 2^{o}23'$ then yields the far field distributions of Figs. 2.4.7 to 2.4.9. The numerical results of the computer calculations show that:

- 1^{st} sidelobe level is at -23.3 dB versus -23.6 dB being the true level from Eq. (3.4.1)
- 2^{nd} sidelobe level is at -31.3 dB versus -31.5 dB.
- the max. amplitude at R_{far} = 1800 m, is 0.23, which value is in perfect agreement with (3.4.1)
- the calculated illumination efficiency is

η = 0.863 versus 0.85975 exactly.

In order to simulate a 20 dB dynamic range in Fresnel field measurements, the samples smaller than 20 dB below the maximum were replaced by zeroes.

Figs. 3.4.10 to 3.4.12 now yield calculated aperture distributions in the case of 20, 30 and 40 dB dynamic range measurements. From these figures it can be concluded that disturbances outside (and also inside) the aperture vanish as the dynamic range of measurements increases. This behaviour can be understood from Figs. 3.4.1 and 3.4.2, showing a fast decay of amplitude for larger azimuth and elevation angles. Hence low dynamic range measurements have here the same effect as truncation of the measurement interval to (too) small angles.

The Fresnel field distribution for m=2 ($R_{Fre} = D^2/\lambda$) in Fig. 3.4.13 already shows a concentration of a main beam and a few sidelobes around the z-axis in the case of the far field.

Fig. 3.10.14 shows the Fresnel field for m=10, calculated from a uniformly circular aperture distribution. This field distribution was truncated for m=15 or from -1.19^{o} to 1.19^{o} in azimuth and elevation. The aperture field that was calculated from this "measured" Fresnel distribution is given in Fig. 3.10.15. The Gibb's effect is again clearly demonstrated. Owing to this effect, large amplitude and phase errors occur c.f. Fig. 3.10.16. The far field calculated from this Fresnel field, Fig. 3.10.17 yields reasonable circular symmetry for the first two sidelobes. Owing to aliasing distortion and reconstruction errors, higher lobes are disturbed.
Numerical results show that:

- the first sidelobe level is carrying from -17.2 dB to -17.9 dB and it should be -17.6 dB
- the second sidelobe level is from -23.3 to -24.7 dB versus the real value of -24.6 dB
- the calculated illumination efficiency was $\eta = 1.000$.

This equals exactly the theoretical value, which clearly shows that the far sidelobes contain very little power and hence their contribution to the calculated gain and illumination efficiency may be neglected (see section 2.10).

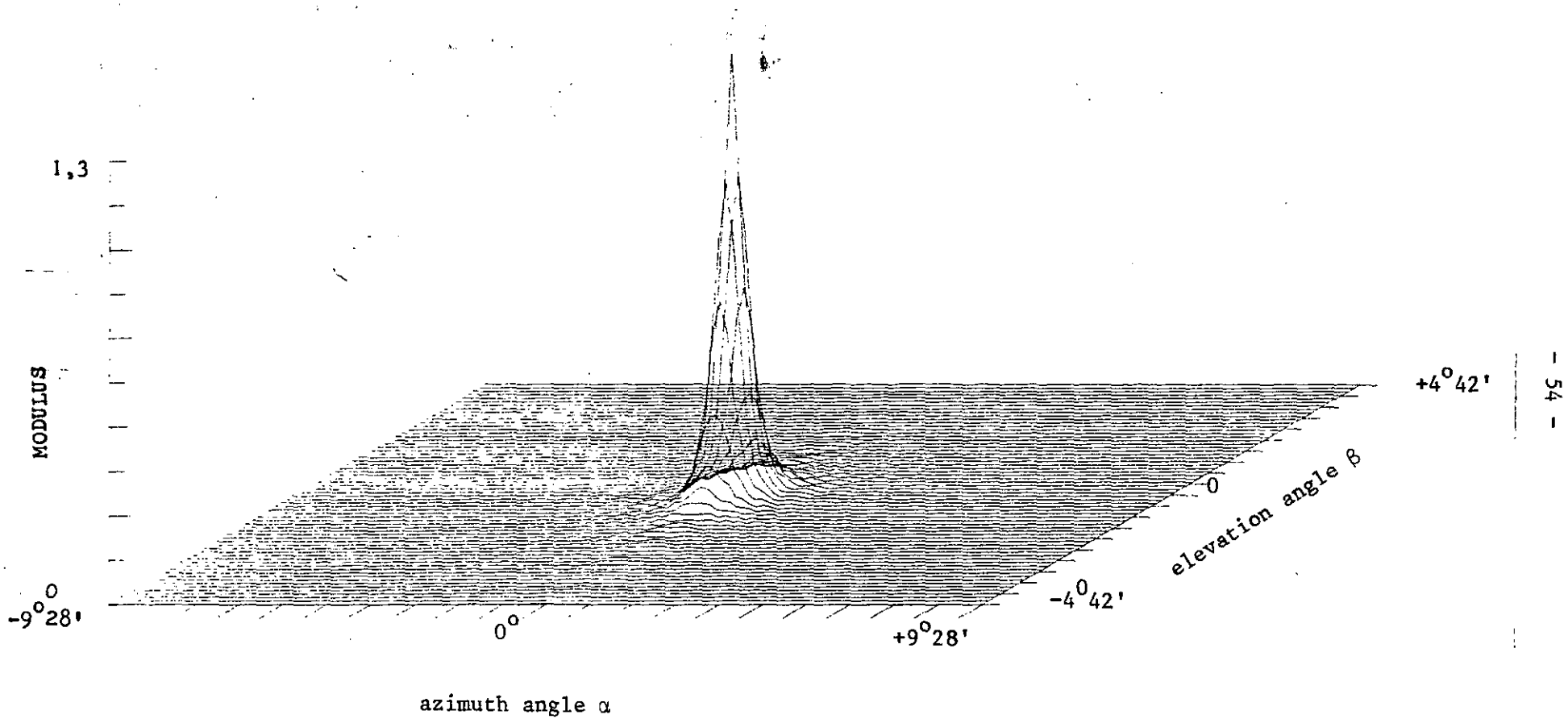

Fig. 3.4.1. Amplitude distribution of the Fresnel field (m = 10)

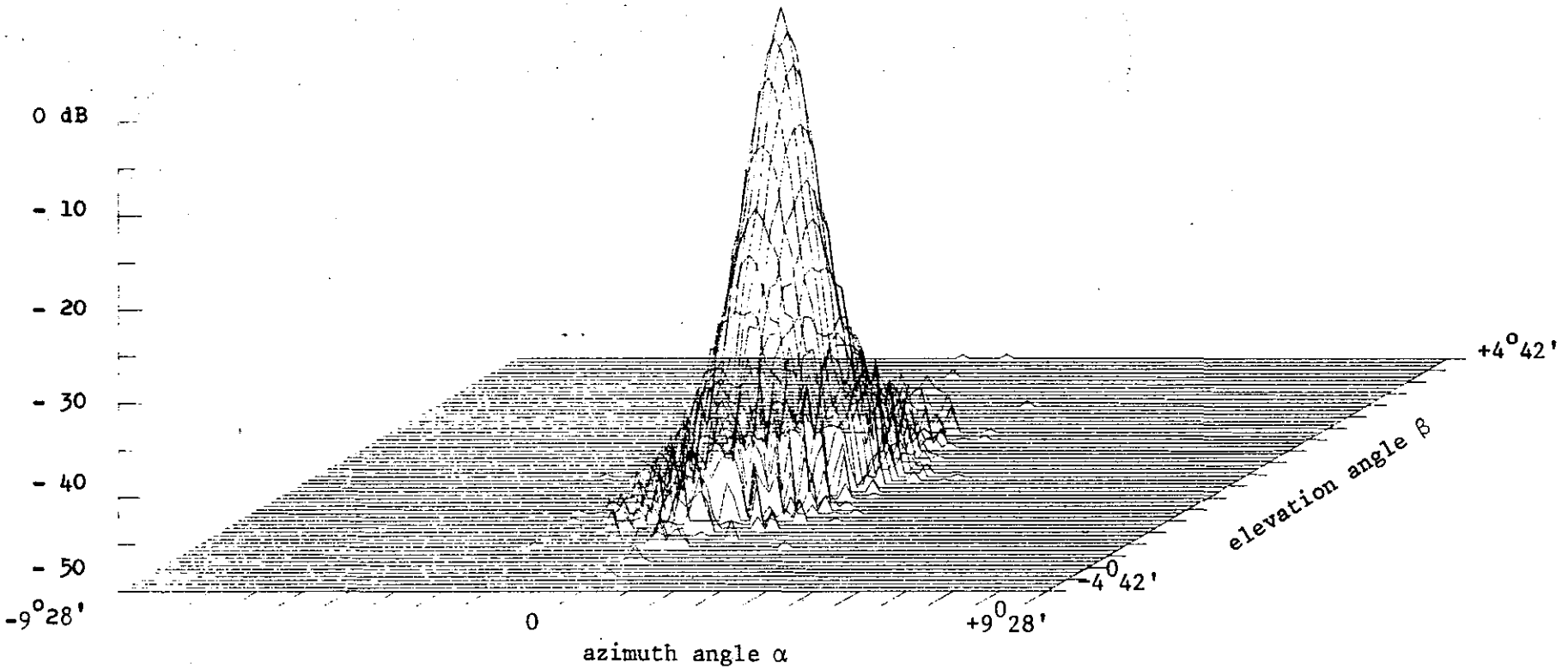

Fig. 3.4.2. Amplitude distribution of the Fresnel field (m = 10)

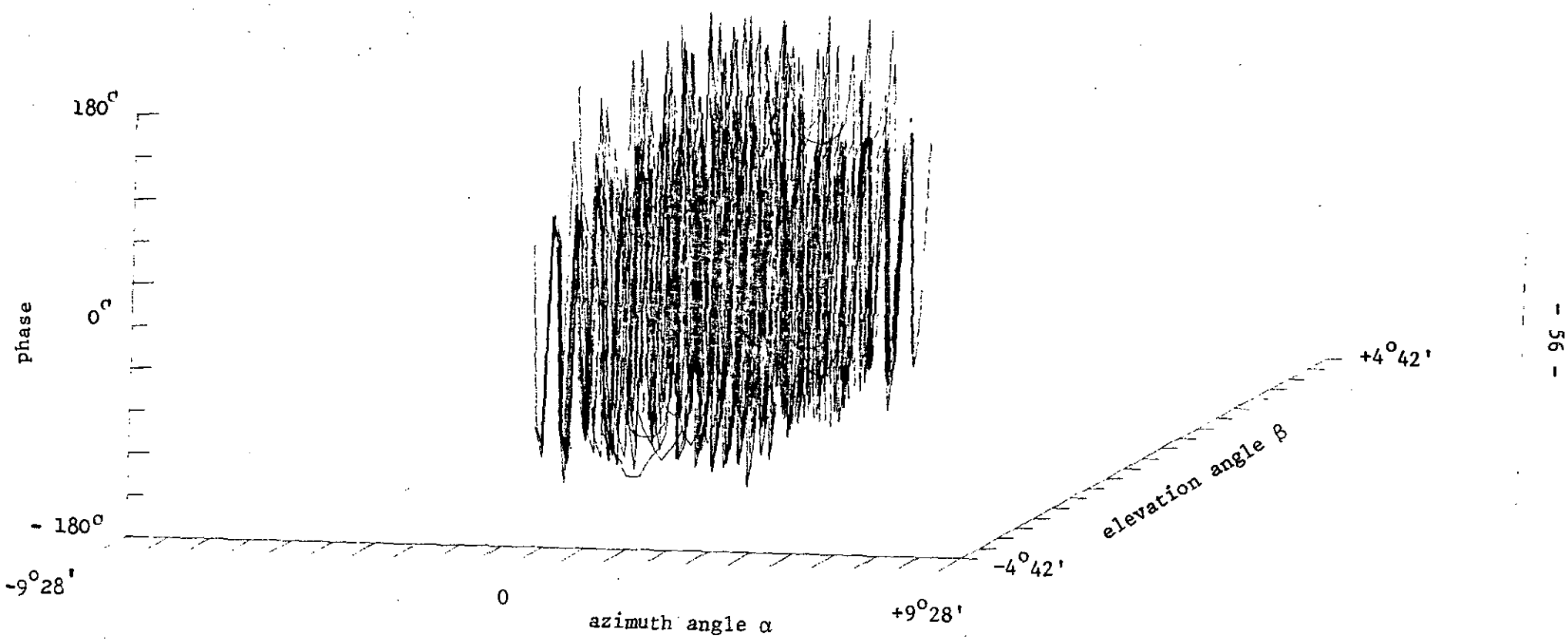

Fig. 3.4.3. Phase distribution of the Fresnel field

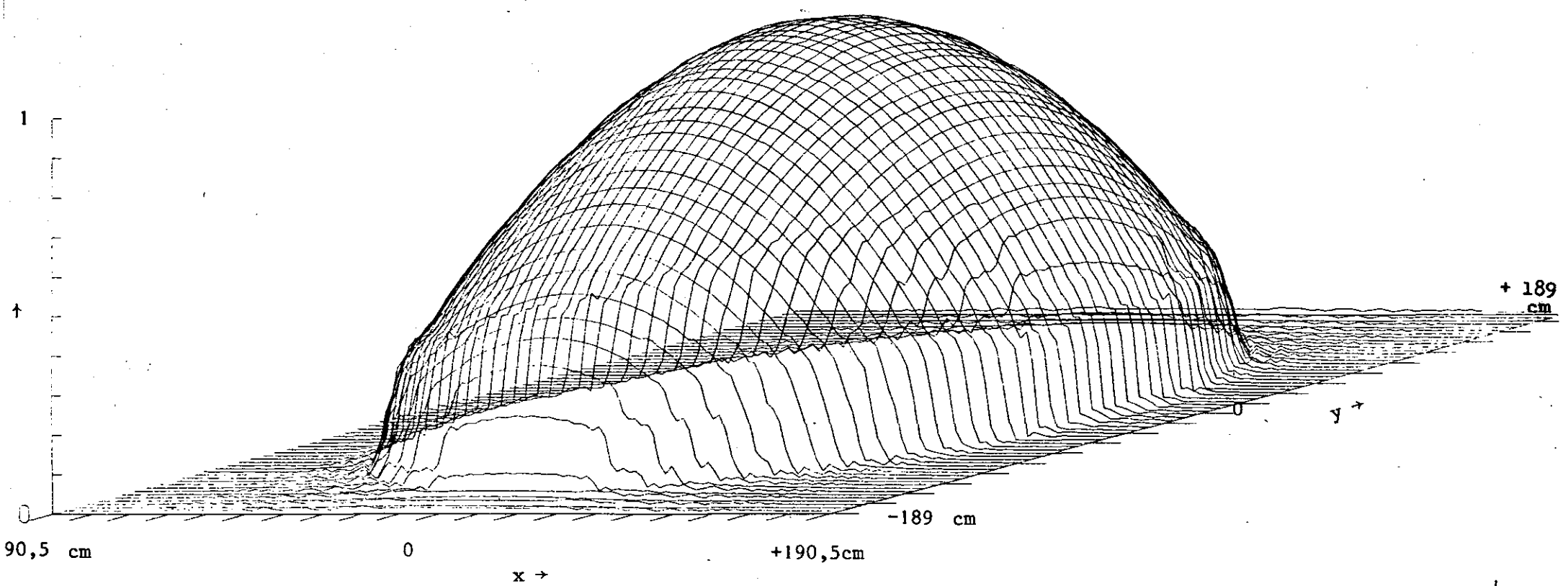

Fig. 3.4.4. Amplitude distribution of the reconstructed aperture field

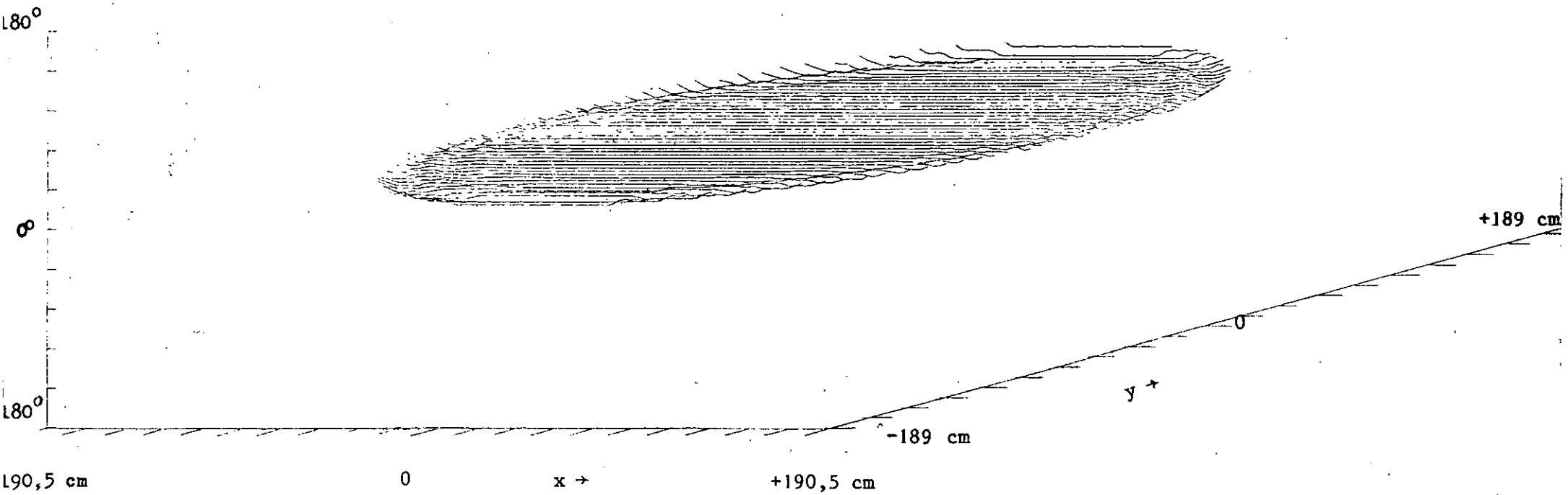

Fig. 3.4.5. Phase distribution of the reconstructed aperture field

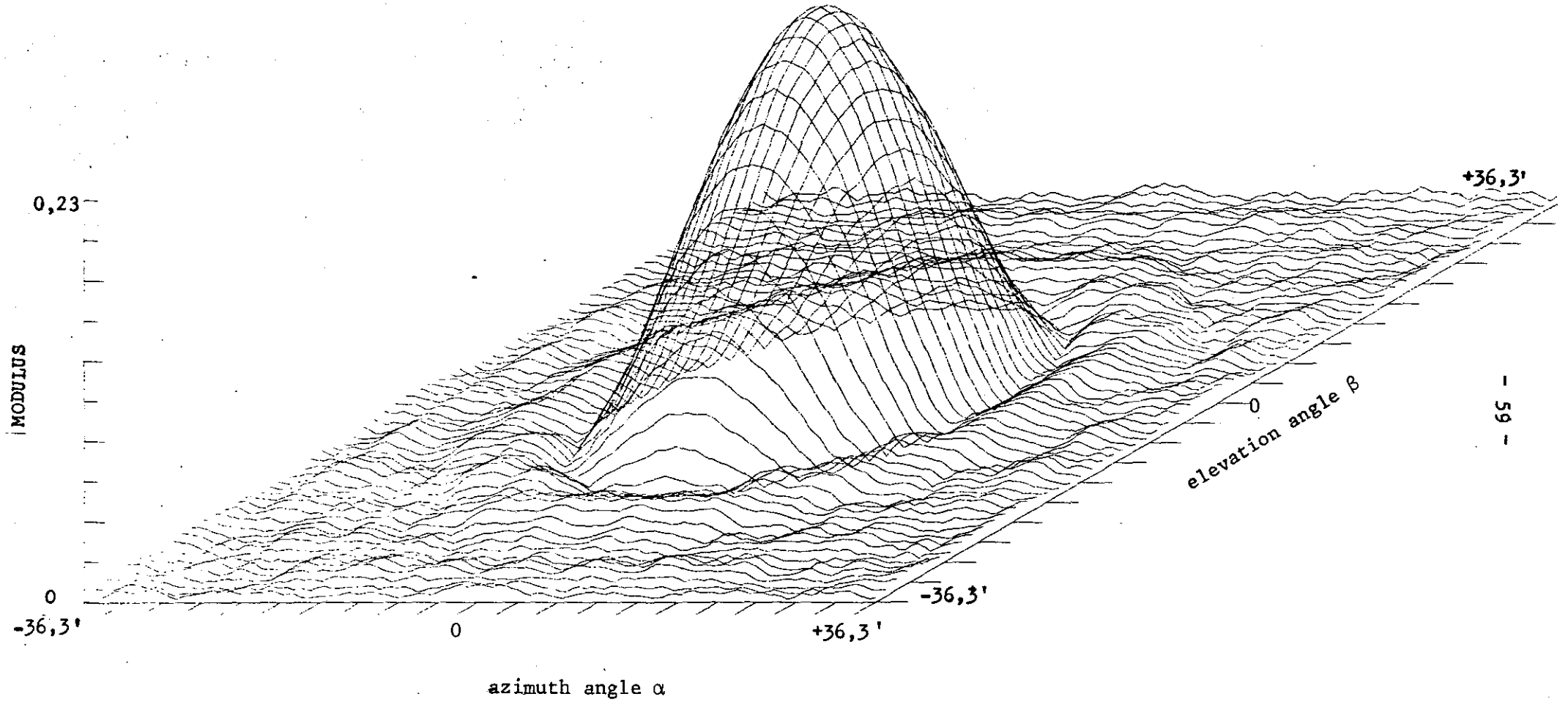

Fig. 3.4.6. Amplitude distribution of the far field, calculated from the truncated Fresnel field

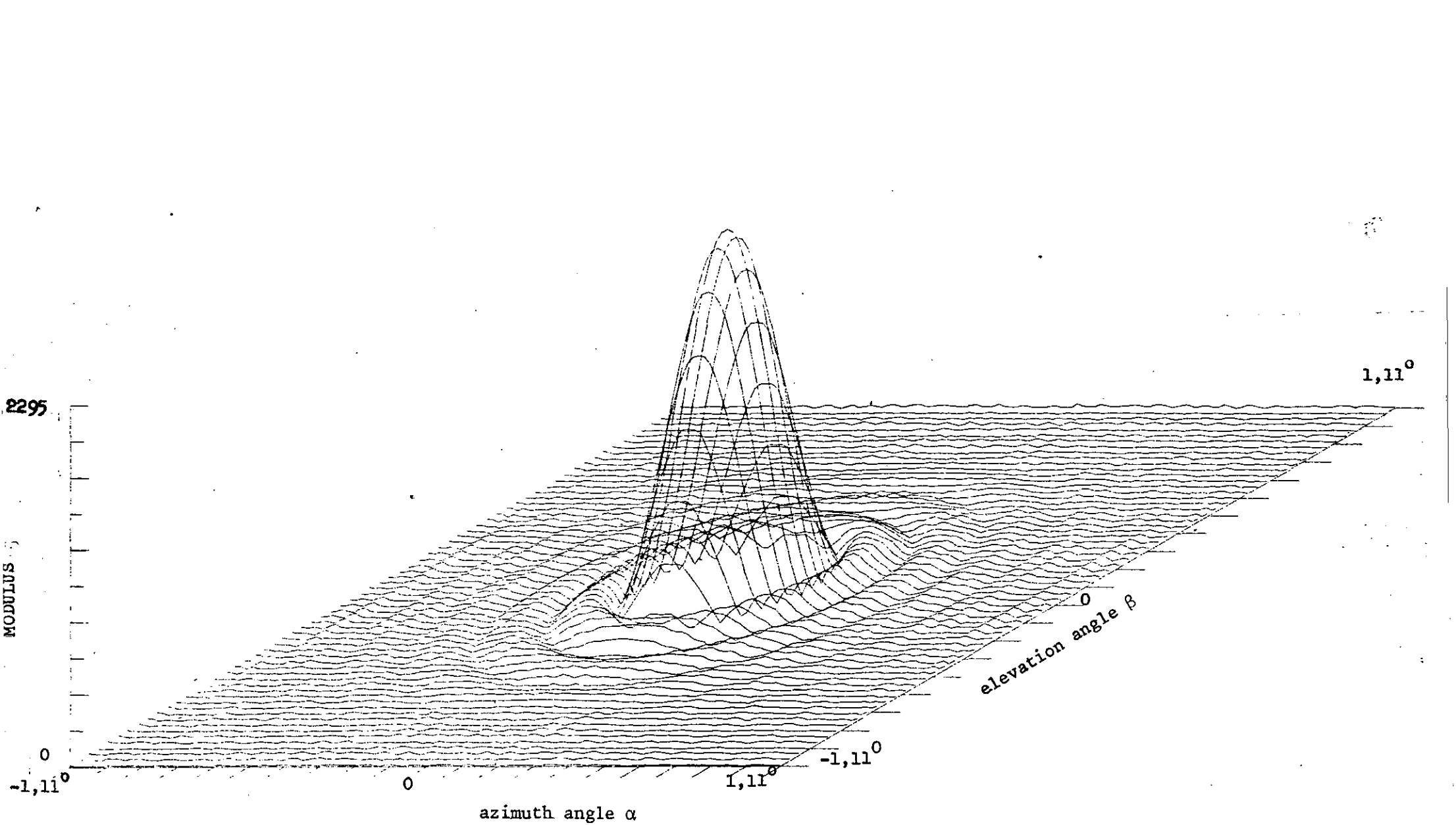

Fig. 3.4.7. Fraunhofer distribution, calculated from the truncated Fresnel field

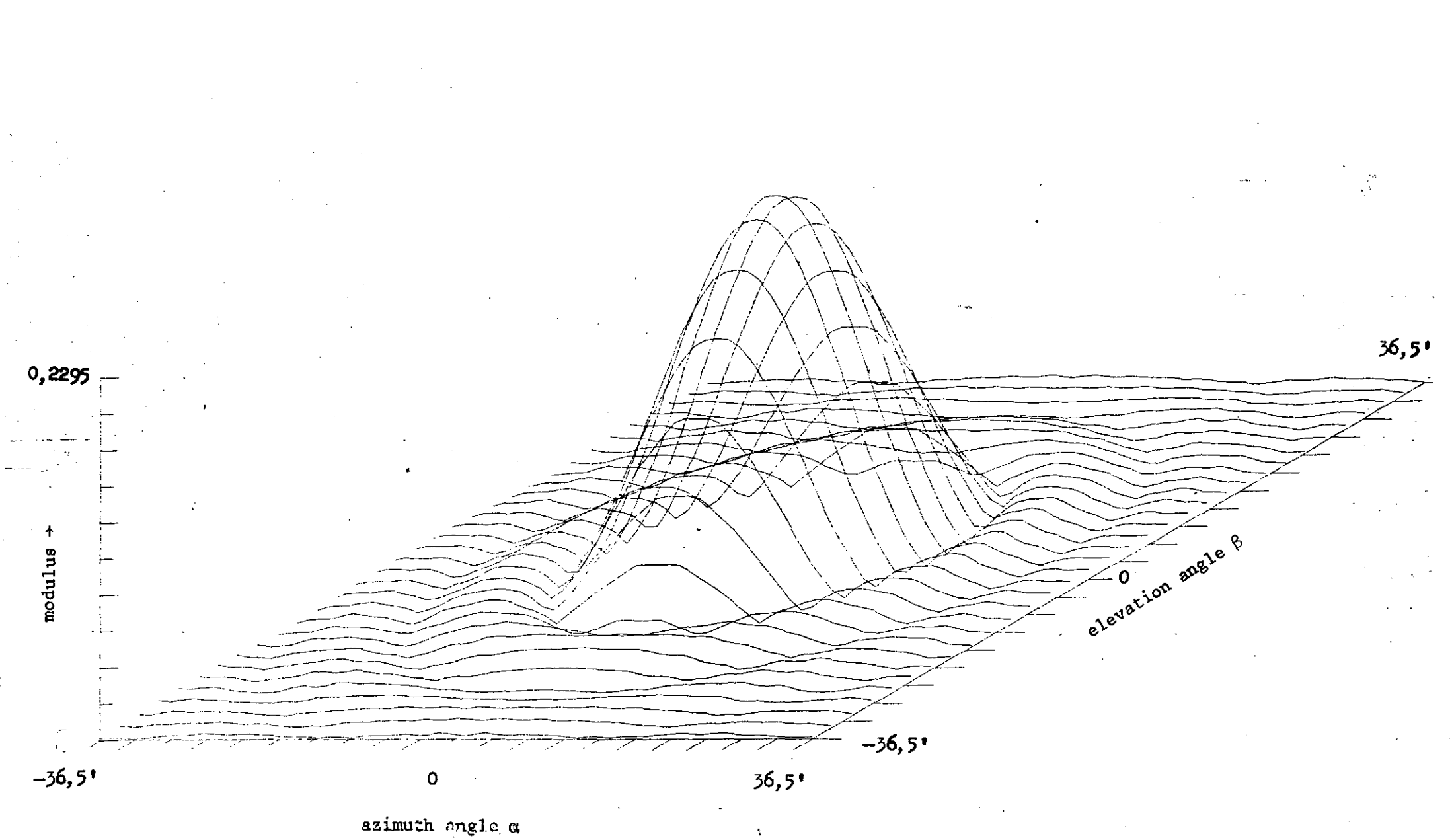

Fig. 3.4.8. Far field distribution, calculated from the truncated Fresnel field

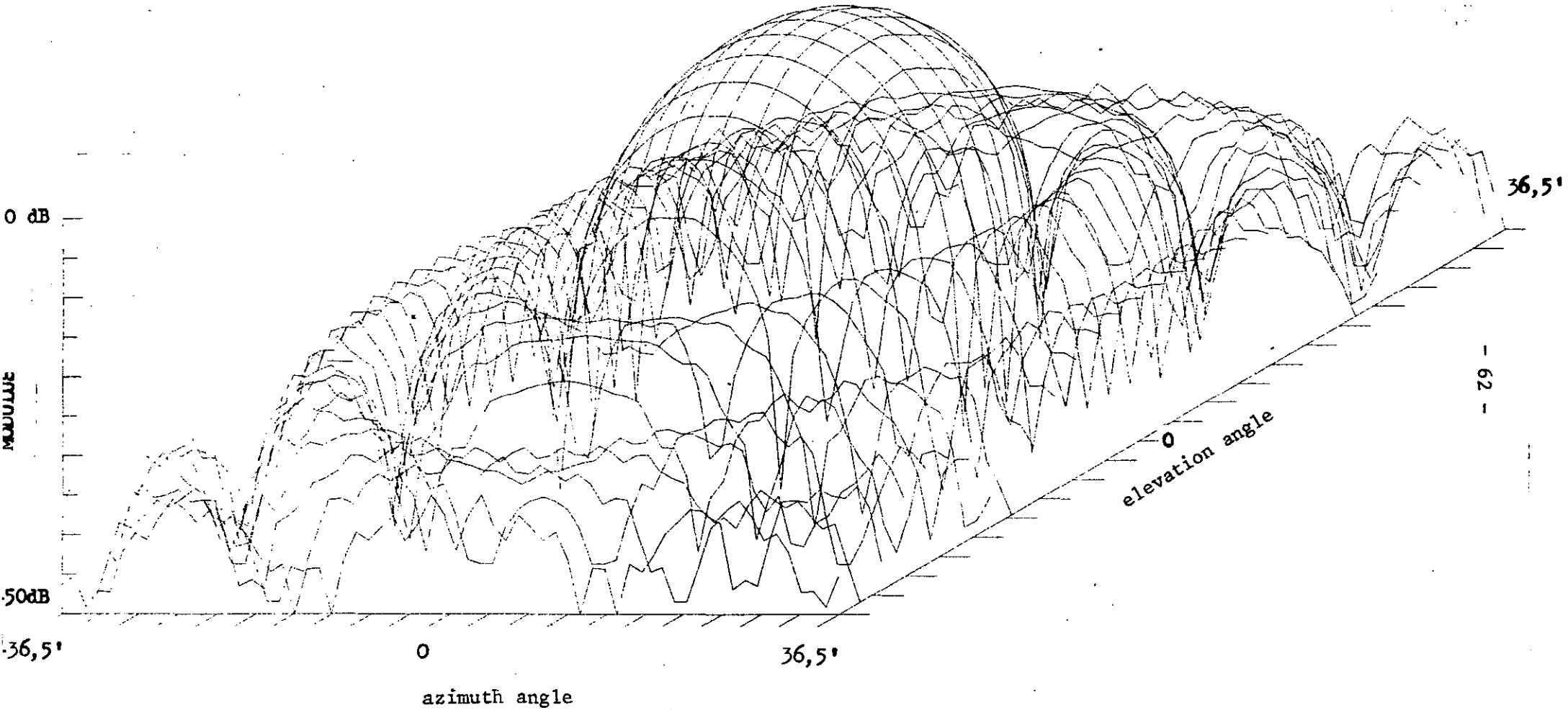

Fig. 3.4.9. Far field distribution of Fig. 3.4.8 with dB-scale

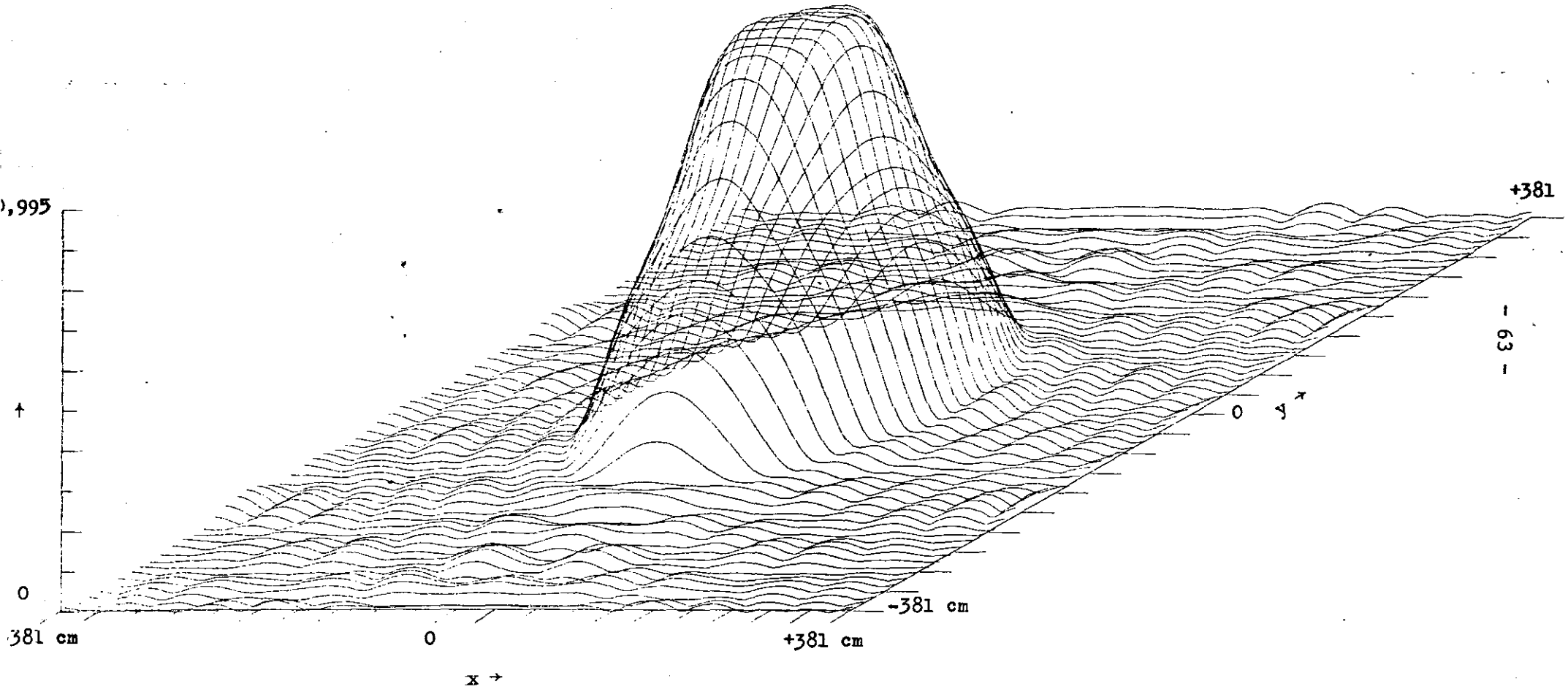

Fig. 3.4.10. Modulus of the reconstructed aperture field as calculated from Fresnel field measurements with a 20 dB dynamic range

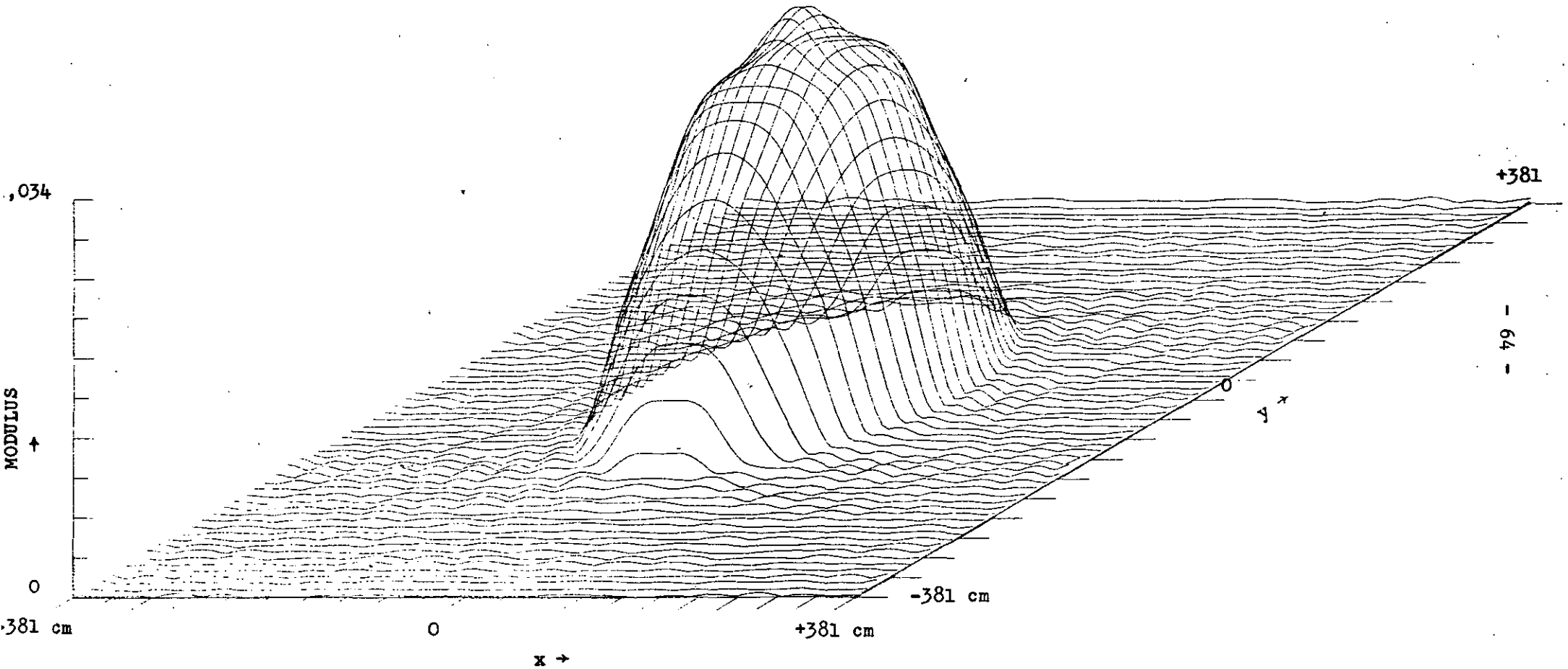

Fig. 3.4.11. Modulus of the aperture field, calculated from 30 dB dynamic range Fresnel field "measurements"

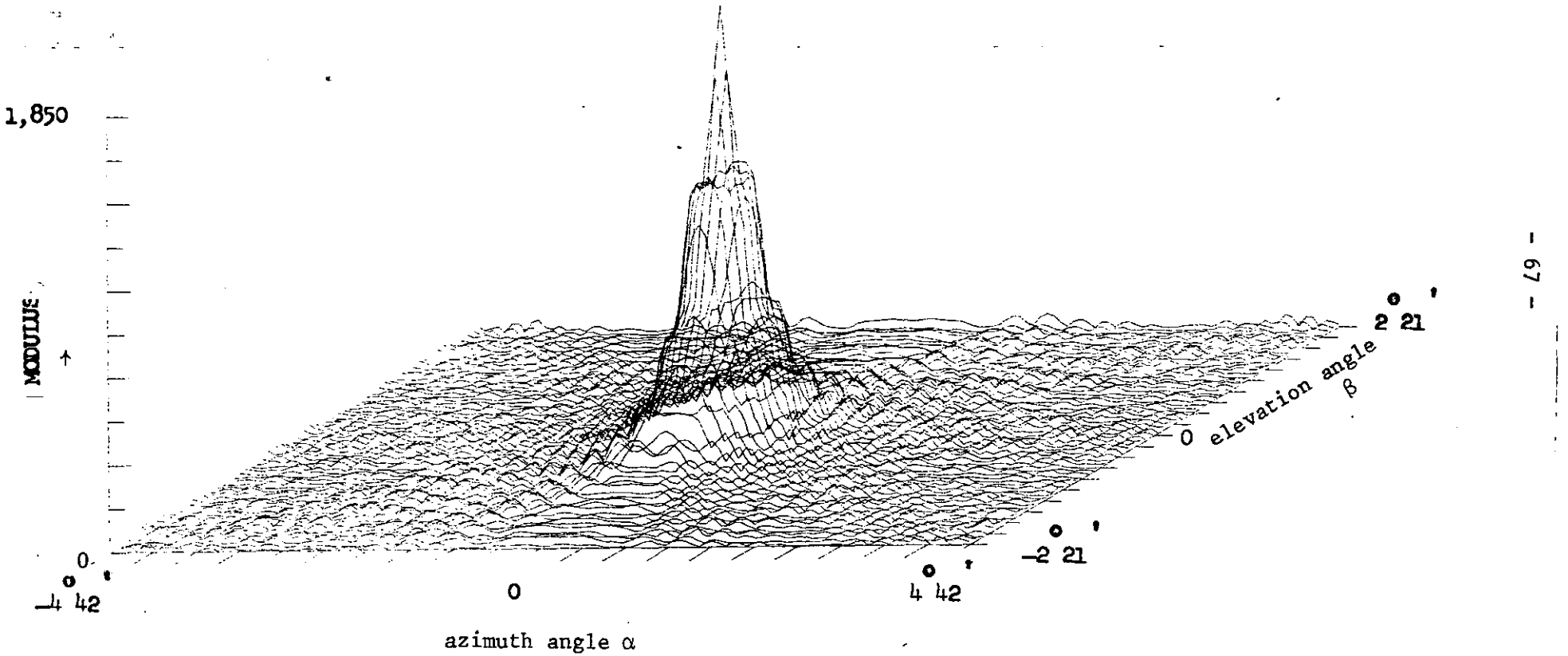

Fig. 3.4.14. Fresnel field distribution of a uniformly illuminated aperture

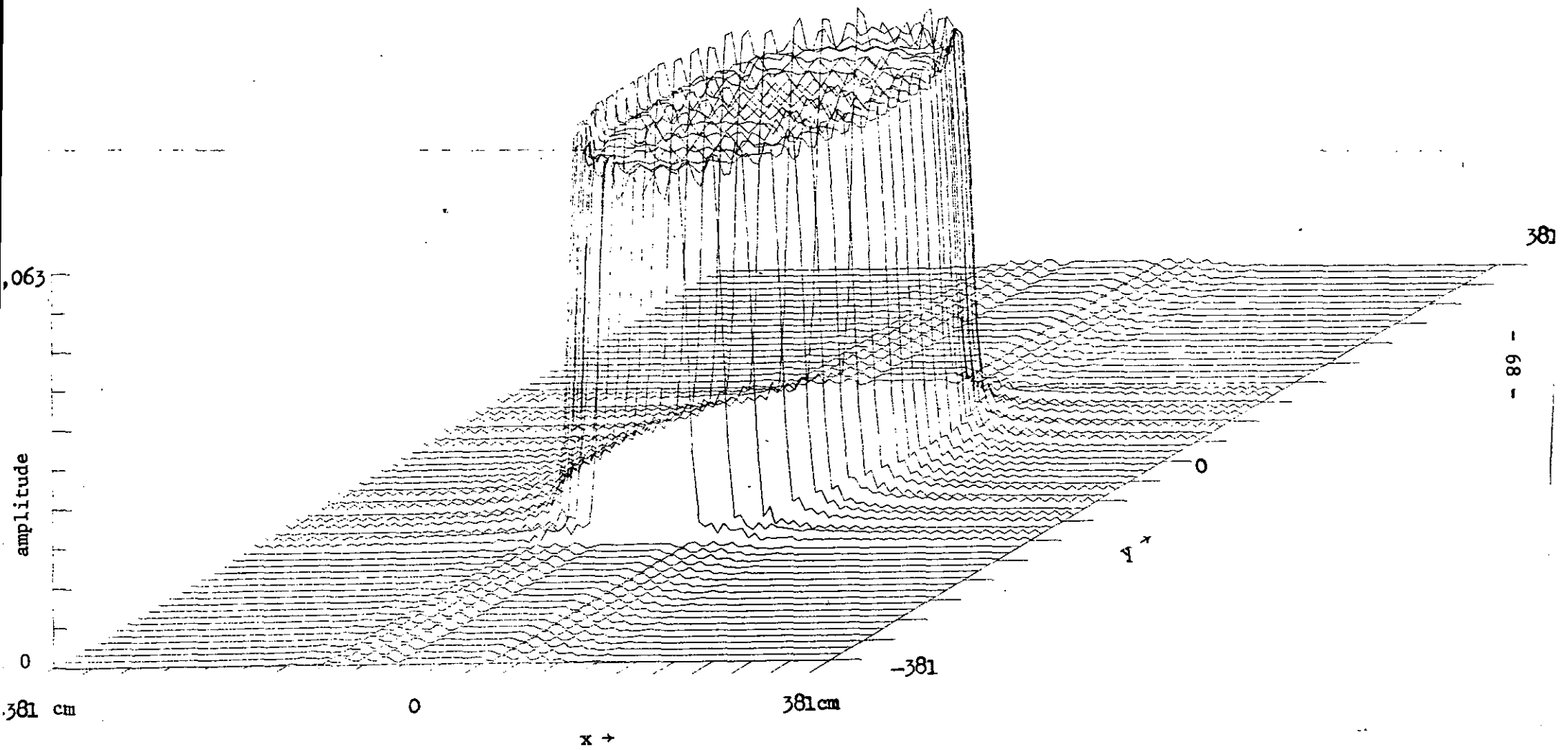

Fig. 3.4.15. Reconstructed aperture field

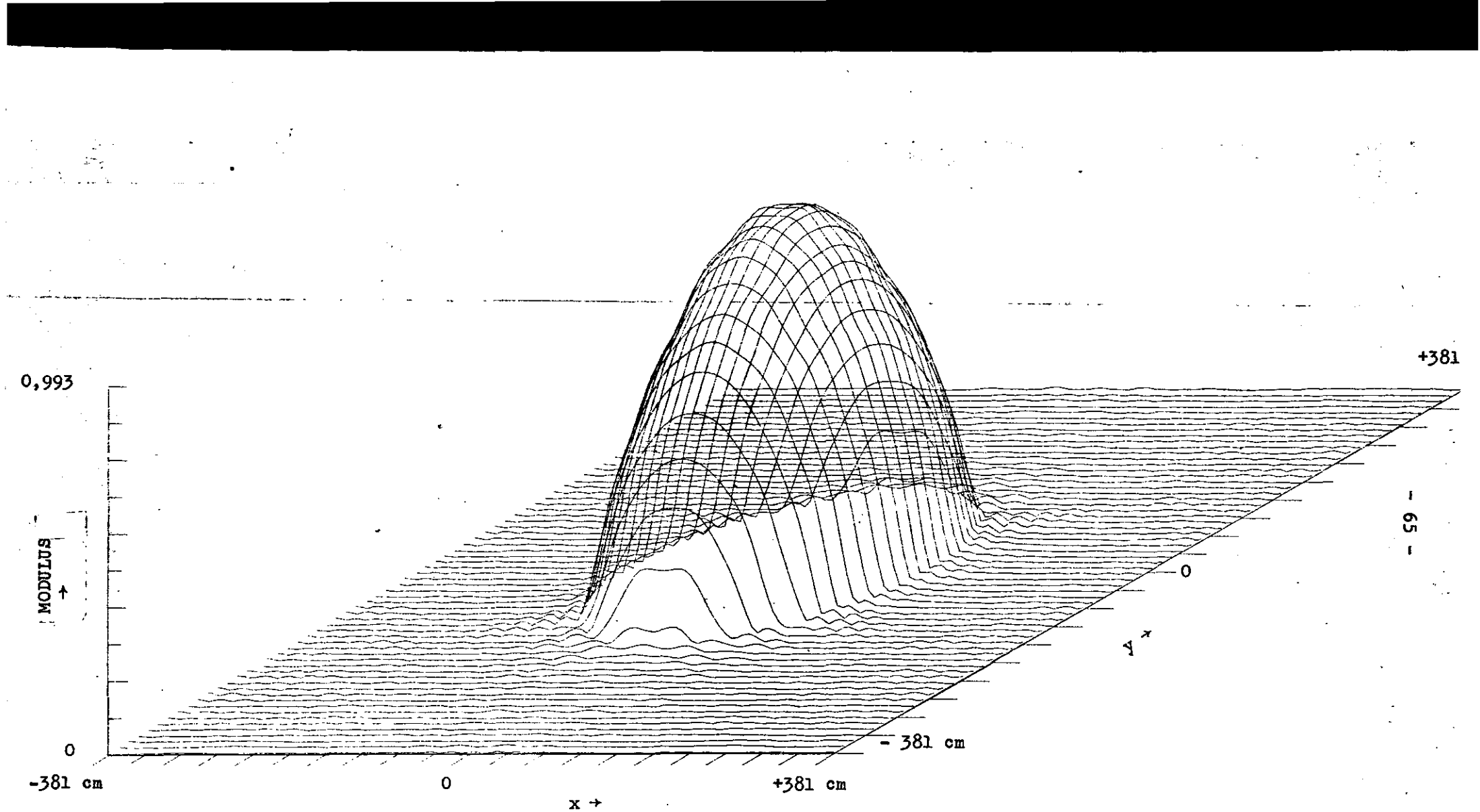

Fig. 4.3.12. Modulus of the aperture field as calculated from 40 dB dynamic range measurements

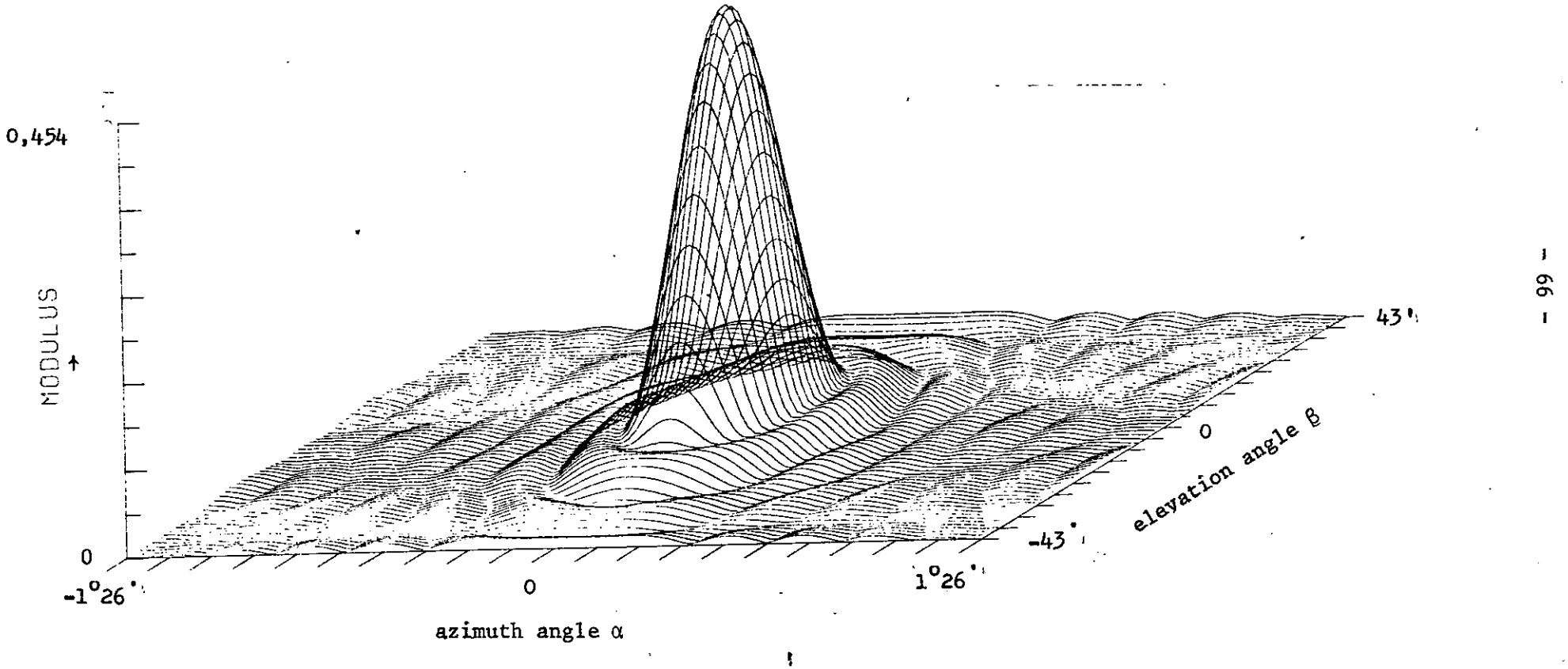

Fig. 3.4.13. Fresnel field distribution for $R_{Fre} = D^2/\lambda$

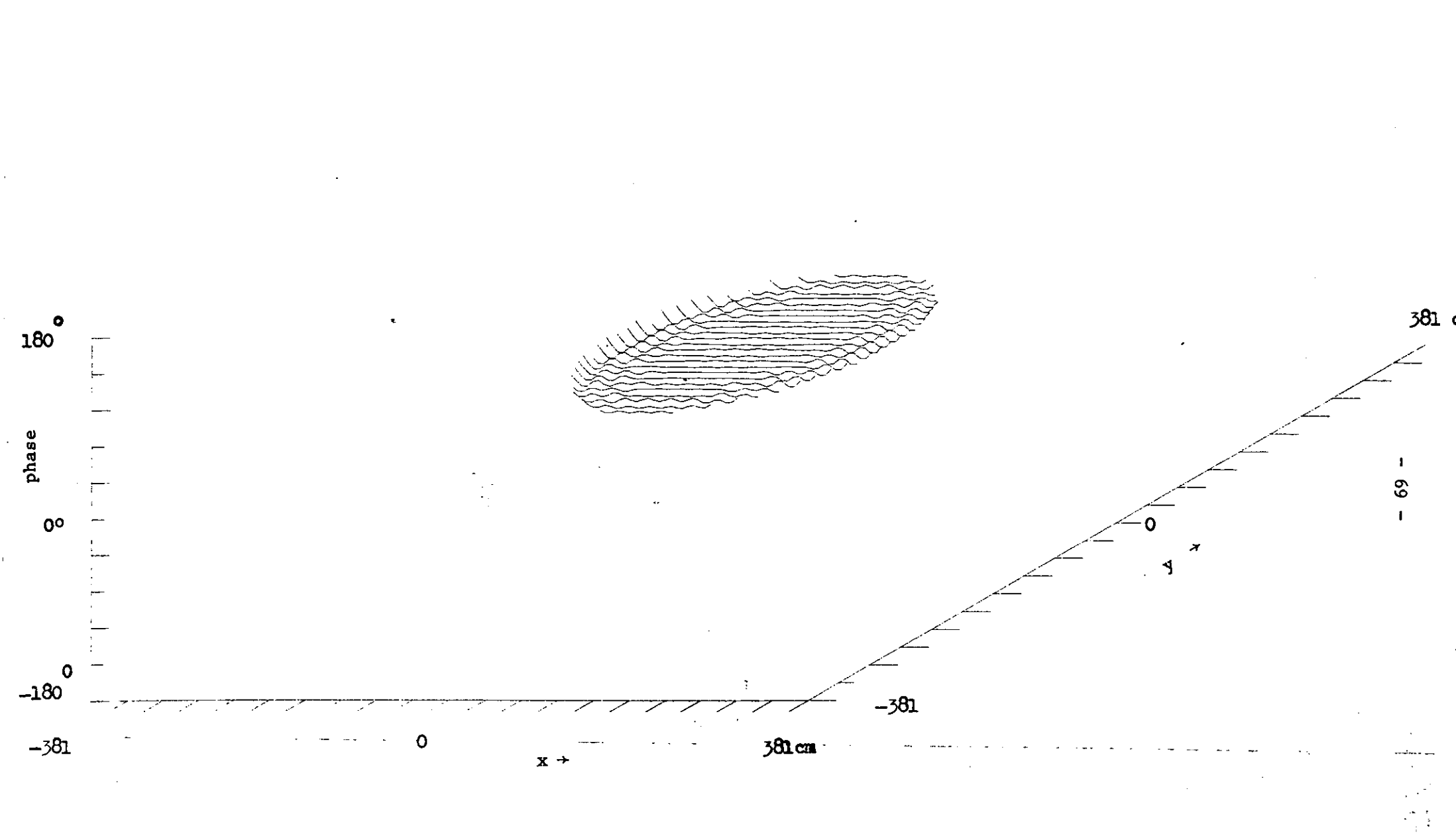

Fig. 3.4.16. Phase distribution of the reconstructed aperture field

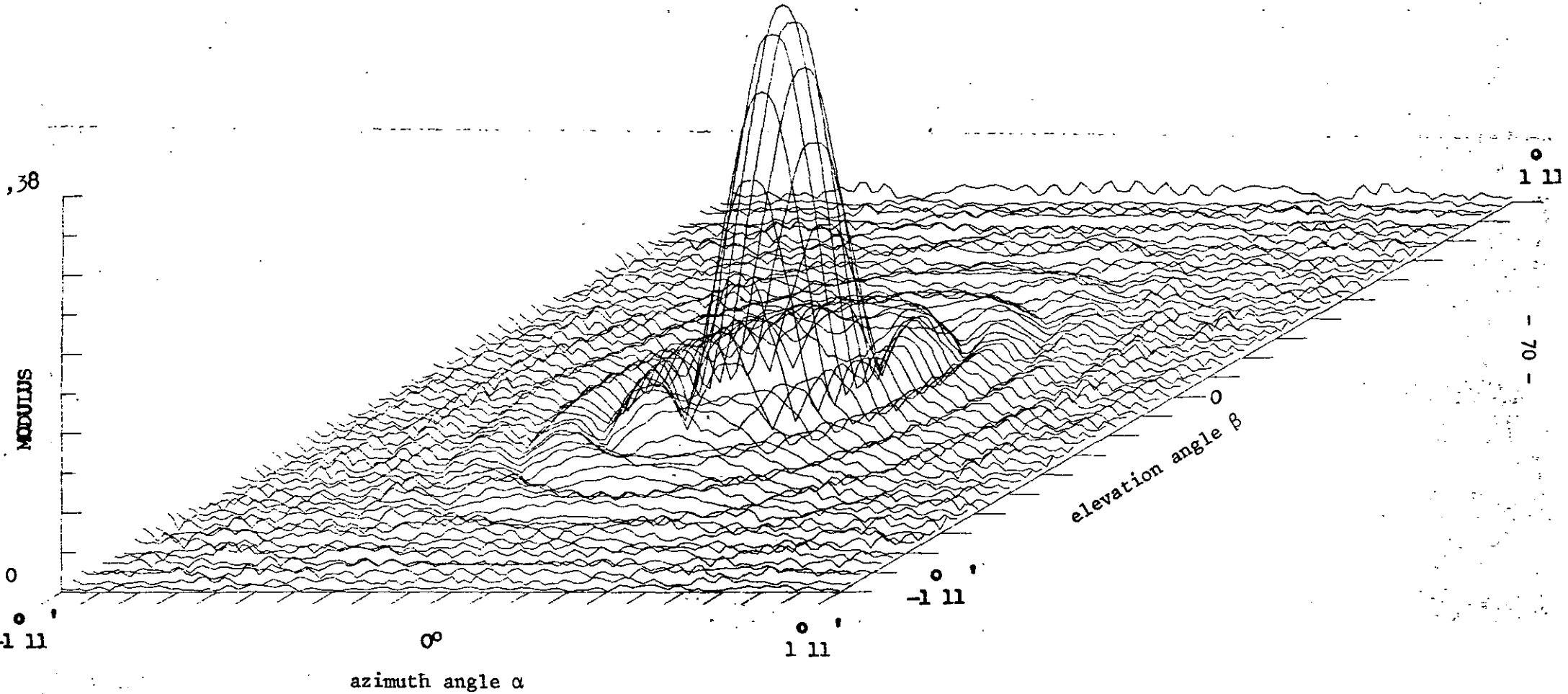

Fig. 3.4.17. Far field distribution as calculated from the truncated Fresnel field.

3.5 Literature

1 W.T. Cochran et al.: "What is the fast Fourier transform" Proc. IEEE, Vol. 55, nr. 10, p. 1664, Oct. 1967.

2 W.C. van Etten: "De diskrete Fourier transformatie", Intern Rapport T.H.E., Nov. 1971.

3 J.A. Glassmann: "A generalisation of the fast Fourier Transform", IEEE Trans. on Comp., Vol. C 19, nr. 2, 1970.

4 V.I. Turchin et al.: "Errors in reconstruction of radiation aptterns of antennas on the basis of near field phase measurements" RE & EP April 1974.

5 C.A.M. Geus: "Antennemetingen m.b.v. microgolfholografie", M.Sc. Thesis Eindhoven University of Technology, 1975.

6 J. Dijk, J.M. Berends, E.J. Maanders: "Aperture blockage in dual reflector antenna systems", THE Report 71-E-23.

4. Fresnel field measurements and results of field reconstructions

4.1. Introduction

Early in 1967, Bakhrakh and Kurohkin [1,2] investigated the use of holographic techniques in order to record Fresnel field distributions totally. From the recorded field distribution, called a microwave hologram, an optical analogon was produced. Holographic reconstruction then yielded the optical analogon of the radiation pattern of the microwave antenna. Because of the low dynamic range of films used for the optical hologram, and the difficulty of obtaining phase distributions, optical reconstruction of the aperture and the far field distributions did not seem very suitable. Napier and Bates [3-7] proposed in 1971 to use the computer for simulating the (optical) holographic reconstruction process. Since then microwave holographic techniques have been used widely for mapping microwave field distributions, while computer reconstruction was mostly used in order to simulate the holographic reconstruction process [8-23].

The holographic recording process is basically a method of encoding spatial phase variations in an intensity modulation. The computer holographic reconstruction process can then be seen as a demodulation process, which, however, requires some inherent approximations [3,4,12].
A much more straightforward method based on the principle of complex microwave holograms will be presented here. Some problems encountered in Fresnel field measurements will be treated and measurement results on an electrically small reflector antenna will be given.

4.2. Recording of microwave fields using complex microwave hologram techniques

Dechamps [20] showed that product detectors, also called correlators in radio astronomy and interferometry, can be used for mapping microwave fields completely. With two harmonic time functions, with complex amplitudes R and S, such a product detector is defined as $\mathrm{Re}(R^{*}S)$.

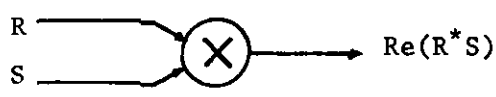

Fig. 4.2.1. Product detector or correlator.

Here * denotes the complex conjugate, and Re the real part. Applocation of an extra 90° phase shift of the R signal then yields $Re([+jR]^*.S) = Im(R^*S)$. A system yielding the real and imaginary parts of R^*S gives a complete recording of the S-signal if R is taken as the known reference.

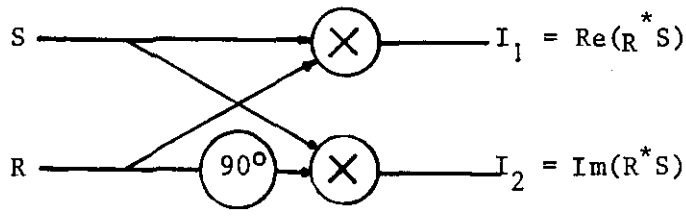

Fig. 4.2.2. Recording of a complex hologram.

With

$$S = |S|e^{j\phi_S}$$

and

$$R = |R|e^{j\phi_R}$$

the amplitude and phase distribution of S can be calculated from I_1 and I_2:

$$|S| = \frac{I_1^2 + I_2^2}{2|R|} \qquad (4.2.1.)$$

$$\phi_S = \phi_R + \arctan\left(\frac{I_1}{I_2}\right) + 2\pi n \qquad (4.2.2)$$

For the purpose of Fresnel field measurements, amplitude and phase distributions are not very suitable since Fast Fourier transform-algorithms require real and imaginary parts of the field. The use of the measurement set-up of Fig. (4.2.2) is then obvious.
Quadrature hybrids (Q) Fig. (4.2.3) can be combined to make a correlator, and with the use of an in-phase power devider (D) a complex hologram-measurement set-up is obtained.

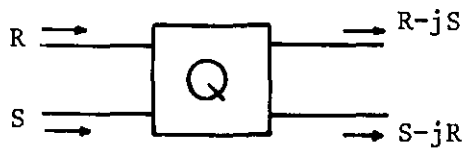

Fig. 4.2.3. Quadrature or 90° hybrid.

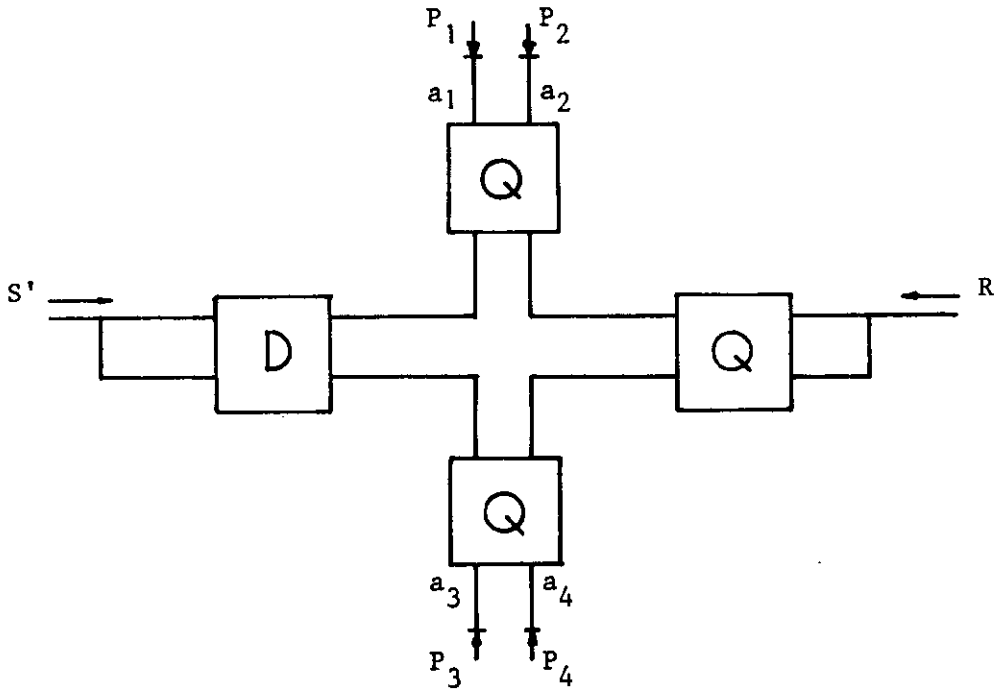

Fig. 4.2.4. Measurement set-up for complex microwave holograms.

In the set-up of Fig. 4.2.4. the complex amplitudes a_i are given by:

$$\begin{aligned} a_1 &= S - R \\ a_2 &= S + R \\ a_3 &= S + jR \\ a_4 &= S - jR \end{aligned} \qquad (4.2.1)$$

The power of the signals with complex amplitudes a_i is then proportional to

$$\begin{aligned} P_1 &= |S-R|^2 = |S|^2+|R|^2-2|SR|\cos(\phi_S-\phi_R) \\ P_2 &= |S+R|^2 = |S|^2+|R|^2+2|SR|\cos(\phi_S-\phi_R) \\ P_3 &= |S+jR|^2 = |S|^2+|R|^2-2|SR|\sin(\phi_S-\phi_R) \\ P_4 &= |S-jR|^2 = |S|^2+|R|^2+2|SR|\sin(\phi_S-\phi_R) \end{aligned} \qquad (4.2.2)$$

The difference of the detected powers then yields:

$$\begin{aligned} P_2 - P_1 &= 4|RS|\cos(\phi_S-\phi_R) \sim \mathrm{Re}(R^*S) \\ P_4 - P_3 &= 4|RS|\sin(\phi_S-\phi_R) \sim \mathrm{Im}(R^*S) \end{aligned} \qquad (4.2.3)$$

The use of diodes with identical quadratic characteristics yields output voltages proportional to the incident microwave power P_i (i = 1, 2, 3, 4).

The voltage difference at the output of these microwave detectors then gives the wanted real and imaginary part of the S-signal if R is taken as a fixed reference signal.

With the use of short slot hybrids as quadrature hybrids and an E-plane T, a waveguide measurement set-up according to Fig. 4.2.4. was realised by the author [27]. The inherent difference in the diode characteristics was solved by applying a large reference signal yielding linear detector output giving a real time output signal with a small dynamic range of 23 dB. Another disadvantage of the system was the small bandwidth of the X-band waveguide structure of approximately 100 MHz.
A solution to these problems is given by the use of co-axial components yielding a large frequency range, and the use of real time computer processing of the various diode characteristics [26]. The main advantage of this concept is that components are commercially available up to 200 GHz, yielding a relatively cheap and simple set-up capable of accurate amplitude and phase measurements in a frequency range where network analysors are not yet available (above 40 GHz).

4.3. Choice of a coordinate system for Fresnel field measurements

The field equations derived in chapter 2, assume a coordinate system which is centered in the aperture plane. In practice, however, it is not possible to rotate a test antenna around the aperture centre or focal point. As a result, in the measured Fresnel field distribution a quadratic phase error is included due to the additional pathlength between the aperture centre and the test probe.

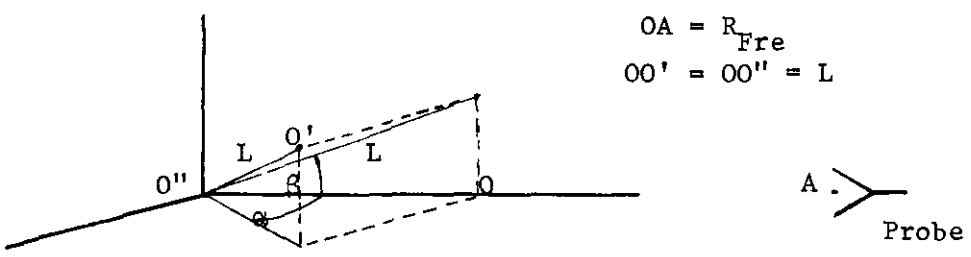

Fig. 4.3.1. Geometry with centre of rotation behind the aperture.

In all formulae the distance R_{Fre} has to be replaced by the distance O'A if the antenna rotates at O" instead of at O. Simple geometry then yields:

$$O'A = \left[(L\sin\beta)^2 + (L - L\cos\beta\cos\alpha + R_{Fre})^2 + (L\sin\alpha\cos\beta)^2\right]^{1/2}$$

A binominal expansion then yields:

$$O'A = R_{Fre} + L(1-\cos\beta\cos\alpha) + \frac{L^2}{2R_{Fre}}\{1 + \sin^2\beta + \sin^2\alpha\cos^2\beta + \cos^2\beta\cos^2\alpha - 2\cos\beta\cos\alpha\}$$

Usually $L^2 << R_{Fre}$ giving

$$O'A = R_{Fre} + L(1 - \cos\beta\cos\alpha)$$

for small values of α and β, a quadratic phase error is apparent from:

$$O'A = R_{Fre} + L(\tfrac{1}{2}\alpha^2 + \tfrac{1}{2}\beta^2) \qquad (4.3.1)$$

The angles α' and β' of the line O"O' with the line O'A do not equal the values α and β as can be seen from the one-dimensional case.

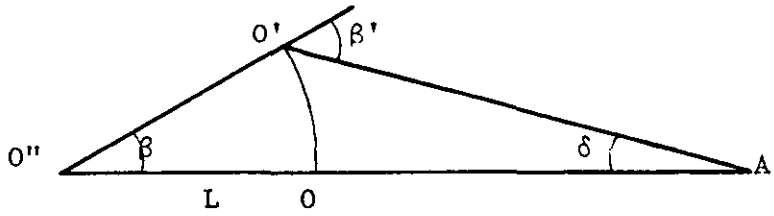

Fig. 4.3.2. Geometry for calculating β'.

It can easliy been seen that

$$\beta' = \beta + \delta$$

where

$$\delta = \arctan\left(\frac{L\sin\beta}{R_{Fre}}\right) \approx \frac{L\sin\beta}{R_{Fre}} \approx \frac{L\beta}{R_{Fre}}$$

if L sin β << R_{Fre} and $\beta \simeq \sin \beta$ giving

$$\beta' \simeq \beta + \frac{L\beta}{R_{Fre}} = \beta(1 + \frac{L}{R_{Fre}}) \qquad (4.3.2)$$

for L << R_{Fre} the error becomes negligible.
The two-dimensional case is much more difficult, but for small angles it can be seen from the one-dimensional case that

$$\alpha' \simeq \alpha(1 + \frac{L}{R_{Fre}}) \qquad (4.3.3)$$

and again for small values of α

$$\alpha' \simeq \alpha$$

If the errors are too large, the sample distances $\Delta\alpha'$ and $\Delta\beta'$ are easily corrected using (4.3.2) and (4.3.3).

4.4. Measurements in the Fresnel zone of a small reflector antenna

Generally the test antenna is capable of rotating and then it is obvious that the test antenna will receive instead of send because in that case a reference signal can easily be received too.

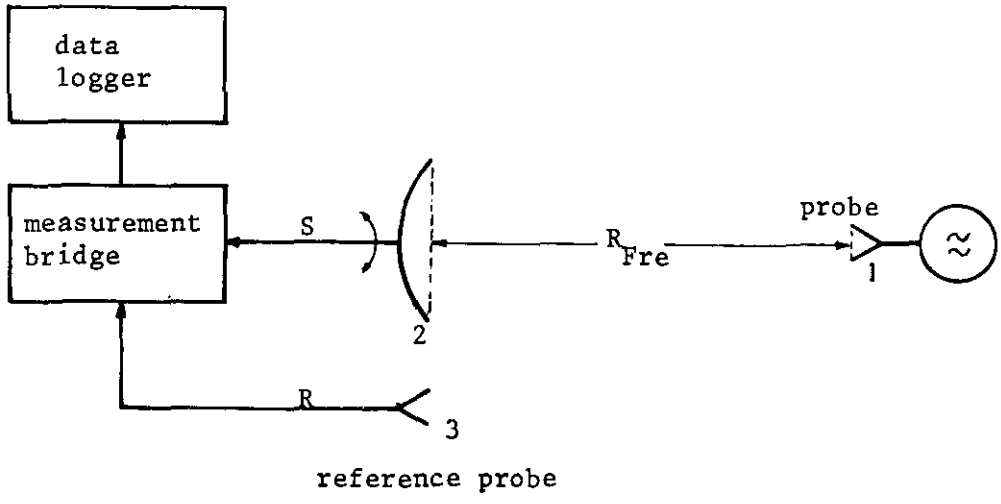

Fig. 4.4.1. Fresnel field measurement set-up.

In the case that the test antenna is used as a transmitter, the sampling probe should be small enough to neglect the averaging effect of the aperture since sampling requires measurement of the field in a point of space.
Kurochkin [8] showed that Fresnel field measurements on a linear test antenna with length D, require a linear probe with maximum dimension l_{max} in order to neglect the influence of the finite dimensions of the probe:

$$l_{max} < \frac{1}{2\pi} \cdot \left(\frac{\lambda}{D}\right) . R_{Fre} \qquad (4.4.1)$$

The proof of (4.4.1) in [8], yields for the two-dimensional case that (4.4.1) is also a good criterion if l_{max} is the maximum dimension of the two-dimansional probe.
Relation (4.4.1) shows that the maximum angular dimension of the probe as seen from the centre of the antenna being investigated, should be approximately one order of magnitude smaller than the width of the lobes of this antenna. Because of reciprocity the probe should have the same dimensions, if used as a transmitter. In order to perform Fresnel field measurements within an anechoic chamber of 2.5 m length, a small reflector antenna was chosen. This antenna rotated at the aperture centre and:

- D = 25 cm
- f = 9.2 GHz (λ = 3.26 cm)
- dipole feed

The far field is at:

$$- R_{far} = 2D^2/\lambda = 3.83 \text{ m} \qquad (4.4.2)$$

Calculation of M = 5 lobes requires

$$m \leq \frac{1}{2}\left(\frac{8D}{5\lambda}\right)^{2/3} - \frac{4}{3} = 2.43 \qquad (4.4.3)$$

The angle of measurement is limited (2.8.19 & 2.8.21) to

$25^o \leq \theta \leq 55^o$ if m = 1.5 or R_{Fre} = 2.54 m
$27^o \leq \theta \leq 45^o$ if m = 2 or R_{Fre} = 2.04 m

The sample distance in the Fresnel field is limited to λ/D:

$$\Delta\alpha \text{ or } \Delta\beta \leq \frac{\lambda}{D} = 7.5^{\circ}$$

Here we chose: $\Delta\alpha = 2^{\circ}$

$\Delta\beta = 4^{\circ}$

and measurements were performed for

$m = 1.5$ and $m = 2$

$-30^{\circ} \leq \alpha \leq 30^{\circ}$

$-32^{\circ} \leq \beta \leq 32^{\circ}$

The probe was an open-ended X-band waveguide, as chosen in agreement with (4.4.1). The measurements were carried out with an H.P. network analyser, yielding amplitude and phase distribution of the Fresnel field.
The Fresnel field measured at 2.54 m was used to calculate the amplitude and phase distribution in the aperture, Figs. 4.4.2 and 4.4.3. The aperture distribution shown in Figs. 4.4.4. and 4.4.5 was calculated from the field measured at $R_{Fre} = 2.04$ m. A good agreement of both reconstructed aperture fields is apparent. Interpretation of the calculated amplitude and phase distribution for the aperture field requires a separate investigation; however, some obvious conclusions can be made here.

- The dip in the amplitude of the aperture field is due to aperture blocking by the feed.
- The lobes outside the aperture, where the field should be zero, are due to the fact that the Fresnel field was measured over too small an angle ($\pm 32^{\circ}$). The same effect can be observed from Figs. 3.4.10 to 3.4.12, since truncation of the dynamic range of measurement resembles a measurement interval which is too small. This resemblance is due to the fact that the Fresnel field intensity decays fast for larger boresight angles. However, measurement of the Fresnel distribution over larger angles is hardly possible, because then α and β are proportional to $\sin\theta$ instead of θ, and, hence, sample distance requires nonconstant azimuth and elevation steps.
- The calculated aperture phase distribution is strongly nonuniform yielding high levels of the far sidelobes of the radiation pattern [27]. However, no far sidelobes may be predicted in case of strongly nonuniform phase distributions because of the assumptions made in sec. 2.2.

The reconstructed field within the aperture was used to calculate the far field patterns 4.4.6 to 4.4.8. The radiation pattern of the antenna was measured in another anechoic chamber, which unfortunately exhibited a strong

reflectivity, yielding high interlobe levels (Fig. 4.4.6) and making the recorded radiation pattern highly inaccurate below -28 dB.

In spite of the small Fresnel field measurement interval, the reconstructed and measured main lobe exhibits good agreement in the E and H planes. The reconstructed sidelobe levels agree within approximately 0.5 dB with the measured levels.
Note that the predicted levels between main lobe and first sidelobe are much lower than the measured values, which are too large due to reflections in the anechoic chamber.

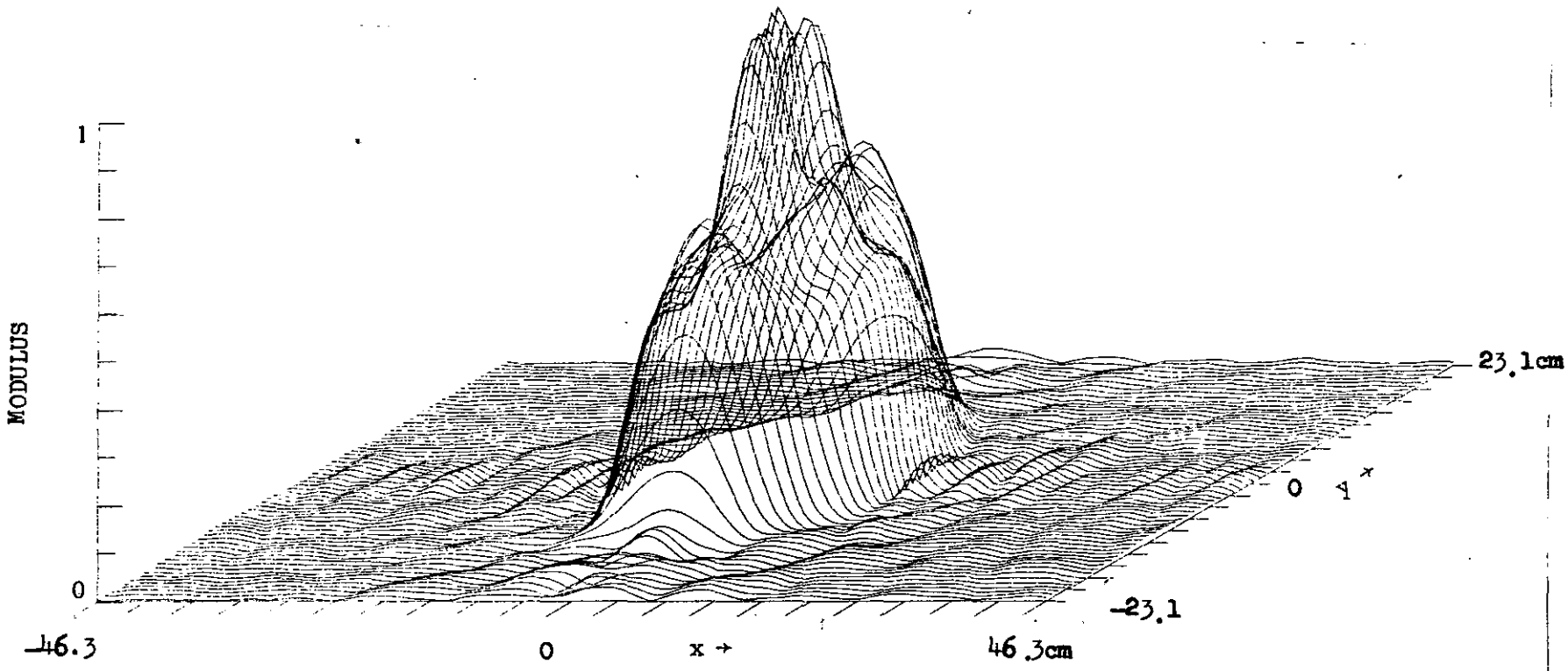

Fig. 4.4.2. Aperture field calculated from Fresnel field measurements at 2.54 m.

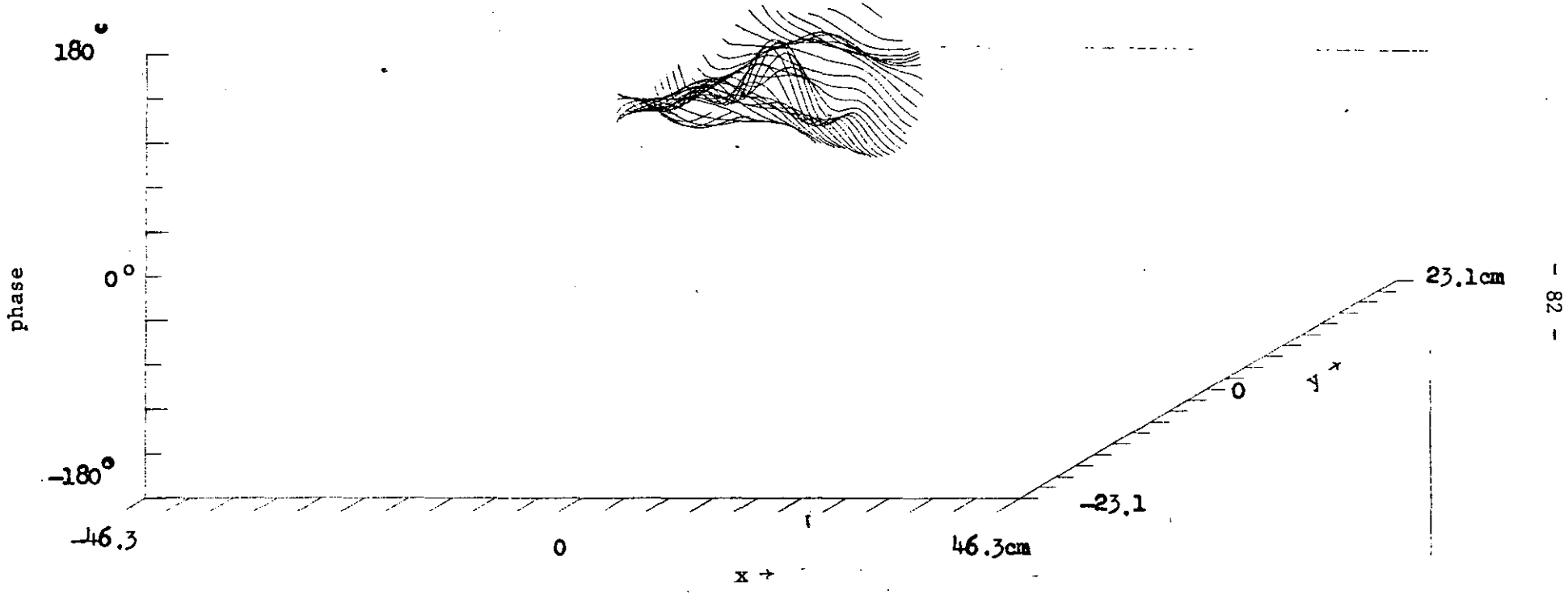

Fog. 4.2.3. Phase distribution of the reconstructed aperture field.

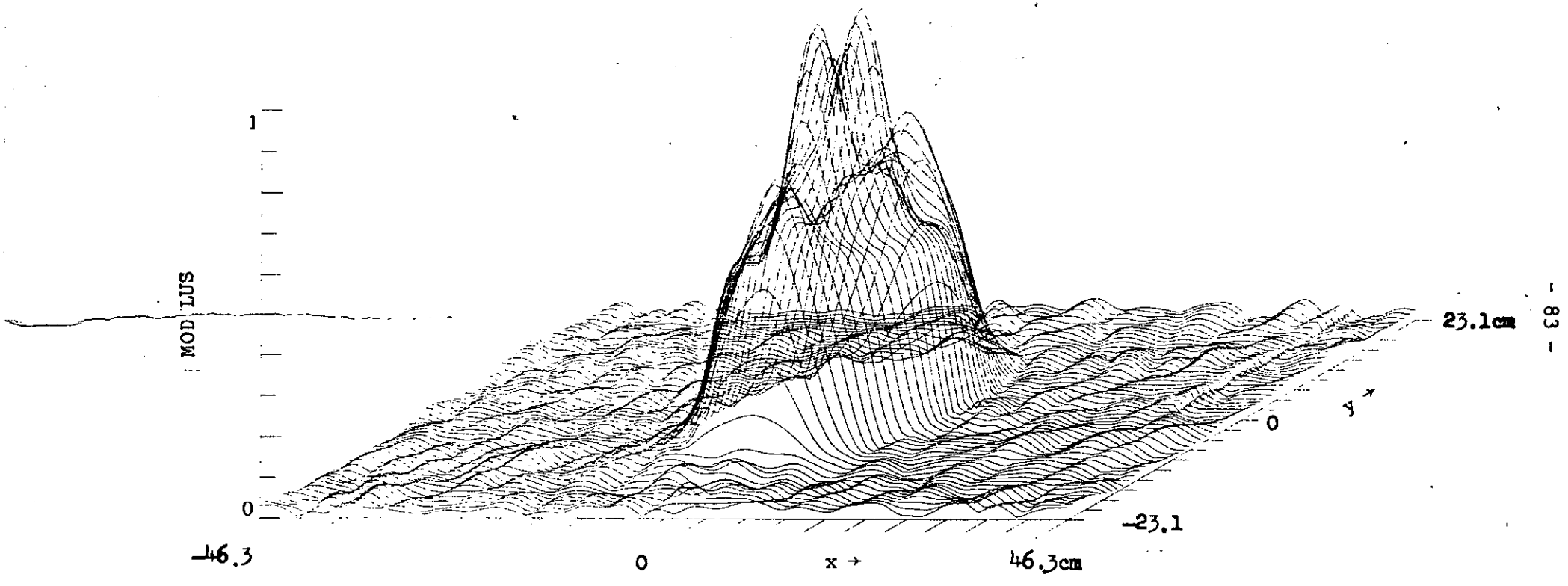

Fig. 4.2.4. Modulus of the aperture field as reconstructed from Fresnel field measurements at 2.04 m.

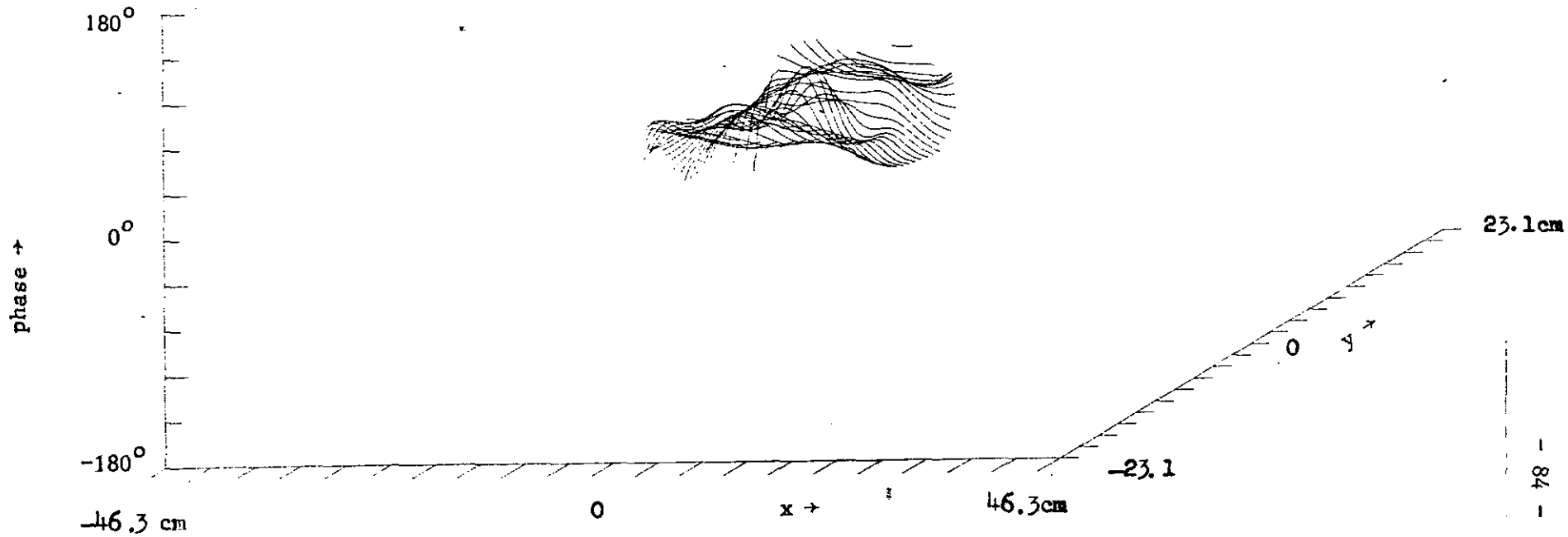

Fig. 4.2.5. Phase distribution of the aperture field as reconstructed from Fresnel field measurements at 2.04 m.

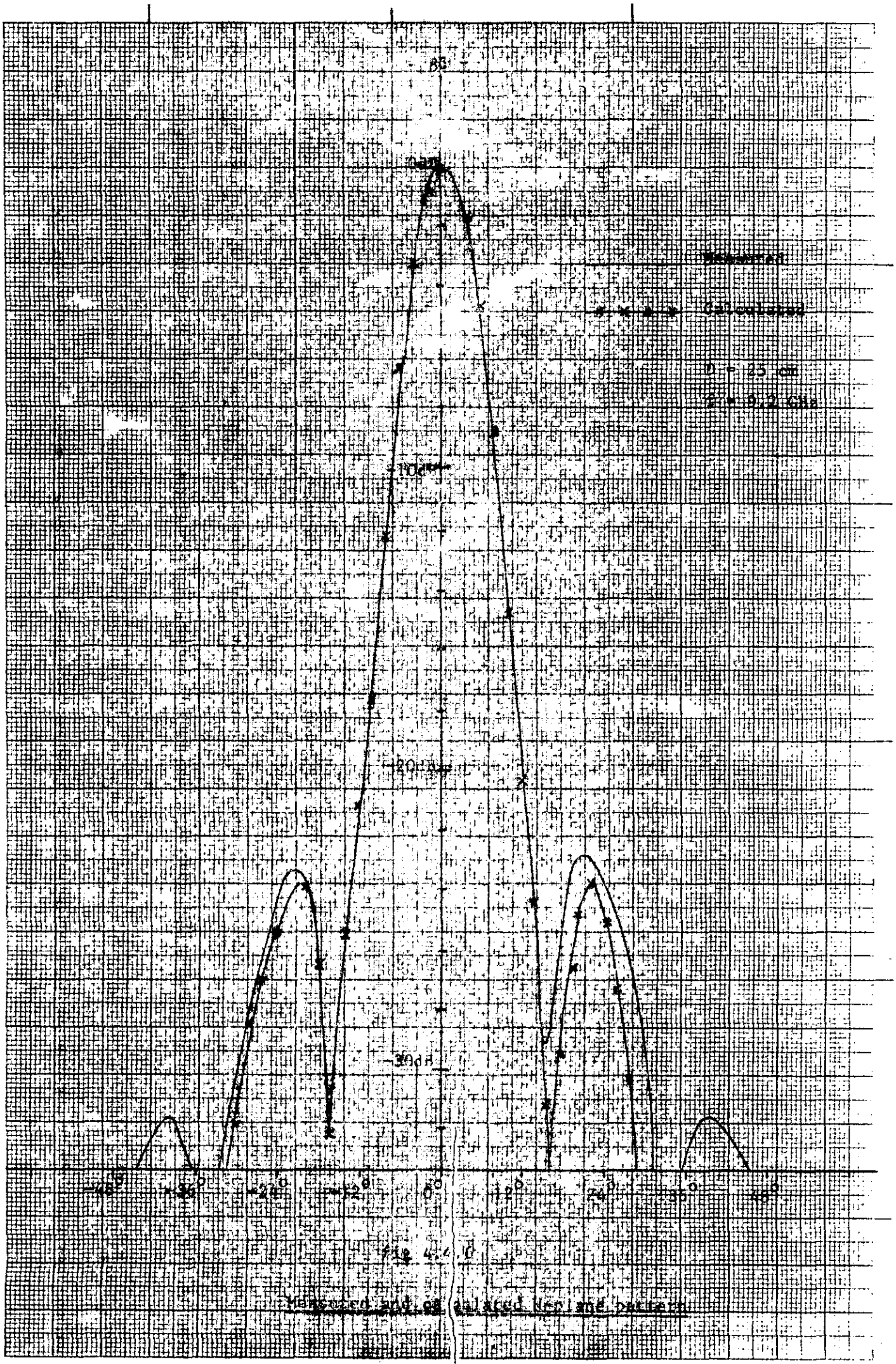

Fig. 4.4 (i)

Measured and calculated H-plane pattern

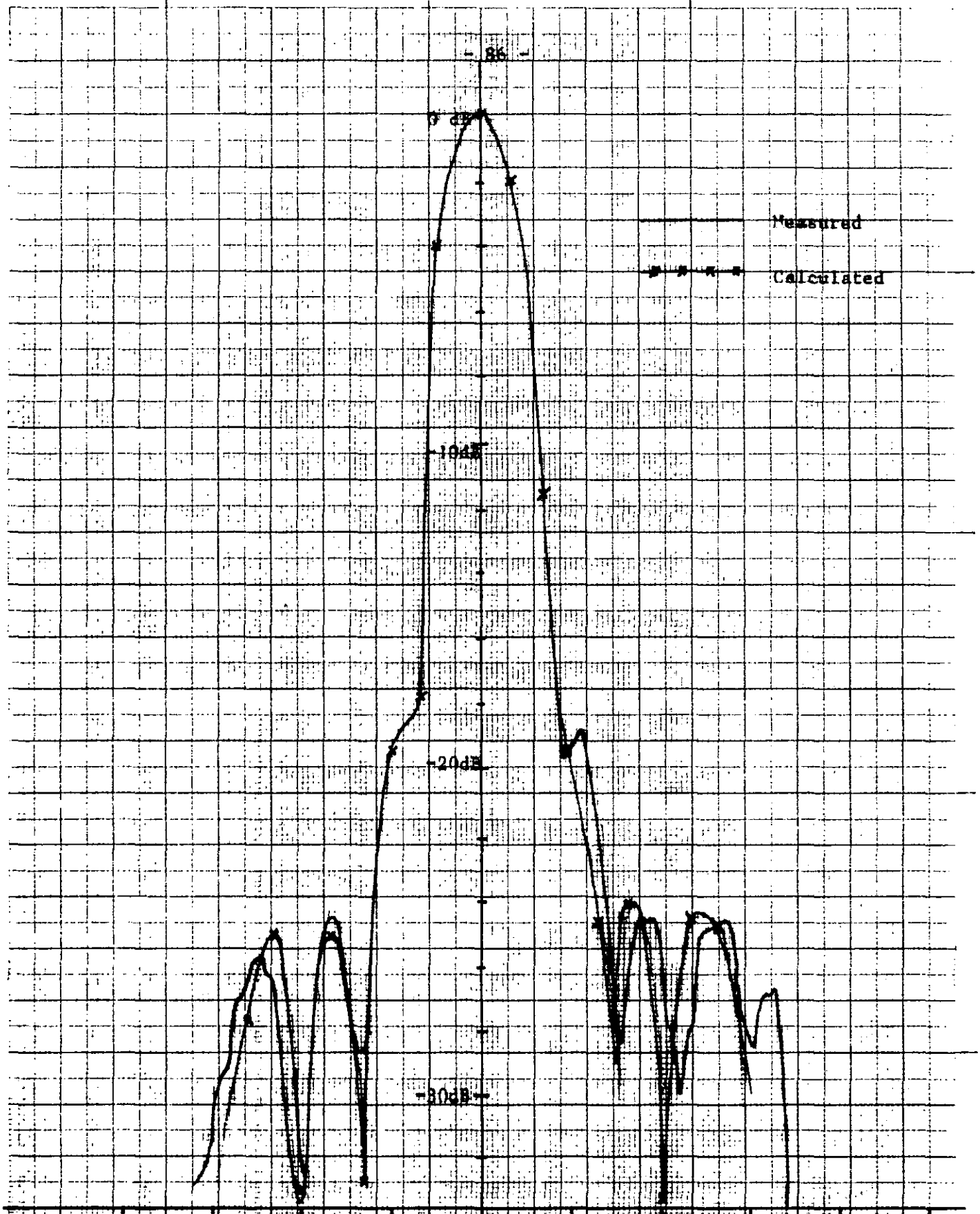

Fig 4.4.7

Measured and calculated E-plane pattern

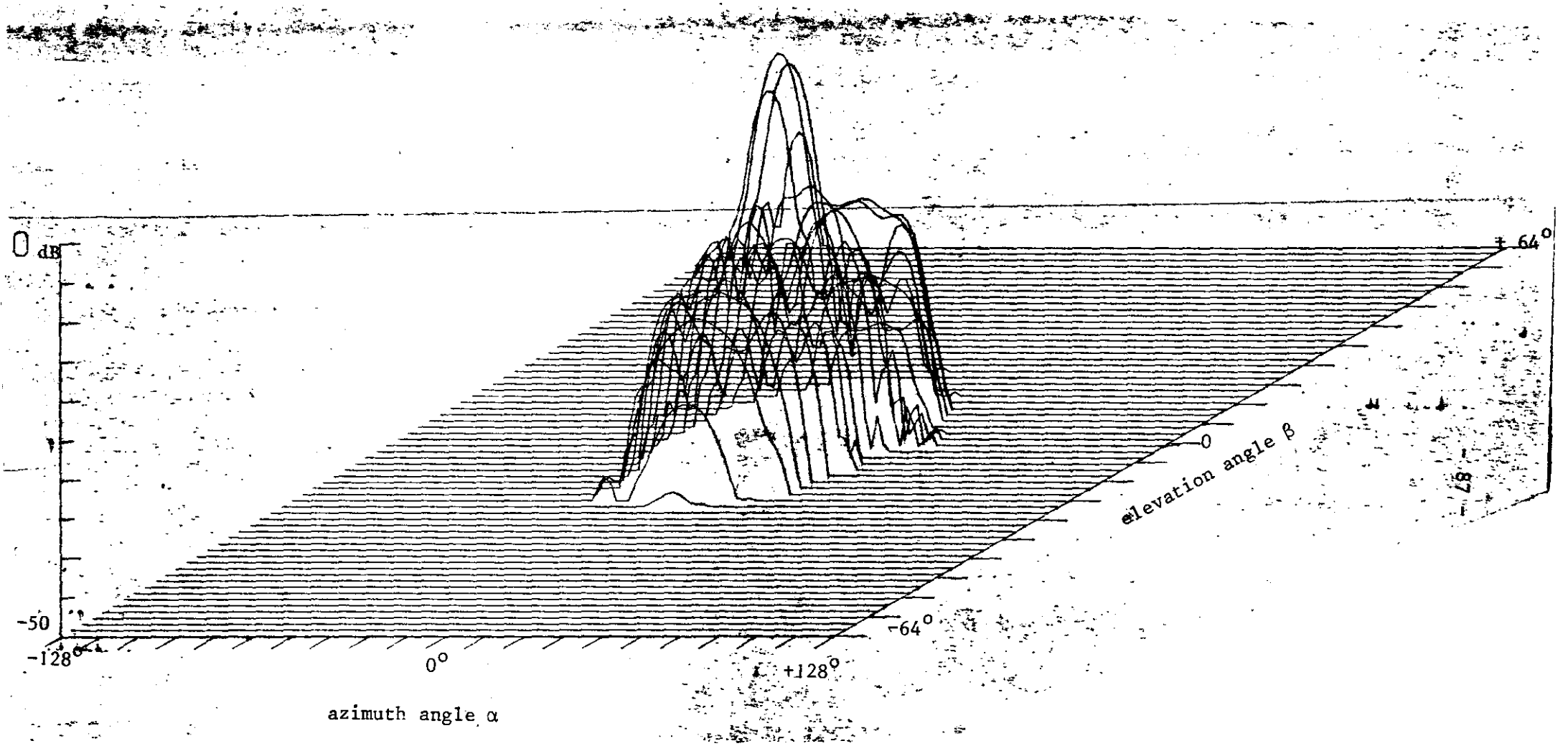

Fig. 4.4.8. Reconstructed radiation pattern.

4.5 Conclusions

The relative simplicity of the Fourier-Fresnel transforms used and the high speed of F.F.T. algorithms are the major advantages of the method described in comparison with near field-far field methods (cf. ref. 1 & 2 of ch. 1). Another advantage of Fresnel field measurements is the use of an often existing antenna mount instead of a special scanning system.
Calculation of radiation patterns from measurements in the Fresnel zone is only meaningful for large D/λ ratios because small ratios yield a small far field distance and a small number of reductions m. Another advantage of a large D/λ ratio is the small angle of measurement yielding a simple relationship between Fresnel field co-polar and cross-polar and aperture field polarisations (cf. 2.5.3 & 2.5.4).
The small measurement angle however might still be too large as in case of the 3 m. Cassegrain antenna of our university which is presently operated on a very special mount [28] at frequencies of 30 and 11.6 GHz. The special mount already mentioned is very stable and accurate, but has some inherent disadvantages being the limited scan angle of 3° and the small rotation and translation as the antenna is scanned. The translation of a few centimeters make accurate phase measurements impossible, while cross-polar measurements are no longer meaningfull due to a small rotation of the antenna.
The most severe restriction is however the limited scan angle of 3°, and a test range of about 16 meters:

D = 3 m; γ = 1 (eq. 2.9.2); M = 5 (sidelobes)								
f	λ	D/λ	λ/D	R_{Fra}	M_{max}	$R_{Fre\ min}$	θ_{max}	θ_{min}
30 GHz	1 cm	300	0.19°	1800 m	60	30 m	5.97°	6.21°
11.6 GHz	2.58 cm	116	0.49°	696 m	31.2	22.3 m	8.36°	10.22°
Equations					2.8.21	2.9.3	2.9.2	2.8.19
Figs					2.9.3	-	2.9.1	-

For small D/λ ratios, Fresnel field measurements are meaningful as far as knowledge of the aperture field distributions is concerned. The interpretation of these distributions and also probe correction could be subject of further study.

4.6 Literature

1. L.D. Bakhrakh and A.P. Kurochkin: "Use of holography in reconstruction of polar diagrams of UHF-antennas from field measurements in the Fresnel zone", Sov. Phys-Tech.Phys., Vol. 11, nr. 2, p. 1102 (June 1967).
2. L.D. Bakhrakh, A.P. Kurochkin, D.A. Dmitrenko, N.M. Tseitlin and Dzh Arutyunyan: "Determination of the radiation pattern of a receiving antenna by means of a source in the Fresnel zone using holography and optical processing", Sov. Phys. Dokl., Vol. 16, nr. 11, p. 1004 (May 1972).
3. R.H.T. Bates: "Holographic approach to radiation apttern measurements", p. 1107-1208, Int. Jrnl. Engng.Sci., Vol. 9, 1071.
4. id. p.1193-1208.
5. R.H.T. Bates and P.J. Napier: "A suggestion for determining antenna pattern phase from holographic type of measurement", Austr.Electr.Comm., p.164, April 1971.
6. P.J. Napier: "Array element modulus and phase measured radiation pattern modulus", Austr.Electr.Comm., p. 466, Dec. 1971.
7. P.J. Napier and R.H.T. Bates: "Antenna aperture distributions from holographic type of radiation pattern measurements", Proc. IEEE 120, Jan. 1973.
8. A.P. Kurochkin: "Measurement properties of radio holograms with a probe", Radio Eng. and Electr. Phys., Vol. 16, nr. 7, p. 1209-1212, July 1971.
9. L.D. Bakhrakh, A.P. Kurochkin, D.A. Dmitrenko, N.M. Tseitlin, Dzh.S. Arutyunyan: "Holographic determination of directional diagram for receiving antenna with source located in Fresnel zone", Dokl.Akad.Wouk SSSR, Vol. 201, nr. 3, p. 580-582 (1971) (In russian).
10. V.A. Varganov, D.A. Dmitrenko, V.I. Turchin et al: "Investigation of cross-polarisation antenna characteristics using microwave holography", Radiophys. and Quantum Electronics, Vol. 16, nr. 1, p. 119-120, 1973.
11. J.C. Bennet, A.P. Anderson, P.A. McInnes, A.I.T. Whitaker: "Investigation of the characteristics of a large reflector antenna using microwave holography", IEEE 1973 S-AP Symposium, p. 298-301.
12. V.I. Turchin, N.M. Tseytlin, A.K. Chandaev: "Measurement of antenna patterns based on radiation from a source in the Fresnel zone with the help of SHF holography and computer processing", Rad Eng and Elect Phys., Vol. 18, nr. 4, p. 527-535 (April 1974).
13. A.A. Arutyunyan, J.S. Arutyunyan et al: "The measurements of antenna far field pattern by machine reconstruction of the microwave hologram in aperture", (in russian), Izv.Akad.Warek.Arm. SSR Fiz.Journal Paper, Vol. 7, nr. 5, p. 373-6 (1972).
14. E.L. Rope, R.A. Hayward, G. Tricoles: "A holographic method for determining antenna near field distributions from phase and intensity measurements on a spherical surface", 1973 G-AP Sy,p. p. 61-64.
15. E.M. Zuikova, L.A. Pasmanik, V.I. Turchin: "Optical processing in non-coherent light, results of radioholographic measurements of antenna radiation pattern", Radio Phys. and Quantum Electron., Vol. 16, p. 1250-1253.
16. E.L. Rope, G. Tricoles: "Microwave and optical holography and diagnostics for antennas and radomes", IEEE J. Quant.Electr.-QE5, nr. 6, p. 315, June '69.
17. "Applications of microwave holography to radomes and antennas", 1971 G-AP Symposium (IEEE), p. 160.
18. V.M. Ginzburg, V.M. Meschankin, B.M. Stepanov: "The use of holographic techniques for microwave measurements", CPEM 74 Digest, (Conference on precision electromagnetic measurement), p. 93-94.
19. "Measurement of the amplitude phase distributions of radio fields by holographic methods", Rad Eng. and Electr. Phys. Vol. 18, p. 166, Febr. 1973.

20. L.D. Bakhrakh, A.P. Kurochkin et al: "The applications of coherent optics and holography to design and measurement of the parameters of high directional antennas", Paper 15-10 of "Applications de l'holographie Univ. Besançon 1971, Papers 15-1,3,6,8 and 2.
21. L.D. Bakhrakh et al: "Antenna synthesis by coherent optical systems", Antennas 5, p. 47-60, 1969, in Russian.
22. V.I. Turchin and N.M. Tseitlin: "Measuring the directivity pattern of antennas in the Fresnel zone", Sov.Phys.-Tech.Phys., Vol. 17, nr. 8, p. 785, Febr. 1973.
23. J.C. Bennet, A.P. Anderson, P.A. McInnes, A.I.T. Whitaker: "Comprehensive measurements of aperture fields near fields and far fields of a large reflector antenna from a microwave hologram", European Microwave Conference Proceedings, 1974.
24. A.P. Kurochkin: "Measurement properties of radio holograms with a probe", Radio Eng. and Electr. Phys., Vol. 16, p. 1209-1212.
25. G.A. Deschamps: "Some remarks on radio frequency holography", Proc. IEEE 55, p. 2162, Dec. 1969.
26. C.A. Hoer: "Using six-port and eight-port junctions to measure active and passive circuit parameters", NBS technical note 673, Sept. 1975.
27. C.A.M. Geus: "Antenne metingen met behulp van microholografie", M.Sc. Thesis Eindhoven University of Technology, Dec. 1975.
28. J. Dijk, E.J. Maanders and J.M.J. Oostvogels: "An antenna mount for tracking geostationary satellites", THE Report 77-E-74, May 1977.